MICROMECHANICAL PROGRESSIVE DAMAGE MODEL FOR PREDICTING RESIN DOMINATED STRENGTH VALUES OF FIBRE REINFORCED COMPOSITES UNDER VARIOUS TYPES OF LOADING

by

Fatih Ertuğrul Öz

B.S., Manufacturing Engineering, Istanbul Technical University, 2008

Submitted to the Institute for Graduate Studies in
Science and Engineering in partial fulfillment of
the requirements for the degree of
Master of Science

Graduate Program in Mechanical Engineering
Boğaziçi University

2012

ACKNOWLEDGEMENTS

I would like to express my gratitude to my thesis advisor Assoc. Prof. Nuri Ersoy for his invaluable patience, guidance and helpfulness throughout my thesis process.

I would also like to acknowledge Prof. Fazıl Önder Sönmez and Assoc. Prof. E. Murat Sözer for their very important guidance and suggestions.

Additionally, I would like to thank my friends. Especially Kenan Çınar for his great helps during experiments and encouragments. Then, Murat Koç and Niyazi Tanlak for all their supports.

Finally, there are no words to describe my indebtness to my family for all their love and encouragement throughout my whole life.

ABSTRACT

MICROMECHANICAL PROGRESSIVE DAMAGE MODEL FOR PREDICTING RESIN DOMINATED STRENGTH VALUES OF A FIBRE REINFORCED COMPOSITE UNDER VARIOUS TYPES OF LOADING

In this study, a three-dimensional Representative Volume Element (RVE) with hexagonally packed array is used to predict the mechanical behaviour of a unidirectional carbon fibre reinforced epoxy under various types of loading. Firstly, elastic moduli, Poisson's ratios, coefficients of thermal expansion (CTE) and shear moduli of a unidirectional carbon fibre reinforced polymer (CFRP) are predicted using proper boundary conditions under various types of loading in ABAQUS Finite Element Software. Secondly, Manufacturer's Recommended Cure Cycle (MRCC) of AS4/8552 composite is modelled as a thermal loading process to calculate the micromechanical residual stresses developed during manufacturing. A user defined material subroutine (UMAT) is developed to model the incremental moduli as well as cure and thermal contraction of the resin as it cures. At the end of the cycle, it is observed that, most of the residual stresses are produced as a result of cooling from curing temperature to room temperature. Stress distributions in fibre-matrix interface at the end of the cycle are presented. Finally, progressive damage model is applied to assess the failure mechanisms of AS4/8552 under various types of loading. Maximum Principal Stress, Raghava's and Bauwen's modified von Misses failure criteria are applied with element stiffness reduction method. Resin-dominated strength values, cited in the manufacturer's data sheet like transverse tensile strength, transverse compression and in-plane shear strength are successfully predicted by using the strength and stiffness values of constituent materials provided by the manufacturer. At the end of the analysis, it is found that, damage initiation and its evolution are highly affected by loading type, loading direction and residual stresses.

ÖZET

KARBON ELYAF TAKVİYELİ BİR EPOKSİ KOMPOZİTİN ÇEŞİTLİ YÜKLEMELER ALTINDAKİ REÇİNE ETKİLİ DAYANIMLARININ ÖNGÖRÜLMESİ İÇİN GELİŞTİRİLEN MİKROMEKANİK İLERLEYİCİ HASAR MODELİ

Bu çalışmada, tek yönlü bir karbon elyaf takviyeli epoksi kompozitin çeşitli yüklemeler altındaki mekanik davranışı ve hasar ilerlemesi, altıgen şeklinde istiflenmiş bir 3 boyutlu Temsili Hacimsel Eleman (THE) kullanılarak öngörülmüştür. İlk olarak, tek yönlü bir karbon elyaf takviyeli epoksi kompozitin elastisite modülleri, Poison oranları, ısıl genleşme katsayıları ve kesme modülleri uygun sınır şartları kullanılarak çeşitli yüklemeler altında ABAQUS sonlu elemanlar programı kullanılarak öngörülmüştür. İkinci olarak, imalat sonucunda oluşan mikromekanik artık gerilmeleri hesaplamak için AS4/8552'ye ait, üreticinin tavsiye ettiği kür çevrimi modellenmiştir. Kullanıcı tarafından tanımlanmış bir alt program geliştirelerek reçinenin kür çevrimi boyuncaki elastisite modülleri, kür ve ısıl büzüşmeleri modellenmiştir. Kür çevriminin sonunda, artık gerilmelerin çoğunun kür sıcaklığından oda sıcaklığına soğuması neticesinde oluştuğu gözlemlenmiştir. Bu artık gerilmelerin elyaf-reçine arayüzlerindeki dağılımları sunulmuştur. Son olarak, AS4/8552'nin değişik yüklemeler altında işgörmezlik mekanizmalarını belirlemek için, ilerleyici hasar modeli uygulanmıştır. Yükleme sırasında Maksimum Asal Gerilme ile Raghava ve Bauwen'in değiştirilmiş vonMisses gerilme kıstasları, rijitlik düşürme yöntemi ile uygulanmıştır. Ürün kataloğunda belirtilen veya deneysel olarak bulunan elyaflara dik yöndeki çeki ve bası ile kısa kiriş kesme gibi reçinenin daha etkili olduğu dayanım değerleri, bu tezde geliştirilen mikromekanik ilerleyici hasar modeli ile başarılı bir şekilde öngörülmüştür. Analizler sonucunda, kompozit malzemelerin dayanımlarının ve kırılma biçimlerinin, yükleme çeşidi, yükleme yönü ve artık gerilmelerden önemli ölçüde etkilendiği gözlemlenmiştir.

TABLE OF CONTENTS

LIST OF FIGURES

LIST OF TABLES

LIST OF SYMBOLS

°C	Celsius
C_{ij}	Stiffness tensor
dc_{ij}	Creep strain increment
de_{ij}	Elastic strain increment
ds	Free shrinkage strain increment due to chemical shrinkage
du_i	Displacement change in direction i
dx	Length of the edge of the model parallel to x direction
dy	Length of the edge of the model parallel to y direction
dz	Length of the edge of the model parallel to z direction
$d\varepsilon_{ij}$	Total strain increment
E_i	Elastic modulus in direction i
G_{ij}	Shear modulus
I_1	First stress invariant
P_i	Concentrated force applied in direction i
S_{ij}	Compliance tensor
V_f	Fibre volume fraction
$\alpha(T)$	Temperature dependent coefficient of thermal expansion
α_i	Coefficient of thermal expansion in direction i
γ_{ij}	Shear strain component
δ_i	Applied displacement in direction i
ΔT	Temperature change

ε_i	Normal strain component in direction i
$\overline{\varepsilon_{ij}}$	Average strain
ε_{TH}	Thermal strain
σ_i	Stress component in direction i
σ_i^C	Compressive strength of composite in direction i
σ_i^T	Tensile strength of composite in direction i
$\sigma_{max,p}$	Maximum principal stress in resin
$\sigma_{min,p}$	Minimum principal stress in resin
$\overline{\sigma_{ij}}$	Average stress
σ_r^T	Tensile strength of resin
σ_{vm}	von Misses stress in resin
τ_{ij}^S	Shear strength of composite
τ_r^S	Shear strength of resin

LIST OF ACRONYMS/ABBREVIATIONS

2D	Two dimensional
3D	Three dimensional
CMC	Ceramic matrix composites
CP	Beginning of cooling stage
CTE	Coefficient of thermal expansion
DOC	Degree of cure
DSTRAN	Mechanical strain increments in user defined material subroutine of ABAQUS
DSTRESS	Stress increments in user defined material subroutine of ABAQUS
EXP	Experimental result
FEA	Finite Element Analysis
FEBM	Finite Element based micromechanics
FEM	Finite Element Method
FRC	Fibre reinforced composites
FRP	Fibre reinforced polymers
GIM	Group Interaction Modelling
GP	Gelation point
GPa	Giga Pascal
MMC	Metal matrix composites
MPa	Mega Pascal
MRCC	Manufacturer’s recommended cure cycle
MVM	Modified von Misses

PMC	Polymeric matrix composites
PS	Predicted strength of composite
RUC	Representative unit cell
RVE	Representative volume element
SCFM	Self-consistent field micromechanics
SOM	Strength of materials
SROM	Simple rule of mixture
UMAT	User defined material subroutine
USDFLD	User defined field subroutine
VP	Vitrification point
WWFE	World-wide failure exercise

1. INTRODUCTION

1.1. Composite Materials

There is a rapid growth in demand for stronger, stiffer and lighter materials in important engineering areas such as aerospace, transportation and construction. High requirements of this kind of materials have raised the interest in the field of composite materials. Composite materials are engineering materials which are evolved to have different and better properties than their constituents. One of the most important characteristics is their low density but high modulus which provides them with higher strength-to-weight ratios. Thus, these materials are more preferential in the engineering applications mentioned above than conventional materials. Besides, composite materials have become the leading research subject in materials and structural engineering areas.

There are various types of composite materials but the most important ones are ceramic matrix composites (CMC), metallic matrix composites (MMC) and polymeric matrix composites (PMC). In this thesis, attention is paid to the PMC. The choice of polymeric matrix can be thermoplastic or thermosetting.

Thermoplastics are resins which melt when heated. They are made-up of linear molecular chains, so they can be reformed with heat and pressure. They derive their strength from high concentration of molecular entanglements. They have anisotropic properties. Thermoplastic composites require high processing pressures, and hence expensive product tooling, as well as significant energy input in heating and cooling the tooling [1].

On the other hand in thermosetting polymers, the liquid resins are converted into hard brittle solids by chemical cross-linking which leads to the formation of a tight three-dimensional (3D) network of polymer chains. They are usually isotropic. Thermosetting polymers do not melt. They are not recyclable. However, thermoset composites are easier to process, requiring less energy and pressure than thermoplastics [1].

Fibres are used as reinforcement in polymeric composites. Fibre and resin are bonded together with an interface. The properties of a composite material are highly affected by the properties of its constituents and the interface. Fibres carry the majority of load and matrix is the binding material of the composite which supports and protects the fibres. These composites can be either called fibre reinforced composites (FRC) or fibre reinforced polymers (FRP). Best mechanical properties are obtained when the fibres are aligned continuously in the matrix. In industrial applications, generally carbon and glass fibres are preferred in polymeric composites. Glass fibres are generally isotropic while carbon fibres are transversely isotropic materials.

The mechanics of fibre-reinforced composites can be considered in macro and micro levels. A composite is considered as an orthotropic, linear elastic solid. In macro-level, the composite is considered as a homogeneous continuum. Damage and failure of composite structures are examined according to overall stress and strain of the structure. However, macromechanical approach does not enable to see the effects of constituents distinctly.

In micro-level, fibre, matrix and the interactions between them are examined particularly. In order to investigate these interactions, micromechanics approach is used. Micromechanics approach enables to predict the overall behaviour of composite in micro-level and shows the detailed effect of fibre and matrix on the mechanical behaviour of composite. Also damage and failure in composites can be modelled at the constituents' level [1].

There are many analytical micromechanics methods. Some of them are; Simple Rule of Mixture (SROM), Strength of Materials (SOM), Halpin-Tsai, Mori-Tanaka, Elasticity Approach and Hahn's Approach. There are also, numerical approaches for micromechanics. The most popular one is Finite Element Analysis (FEA). In finite element micromechanical analysis, the first step is to construct a representative volume element (RVE) that represents the whole composite. It should correspond to a periodic fiber-packing sequence. Frequently used arrangements are square and hexagonal packing arrays. Two dimensional (2D) sketchs of them are shown in Figure 1.1. Secondly, appropriate boundary conditions should be applied to RVE for different loading modes. The

periodicity of the model and symmetry of the deformation in the model can be obtained with correct boundary conditions only.

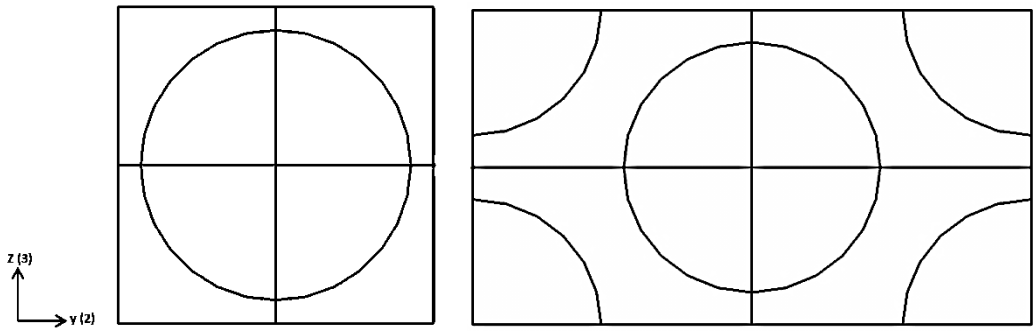

Figure 1.1. Square and hexagonally packed representative volume elements.

Finite element micromechanics approach enables to see the stress-strain distribution under different types of mechanical loading, and also allows to study thermal residual stresses arising from manufacturing process.

Generally, a high-temperature process is required for manufacturing of composite materials. This process is generally named as cure cycle. Basically, a cure cycle consists of three main steps. First of all, the material is heated up to a temperature. Polymer resin expands while heating. Secondly, isothermal curing process (polymerization) takes part at a constant elevated temperature. In this step, polymer shrinks as a result of chemical reaction (chemical shrinkage) and develops stiffness. Finally, the composite is cooled from cure temperature to room temperature. In the last step, fibre and matrix both contract.

1.2. Cure Cycle Process

Manufacturing of composites is a high-temperature process. This process is generally named as “Cure Cyle”. Cure cycle can be defined as a time period in which the temperature of the part follows a defined profile over time. A typical cure cycle consists of three main steps. These steps are, increasing the temperature to a set point at a specific rate, holding the temperature until the part cures to a reasonable extent and then cooling the part to room temperature. Generally an earlier dwell is applied when thermosetting composites are considered [2]. Figure 1.2 represents a typical cure cycle with two hold

temperatures. The first dwell is for the consolidation of the laminate and the second dwell is for the curing of the matrix.

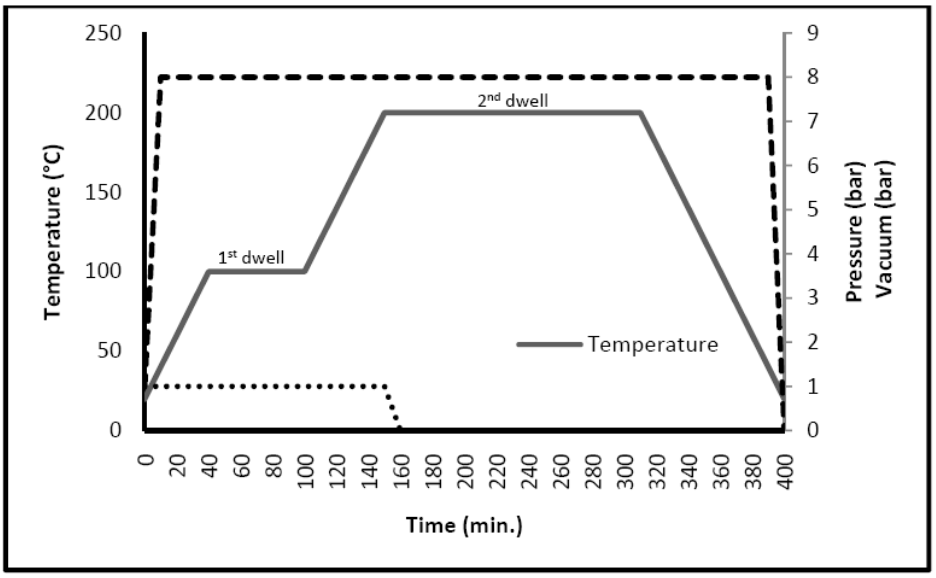

Figure 1.2. A typical cure cycle [2].

Curing is a complex series of chemical reactions that takes place in thermosetting composites. Sometimes it is named as polymerization or cross-linking. Initially a thermosetting resin is liquid at room temperature. When exposed to heat, curing reaction initiates. During the curing of a thermosetting resin, molecular chains forms a three-dimensional cross-linked network. This builds up the stiffness and strength of the material [2]. Development of degree of cure of AS4/8552 during cure cycle can be seen in Figure 1.3. Also, development of glass transition temperature is given in Figure 1.3. The gel point which is defined as the point where the prepreg is cured enough to sustain stress and the vitrification point is the point at which glass transition temperature reaches the process temperature are also indicated in Figure 1.3 [3].

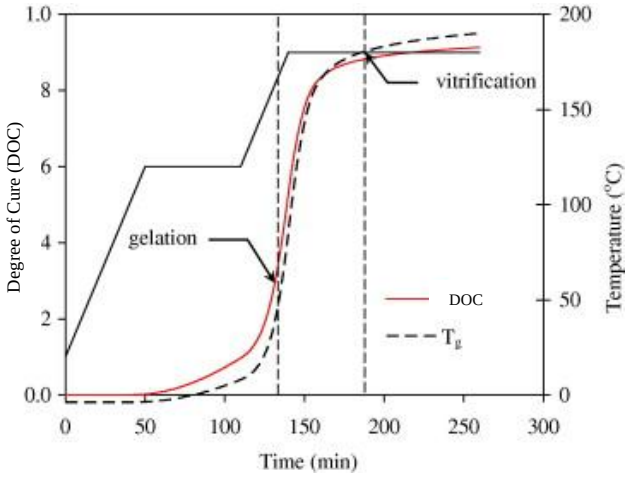

Figure 1.3. Development of degree of cure and the glass transition temperature of AS4/8552 through cure [3].

During polymerization of composite at an elevated temperature, polymeric resin shrinks. This is the chemical shrinkage of the resin. The contraction of polymeric resin is constrained by the fibres. While cooling to room temperature, both constituents contract but due to the different Coefficient of thermal expansion (CTE) of fibre and matrix, they do not contract the same amount. Coefficient of thermal expansion of polymeric resin is greater than the fibre. Full thermal shrinakge of resin is constrained by fibre, while the fibre contracts due to its own coefficient of thermal expansion and also, it is compressed by the constrained contraction of the resin. Significant part of the residual stress is generated during cooling step. This result in the development of residual stress inside the bulk resin, fibre and as well as the fibre/matrix interface. While tensile residual stresses are induced in the resin, compressive residual stresses are induced in the fibre after cooling down.

1.3. Mechanics of Composite Materials

A composite is considered as an orthotropic, linear elastic continuum. Actually, composites are transversely isotropic structures. An orthotropic material is the one which has different material properties in each orthogonal directions. Transversely Isotropic materials have the same material properties in one plane and different properties in its normal direction. Consider a unidirectional laminae as shown in Figure 1.4. Direction 1 is the fiber direction. This composite has same properties in (2-3 plane) but its properties are different in its normal direction (1).

Mechanics of composites are divided into two in this thesis. Macromechanics and micromechanics. They are described in details in further sections.

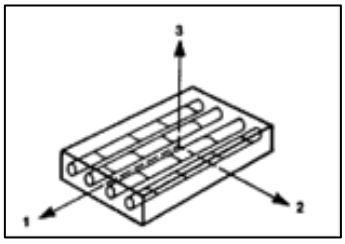

Figure 1.4. Coordinate system of a unidirectional laminae [4].

1.3.1. Macromechanics of Composite Materials

Figure 1.5. illustrates the stress state on an elastic body. Elastic stress and strain tensor components are $\sigma_1, \sigma_2, \sigma_3, \sigma_{12}, \sigma_{13}, \sigma_{23}$, $\varepsilon_1, \varepsilon_2, \varepsilon_3, \gamma_{12}, \gamma_{13}, \gamma_{23}$. Anisotropic stiffness and compliance matrices of composite are obtained by using these stress-strain components.

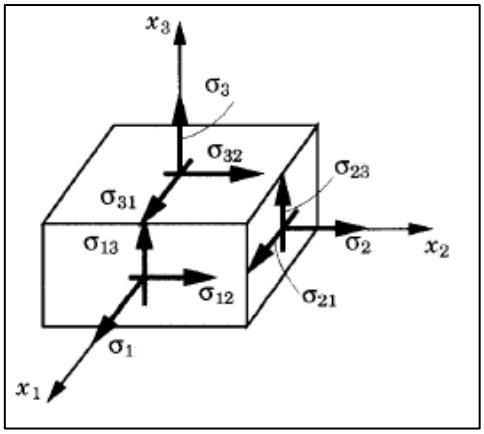

Figure 1.5. Stresses acting on an elastic body.

General equations for normal and shear strain components in terms of displacement are given in Equation 1.1 and 1.2 respectively. Poisson's ratio is defined in Equation 1.3.

$$\varepsilon_{ij} = \frac{1}{2}\left(\frac{\partial u_i}{\partial x_j} + \frac{\partial u_j}{\partial x_i}\right) \tag{1.1}$$

$$\gamma_{ij} = 2 \cdot \varepsilon_{ij} \tag{1.2}$$

$$\nu_{ij} = -\frac{\varepsilon_j}{\varepsilon_i} \tag{1.3}$$

A three dimensional (3D) rectangular unidirectional composite lamina is considered and the dimensions of this body are x_1, the length of the edge parallel to direction 1; x_2, the length of the edge parallel to direction 2; and x_3, height of the body. Deformation of the element under tensile and shear loading in various directions are shown in Figures 1.6-1.9. Stress-strain and strain-displacement relationships under different types of uniaxial loadings are derived in details in Equation 1.4 – 1.17.

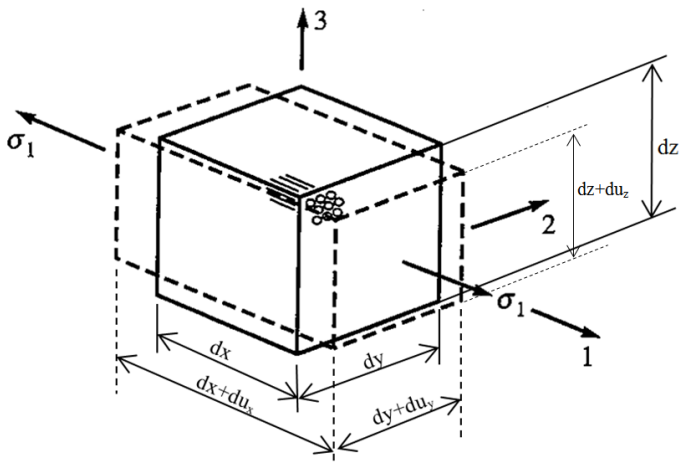

Figure 1.6. Deformation in fiber direction [5].

$$\varepsilon_1 = \frac{du_x}{dx} \tag{1.4}$$

$$\varepsilon_1 = \frac{\sigma_1}{E_1} \tag{1.5}$$

$$\nu_{12} = -\frac{\varepsilon_2}{\varepsilon_1} \tag{1.6}$$

$$\nu_{13} = -\frac{\varepsilon_3}{\varepsilon_1} \tag{1.7}$$

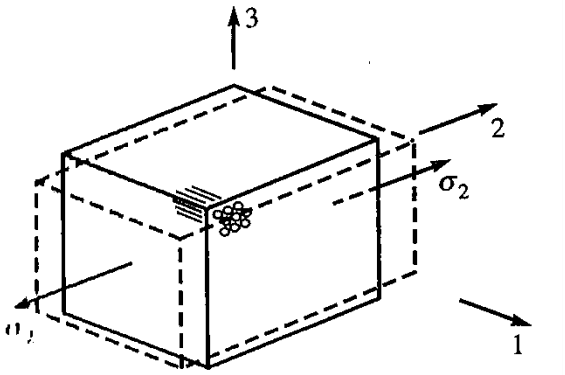

Figure 1.7. Deformation in transverse direction [5].

$$\varepsilon_2 = \frac{du_y}{dy} \tag{1.8}$$

$$\varepsilon_2 = \frac{\sigma_2}{E_2} \tag{1.9}$$

$$\nu_{21} = -\frac{\varepsilon_1}{\varepsilon_2} \tag{1.10}$$

$$\nu_{23} = -\frac{\varepsilon_3}{\varepsilon_2} \tag{1.11}$$

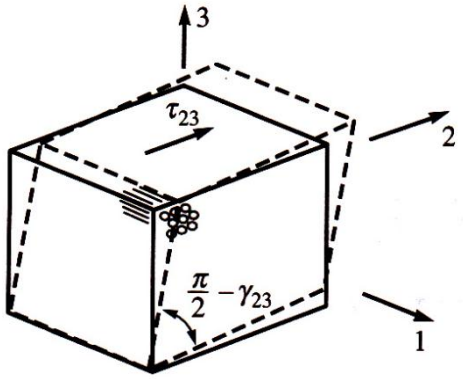

Figure 1.8. Deformation due to transverse shear [5].

$$\gamma_{23} = \frac{du_y}{dz} + \frac{du_z}{dy} \tag{1.12}$$

$$\gamma_{23} = \frac{\tau_{23}}{G_{23}} \tag{1.13}$$

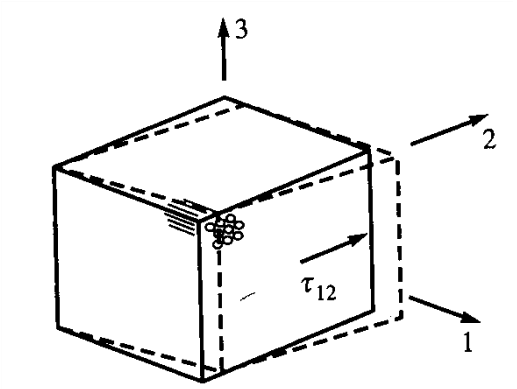

Figure 1.9. Deformation due to τ_{12} [5].

$$\gamma_{12} = \frac{du_x}{dy} + \frac{du_y}{dx} \tag{1.14}$$

$$\gamma_{12} = \frac{\tau_{12}}{G_{12}} \tag{1.15}$$

Aside from the deformation due to mechanical loading, a material can be deformed as a result of thermal loading when heated or cooled. When an isotropic material is heated or cooled, it expands or shrinks an amount proportional to its coefficient of thermal expansion (CTE) in each direction. Due to the anisotropic structure of composites, they generally expand or shrink with different amounts in each direction. Also, while a carbon fibre reinforced composite expands in two directions, it may shrink in the fibre direction due to negative CTE of carbon fibres in longitudinal direction as shown in Figure 1.10.

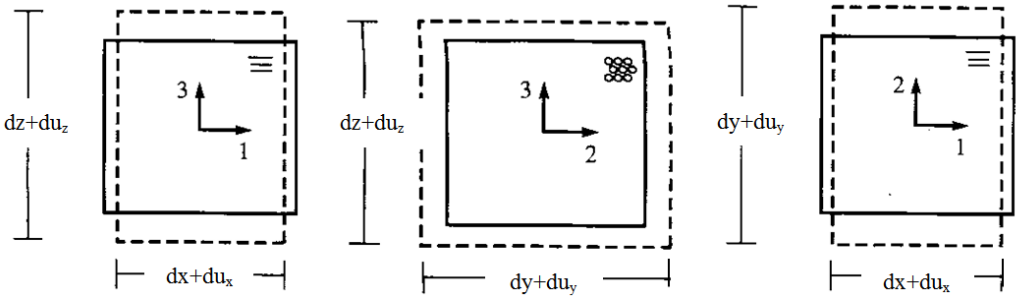

Figure 1.10. Deformation due to thermal loading [5].

The change in length in a particular direction due to thermal effect is given by Equation 1.16 where α_i is the CTE in that direction and the thermal strain is given in Equation 1.17.

$$dx_i = x_i \cdot \alpha_i \cdot \Delta T \tag{1.16}$$

$$\varepsilon_T = \frac{dx_i}{x_i} = \alpha_i \cdot \Delta T \tag{1.17}$$

Stress-strain relationship of composites with anisotropic compliance and stiffness matrices is as follows:

$$\sigma_i = C_{ij} \cdot \varepsilon_{ij} \tag{1.18}$$

C_{ij} is the stiffness matrix of the composite. The compliance matrix is the inverse of it. $\left(S_{ij} = {C_{ij}}^{-1}\right)$. Compliance matrix of a transversely isotropic material is presented below.

$$ {C_{ij}}^{-1} = S_{ij} = \begin{bmatrix} \frac{1}{E_1} & -\frac{\nu_{21}}{E_2} & -\frac{\nu_{21}}{E_2} & 0 & 0 & 0 \\ -\frac{\nu_{21}}{E_2} & \frac{1}{E_2} & -\frac{\nu_{23}}{E_2} & 0 & 0 & 0 \\ -\frac{\nu_{21}}{E_2} & -\frac{\nu_{23}}{E_2} & \frac{1}{E_2} & 0 & 0 & 0 \\ 0 & 0 & 0 & \frac{1}{G_{12}} & 0 & 0 \\ 0 & 0 & 0 & 0 & \frac{1}{G_{12}} & 0 \\ 0 & 0 & 0 & 0 & 0 & \frac{1}{G_{23}} \end{bmatrix} \tag{1.19}$$

There are five independent material constants for a transversely isotropic material. These are E_1, E_2, G_{12}, ν_{12} and ν_{23}. Because:

$$E_2 = E_3;\ G_{12} = G_{13};\ \frac{\nu_{21}}{E_2} = \frac{\nu_{12}}{E_1} \tag{1.20}$$

$$G_{23} = \frac{E_2}{(1 + \nu_{23})} \tag{1.21}$$

In order to fully characterize a composite's elastic behaviour, these constants should be either found experimentally or evaluated by micromechanics using the constituent properties.

1.3.2. Micromechanics

In macromechanical analysis, elastic constants of composite are required for the stiffness and compliance matrices. The most certain way to obtain these constants is experiment. However, experimental studies with composite structures require too much time and cost. Basically, different test setups and procedures are required to determine each elastic constant. Besides, it is not as easy as in isotropic materials. Therefore, elastic constants of a composite can be determined from its constituents' properties by micromechanics method. It is a solution for the situation when the mechanical properties cannot be determined experimentally.

Micromechanics is the analysis of a composite material to predict its overall mechanical behaviour by modelling the structure at the fibre and matrix level. Many questions about the failure of a composite arise at micro level. There are several analytical micromechanical methods. Some of them are; Simple Rule of Mixture (SROM), Advanced Strength of Materials (ASOM), Elasticity Approach, Hahn's Approach and Halpin-Tsai method. Details of analytical micromechanics approaches can be found in standard textbooks on composite materials, for example [4,5].

These calculations are very good for predicting a composite's mechanical constants. However they are not able to show the constituents' interactions with each other. In this regard, numerical micromechanics approaches are employed. The most important numerical micromechanics method is Finite Element Analysis.

In finite element micromechanical analysis, it is assumed that the fibres lie inside the matrix within the same cross-section and packed in a periodic array. Generally for fibre reinforced polymeric composites, square and hexagonally packed arrays are considered.

These arrays should represent the whole composite correctly. Therefore these elements are called Representative Volume Elements (RVE) or Representative Unit Cell (RUC). Thus, only one identical RVE is required to analyse the whole composite. Square and hexagonally packed RVEs are shown in Figure 1.11 and different types of hexagonally packed array are presented in Figure 1.12. Appropriate boundary conditions should be applied to RVE under different load modes. The periodicity and symmetry of the resulting deformation can be obtained with correct boundary conditions only. Generally, for simplicity of the solution and due to the symmetrical geometry, only ¼ of the elements are employed in published studies.

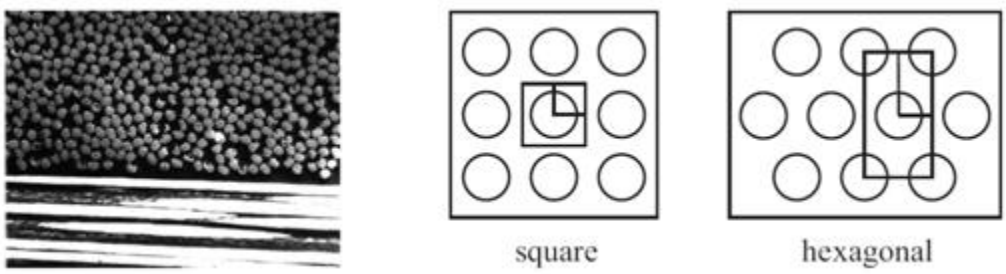

Figure 1.11. Square and hexagonally packed RVE [6].

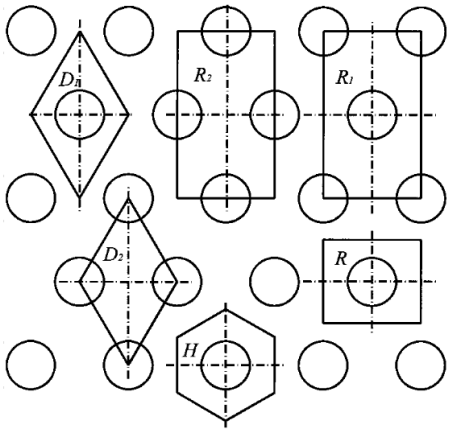

Figure 1.12. Different RVE for hexagonal packing [7].

Finite element micromechanics approach enables to see the stress-strain distribution after different types of loading. Additionally it allows the study of residual stresses arising from manufacturing process.

1.4. Damage and Failure in Polymeric Composites

Failure in a structural component can be defined as the inability of a component to carry load. Damage and failure mechanism of composite structures is a progressive series of events. Stiffness and strength of a composite can reduce due to damage accumulation such as matrix cracking or fibre breakage during loading [5]. Failure usually initiates as a tiny crack at the fibre-matrix interface in the matrix and the on-going loading evolves this crack and forms multiple cracks in the lamina. These cracks decrease the stiffness of composite and cause the surrounding lamina to carry stress over its capacity. Redistribution of stress indicates the damage path until global failure of composite.

1.4.1. Progressive Failure

A progressive failure theory can be described by degradation of a material's stiffness properties as damage accumulates until global failure. The aim of this theory is to predict the strength of a ply and response of a damaged ply. A progressive failure theory consists of three main elements. First element is a constitutive law to describe the stress-strain relationship of the material, second, a failure theory to identify damage and failure of the ply and finally, a degradation model to describe post-failure behaviour of the composite structure.

While modelling the progressive failure analysis of a composite, the first distinction of damage may not be associated with the ultimate strength of the structure. The failed material unloads and the load is redistributed to the undamaged material. Material property degradation proceeds through the structure according to the failure criterion until no additional load can be sustained [8].

Several analytical and numerical methods are developed to investigate the progressive failure of a composite. Finite elements method can be employed to composite structures in macro and micro levels. Macromechanical approach does not consider the distinctive modelling of constituents. However, micromechanical approach allows seeing the influence of constituents to the damage and failure of the overall composite.

Finite element micromechanical analysis enables to see the damage progression and stress re-distribution within the fibre, matrix and their interface during loading.

1.4.2. Failure Types

Logically, it is assumed that failure at a point begins when certain conditions are governed. Damage mechanism of a fiber-reinforced composite material is unique for various types of loading.

The formation of residual stress is generally detrimental in the production of polymer-matrix composite parts, since the stress can be sufficient enough to initiate damage before loading. Initial damage can reduce the stiffness and the strength of the material. Therefore, residual stress should be taken into account in order to study damage and fracture mechanics of polymeric composites. Initial damage due to residual stress can cause interface debonding and matrix micro-cracking as shown in Figure 1.13 [9].

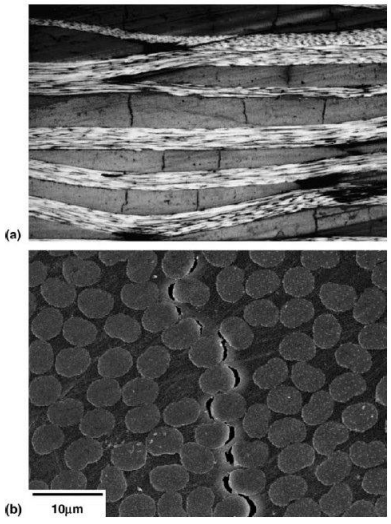

Figure 1.13. Micro-cracks in a woven graphite polymide a) tow micro-crack b) fibre/matrix debonding [9].

Generally mechanical loadings are the main reason of failure and different types of loading cause different types of failure in composites. When a composite is subjected to a tensile loading in fiber direction, global failure is due to fiber tensile fracture. Representation of this situation is shown in Figure 1.14. One fiber breaks and the load is

transferred to the neighbouring fibers through matrix. These fibers are overloaded, and with a small increase they fail. Failure propagates rapidly. When a compressive stress is applied in fiber direction, composite fails by fiber kinking or microbuckling as shown in Figure 1.15. The primary mechanism responsible for this behaviour is yielding or softening of the matrix as the stress within it increases to suppress fiber buckling [5].

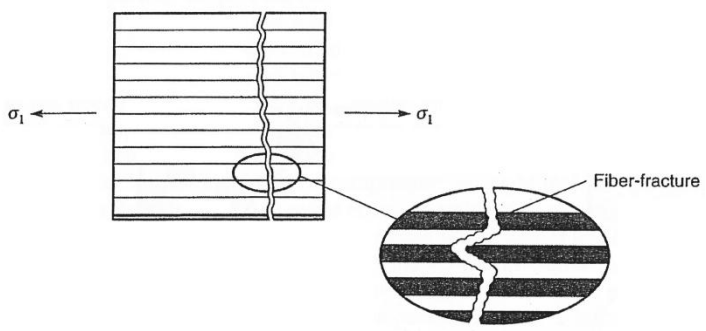

Figure 1.14. Failure under longitudinal tensile loading [5].

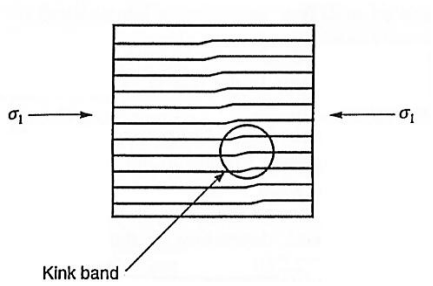

Figure 1.15. Failure under longitudinal compressive loading [5].

Generally a tensile failure perpendicular to the fiber is due to a combination of three possible micromechanical failures; tensile failure of matrix, tensile failure of fibre across its diameter and failure of the interface. Figure 1.16 represents this situation. Failure in compression perpendicular to the fibres as shown in Figure 1.17 is due to material crushing.

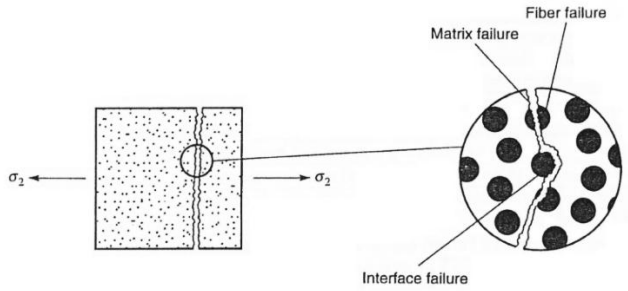

Figure 1.16. Failure under transverse tensile loading [5].

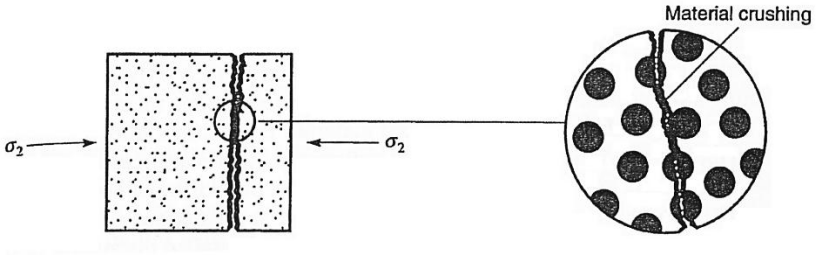

Figure 1.17. Failure under transverse compressive loading [5].

Shear stress in perpendicular direction to fibres causes matrix tensile failure across its diameter. In-plane shear strength of composite is limited by the shear strength of the matrix, fibre and the interfacial shear strength between fibre and matrix. Failure under shear loadings are presented in Figures 1.18 and 1.19 [5] respectively.

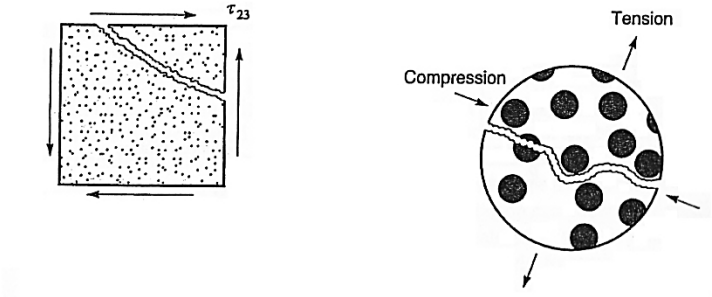

Figure 1.18. Failure under transverse shear loading [5].

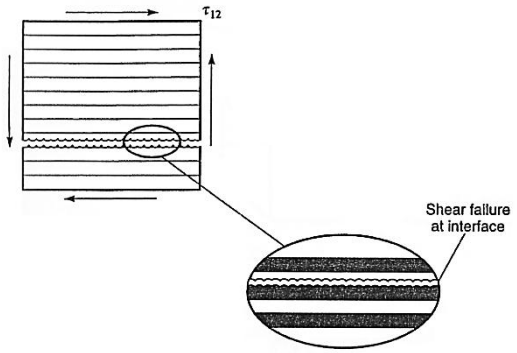

Figure 1.19. Failure under in-plane shear loading [5].

1.4.3. Failure Criteria of Composites

Failure in a ply has dissimilar mechanism depending on where damage initiates under various types of loading as mentioned before. Therefore appropriate failure criteria should be selected to predict where failure initiates.

There are many failure criteria to predict damage in composites. In macro level, mostly, Maximum Stress and Tsai-Wu failure criteria are used. Maximum Stress failure criterion is a non-interactive failure criterion but Tsai-Wu is an interactive theory and the influence of stress component interactions is observed [5].

According to maximum stress failure criterion, a fibre-reinforced composite does not fail under these circumstances:

$$\begin{aligned} {\sigma_1}^C < \sigma_1 < {\sigma_1}^T \\ {\sigma_2}^C < \sigma_2 < {\sigma_2}^T \\ |\tau_{12}| < {\tau_{12}}^S \end{aligned} \tag{1.22}$$

where σ_i is the normal stress in direction *i*, τ_{ij} is the shear stress in plane *i*, direction *j*, ${\sigma_i}^T$ is the tensile strength of composite in direction *i*, ${\sigma_i}^C$ is the compressive strength of composite in direction *i* and ${\tau_{ij}}^S$ is the shear strength of composite

Here 1 refers to fibre direction and 2 refers to transverse direction of the composite.

Tsai-Wu is an interactive second-order failure criterion. It investigates the interactions between instantaneous stresses during loading and the strength of composite. Since composites are transversely isotropic materials, their strength is different in each direction and under different load modes. Tsai-Wu failure criterion can be expressed mathematically as:

$$F_1\sigma_1 + F_2\sigma_2 + F_{11}{\sigma_1}^2 + F_{22}{\sigma_2}^2 + F_{66}{\tau_{12}}^2 - \sqrt{F_{11}F_{22}}\sigma_1\sigma_2 = 1 \tag{1.23}$$

in which

$$F_1 = \left(\frac{1}{{\sigma_1}^T} + \frac{1}{{\sigma_1}^C}\right)$$

$$F_2 = \left(\frac{1}{{\sigma_2}^T} + \frac{1}{{\sigma_2}^C}\right)$$

$$F_{11} = -\frac{1}{{\sigma_1}^T{\sigma_1}^C} \tag{1.24}$$

$$F_{22} = -\frac{1}{{\sigma_2}^T{\sigma_2}^C}$$

$$F_6 = \left(\frac{1}{{\tau_{12}}^S}\right)^2$$

In micro-level, different failure criteria can be applied to fiber, matrix and even their interface. For this purpose, several criteria can be applied to constituents. Within the scope of this thesis, only resin dominated failures are interested. Resin dominated failure modes for composite materials can be seen in Figure 1.20 [6]. So, only failure criteria applied to polymeric materials are explained below.

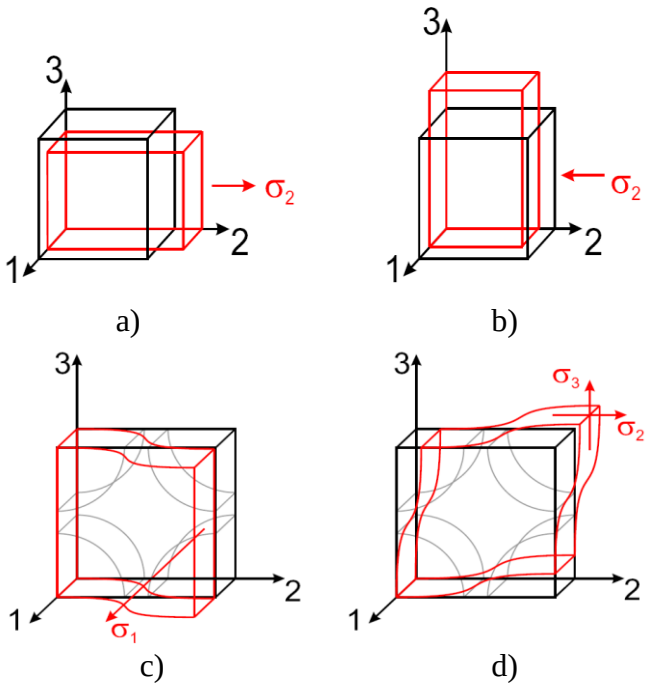

Figure 1.20. Resin dominated failure modes a)Transverse tension b) Transverse compression c) Longitudinal shear d) Transverse shear loading [6].

Maximum Principal Stress and von Misses Stress criteria can be applied to the polymeric resin. Equation for Maximum Principal Stress and von Misses stress criteria are given in Equation 1.25 and 1.26 respectively. In Equation 1.26, subscripts represent the direction of stresses in resin.

$$|\sigma_{maxP}| < {\sigma_r}^T \qquad\qquad |\sigma_{minP}| < {\sigma_r}^C \tag{1.25}$$

$$\sigma_{vm} = \sqrt{\frac{1}{2}[(\sigma_1 - \sigma_2)^2 + (\sigma_1 - \sigma_3)^2 + (\sigma_2 - \sigma_3)^2 + 6({\tau_{12}}^2 + {\tau_{13}}^2 + {\tau_{23}}^2)]} \tag{1.26}$$

in which σ_{maxP} is the maximum principal stress in resin, σ_{minP} is the minimum principal stress in resin, σ_{vm} is von Misses stress in resin, ${\sigma_r}^T$ is the tensile strength of resin and ${\sigma_r}^C$ is the compressive strength of resin.

In particular, although the polymeric resins are isotropic, their yield behaviour is dependent to the hydrostatic pressure and as a consequence, in reality the yield stress in tension is different from compression. Some authors [10,11] found that failure of

composites do not only depend on deviatoric stress invariant, it also depend on volumetric stress invariant such as the first stress invariant (I_1). So, they modified the von Misses (MVM) stress criterion for polymeric resins.

Raghava *et al.* suggested a modified version of the von Mises criterion [10] which is named as Raghava's modified von Misses (MVM) failure criterion as given in Equation 1.27.

$$\frac{{\sigma_{VM}}^2}{{\sigma_r}^C \cdot {\sigma_r}^T} + \left(\frac{1}{{\sigma_r}^T} - \frac{1}{{\sigma_r}^C}\right) I_1 = 1 \tag{1.27}$$

Bauwens developed another version of modified von Mises (MVM) criterion [11] with the name Bauwens' MVM failure criterion as defined in Equation 1.28.

$$\frac{1}{2}\left(\frac{1}{{\sigma_r}^T} - \frac{1}{{\sigma_r}^C}\right)\sigma_{VM} + \frac{1}{2}\left(\frac{1}{{\sigma_r}^T} - \frac{1}{{\sigma_r}^C}\right) I_1 = 1 \tag{1.28}$$

in which I_1 is the first stress invariant $(\sigma_1 + \sigma_2 + \sigma_3)$

Failure criterion proposed by Tresca indicates that failure occurs when the maximum shear stress induced in the resin reaches the critical value as mentioned in Equation 1.29.

$$\frac{1}{2}\left|\sigma_i - \sigma_j\right| = {\tau_r}^S \tag{1.29}$$

where ${\tau_r}^S$ is the shear strength of resin

The selection of proper failure criterion for resin plays a very important role for prediction of damage initiation and progressive failure response of composites under different types of loading. Micromechanical finite element analysis is an elaborate solution method for this purpose.

1.5. Literature Review

There are extensive amount of literature about the macromechanical behaviour of composite materials. This thesis is based on micromechanical approach to predict the resin dominated failure modes of fibre reinforced polymeric materials. Therefore the literature review is focused on the micromechanical studies of polymeric composite materials.

Adams and Crane [12] modelled the micro structure of a composite with plane strain assumption by using finite elements micromechanical method. They used 2D square packed quarter RVE. They investigated the stress distribution under tensile and axial shear loadings. Material properties of resin are assumed as temperature and moisture dependent. They obtained a good correlation with available experimental results.

King *et al*. [13] developed a finite element micromechanical model to predict the shear strength of composites. They examined different fiber reinforced polymeric composite materials with a 2D square-packed representative unit cell (RUC). The effects of matrix properties, interfacial bond strength and fibre volume fraction on the longitudinal shear strength of composites was investigated. Material properties of resin were assumed to be temperature-dependent. Fibre/Matrix interfacial bond strength was adjusted in the micromechanics analysis until the predicted composite shear strength matches with experimental value. Crack initiation and propagation schemes are presented in Figure 1.21.

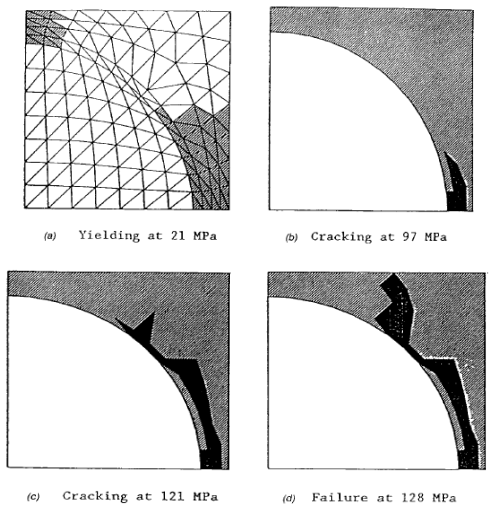

Figure 1.21 Crack initiation and propagation of Tonen HM/Hercules 3501-6 under longitudinal shear loading [13].

Nedele and Wisnom [14] examined the simultaneous thermal and shear loading of a unidirectional composite with finite elements micromechanical analysis. Three-dimensional quarter square packed Representative Unit Cell (RUC) was used in their study. They investigated the effect of different parameters on the axial shear modulus. Akzo HTA carbon fibre and Ciba-Geigy F922 epoxy matrix were used as constituents. They found that the shear moduli of the constituents, especially resin, have important effect on the shear moduli of the composite but the maximum shear stress in the matrix is not affected as much as the moduli. Fibre volume fraction has important influence on the shear moduli of composite and also the maximum shear stress in it. By including the non-linear behaviour of matrix, the shear stress-strain behaviour of the composite was plotted and it showed a very good correlation with experimental data. At the end of the study, it was mentioned that appropriate failure criteria should be developed to predict failure modes of the composite.

Sun and Vaidya [15] predicted the properties of a composite with finite element micromechanics approach. They used 3D square and hexagonal quarter representative unit cells (RUC) to predict elastic moduli. Transverse shear modulus (G_{23}) was obtained by a 2D square-packed whole representative volume element (RVE) under pure shear loading. Finally, longitudinal shear modulus (G_{12}) was predicted with a 3D whole square-packed RVE. Representative volume elements used by Sun and Vaidya are presented in Figures 1.22 and 1.23.

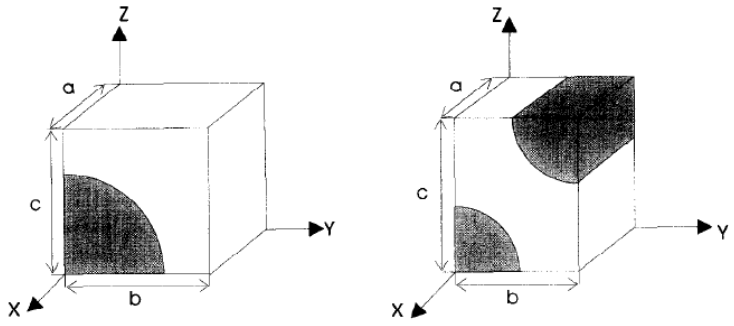

Figure 1.22. ¼ RVE of square and hexagonal-packed arrays [15].

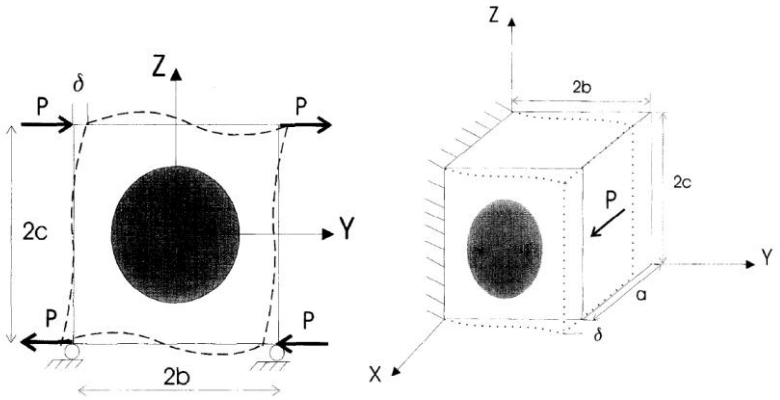

Figure 1.23. 2-D and 3-D whole square-packed representative volume elements under transverse pure and longitudinal shear loadings respectively [15].

The average stress was calculated by using the strain energy equivalence principle to relate the energy stored in the RVE to the external work done on it. The relevant composite modulus was obtained by dividing the average stress to the average strain. For example, enery equivalence and elastic modulus in fibre direction of the models shown in Figure 1.22 are given in Equation 1.30 and 1.31 respectively.

$$\frac{1}{2}P_1\delta_1 = \frac{1}{2}\bar{\sigma}_{11}\bar{\varepsilon}_{11}V \tag{1.30}$$

where P_1 is the concentrated force applied on front surface of the RUC in Figure 1.22, δ_1 is the displacement of front surface which is constant for all nodes on that surface, $\bar{\sigma}_{11}$ is the average normal stress which is $\bar{\sigma}_{11} = \frac{P_1}{bc}$ and $\bar{\varepsilon}_{11}$ is the average normal strain which is $\bar{\varepsilon}_{11} = \frac{\delta_1}{a}$

$$E_{11} = \frac{\bar{\sigma}_{11}}{\bar{\varepsilon}_{11}} = \frac{P_1 a}{bc\delta_1} \tag{1.31}$$

This procedure was applied for other types of loading. Comparison of their results with a micromechanical [16] and an experimental study [17] is shown in Table 1.1.

Table 1.1. Comparison of results Elastic Moduli of AS4/3501-6 (V_f=60%) [15].

Elastic Constants	FEM Square-Array [15]	FEM Hexagonal-Array [15]	Micromechanical [16]	Experimental [17]
E_1 [GPa]	142.6	142.6	142.9	142
E_2 [GPa]	9.6	9.2	9.79	10.3
G_{12} [GPa]	6	5.88	6.53	7.6
G_{23} [GPa]	3.1	3.35	3.01	3.8
ν_{12}	0.25	0.25	0.26	-
ν_{23}	0.35	0.38	0.42	-

Chen, Xia and Ellyin [18] investigated the effect of viscoelasticity of matrix on the evolution of residual stress, due to cooling from cure temperature (149 °C) to room temperature (20 °C), in a unidirectional and cross-ply 3M Scotch type 1003 continous E-glass fibre/epoxy composite by finite elements method. They used square packed RVE and tested temperature-independent elastic and viscoelastic matrix materials. Material properties at room temperature are used. Also, effect of different cooling rates on the residual stress was studied. It was found that higher cooling rates results with higher residual stresses in resin and elastic resin accumulates higher residual stress than visco-elastic composite at the end of the cooling process in composite as seen in Figures 1.24 and 1.25. Relaxation of residual stress with time was presented and it became independent of cooling rate at the end. As it is seen in Figure 1.25, composite with elastic resin matrix does not relax.

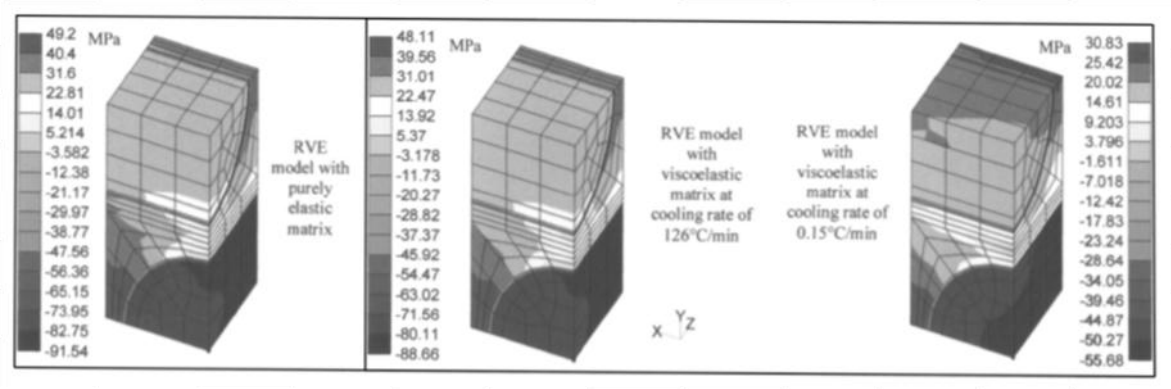

Figure 1.24. Residual stress distribution in longitudinal direction (σ_{zz}) for cross-ply laminate with two different cooling rates and two different matrix materials [18].

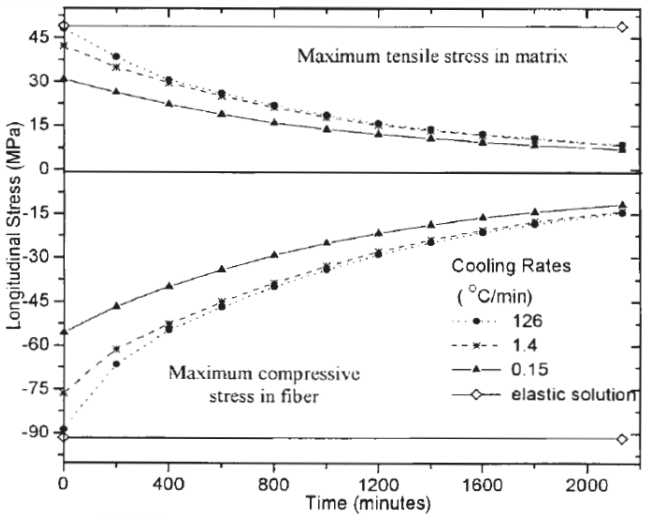

Figure 1.25. Residual stress relaxation in cross-ply model for different cooling rates [18].

Zhang improved the same study with Xia and Ellyin [19] to investigate the response of the same material (3M Scotch type 1003 continous E-glass fibre/epoxy composite) for subsequent mechanical loading. The resin is modelled as non-linear, viscoelastic and temperature-dependent material. Evolution of damage under subsequent tensile loading with and without residual stresses was observed. Maximum principal strain criterion was used for damage assessment. Resulting damage initiation and its evolution with respect to maximum principal strain criterion can be seen in Figure 1.26. Damage initiates at fibre-matrix interface, then spreads along the interface and through the thickness of the RVE with residual stress, however, without the effect of residual stress, damage initiates in bulk resin and progresses through the thickness and depth of the RVE as seen in Figure 1.26.

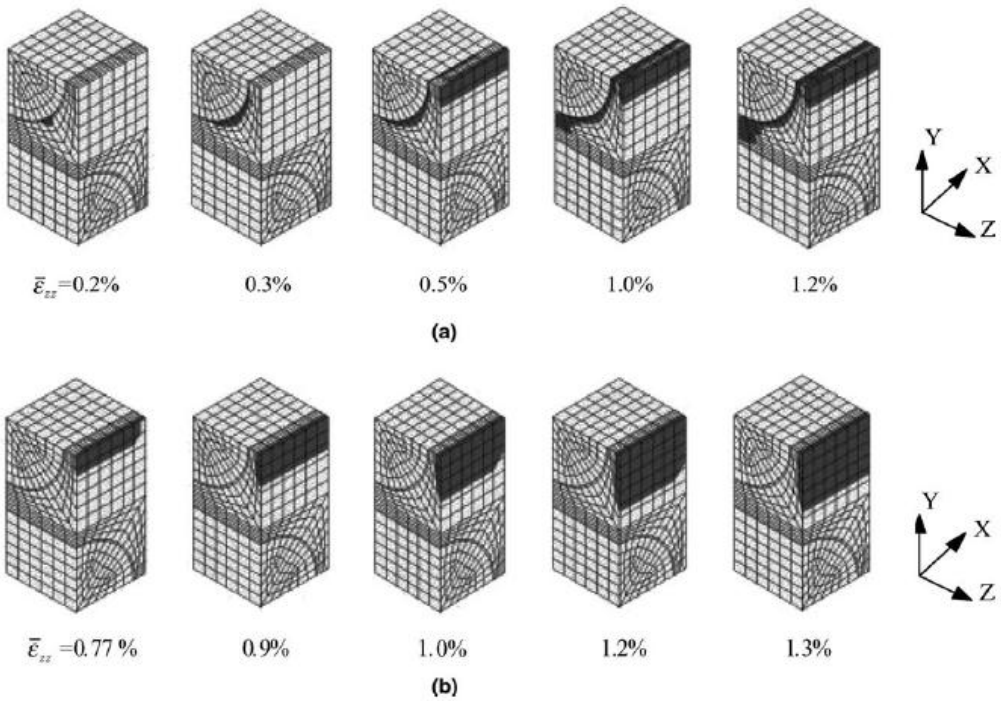

Figure 1.26. Damage evolution (a) with residual stress/strain and (b) without residual stress/strain under transverse tensile loading [19].

Further investigation with the same material properties in [18,19] was carried out by Zhao, Warrior and Long [20]. Effect of residual stress on transverse failure was investigated. Material properties of resin were assumed as elastic and temperature-dependent. Square-packed representative volume elements were selected. While a quarter RVE was used for subsequent transverse tensile loading, a whole RVE was preferred for transverse shear loading. Maximum Principal Stress criterion with element stiffness degradation technique was used for failure prediction. Also, effect of curing temperature and different resin strength were observed. It was found that damage pattern is highly affected with the presence of residual stress and loading mode as can be seen in Figures 1.27 and 1.28. Beneficial consequences of residual stress for transverse tensile loading and detrimental consequences for transverse shear loading were proven for this material and this is presented in Figure 1.29.

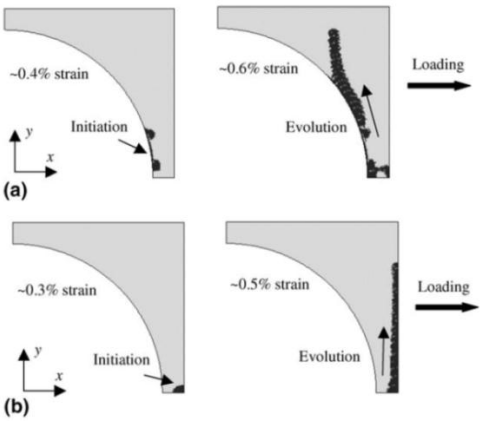

Figure 1.27. Damage initiation and evolution under uniaxial transverse tensile loading a) with residual stress b) without residual stress [20].

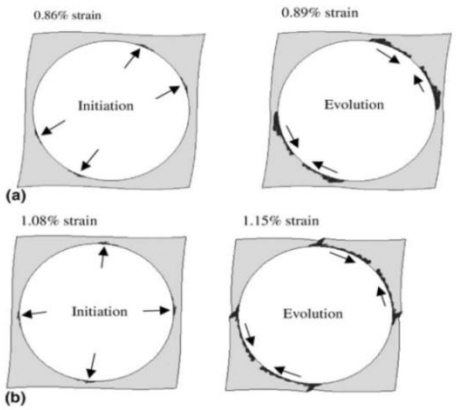

Figure 1.28. Damage initiation and evolution under transverse pure shear loading (a) with residual stress (b) without residual stress [20].

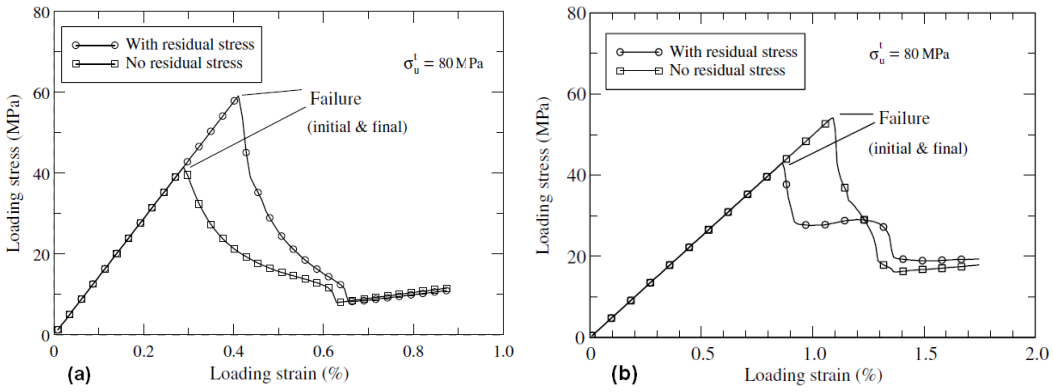

Figure 1.29. Global stress-strain curve under (a) transverse tensile (b) transverse pure shear loading [20].

Same authors [21] studied the effect of residual stress on 3M Scotch type 1003 continous E-glass fibre/epoxy composite for longitudinal shear, longitudinal and transverse normal loadings. Resin properties were modelled as viscoelastic. In this study, cure cycle was modelled with two steps. Curing at 150 °C and cooling to room temperature. At the end of the cure-cycle, residual stresses relaxed to a lower value. Same RVEs in [20] and additionally a hexagonally packed RVE, shown in Figure 1.30, were used to see the effect of fibre packing geometry. Also, influence of fibre volume fraction was investigated. Response of composite under uniaxial and biaxial transverse normal and longitudinal shear loading was presented. Maximum Principal Stress failure criterion was preferred for failure prediction. As found in [20], it was seen again that the presence of residual stress highly effects the initiation and evolution of damage as shown in Figure 1.31. Also, different fibre volume fractions and fibre packing geometries had different effects on damage progression.

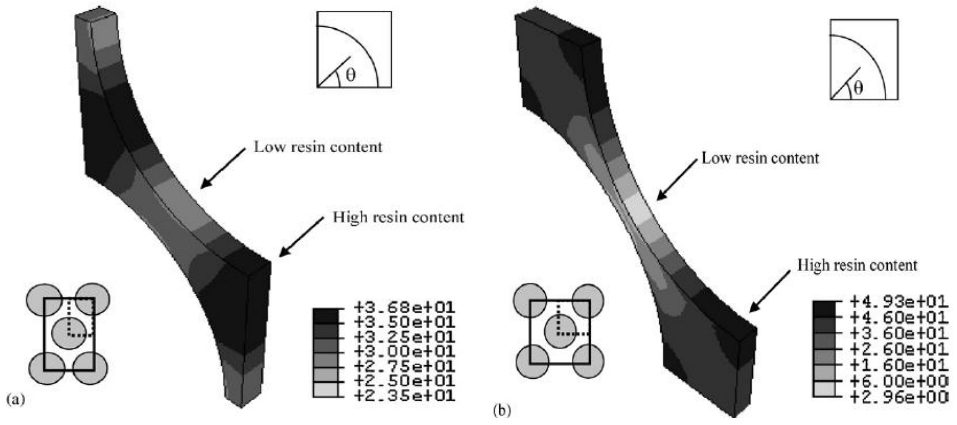

Figure 1.30. Maximum principal residual stress (MPa) distribution within the matrix (V_f=60%) for (a) hexagonal packing (b) square-diagonal packing [21].

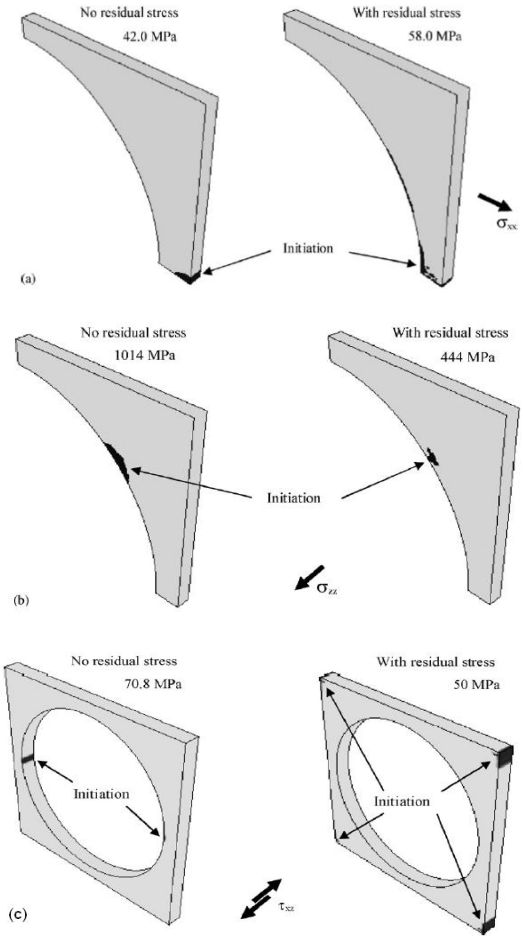

Figure 1.31. Effect of residual stress on damage initiation for (a) transverse tensile (b) longitudinal tensile (c) longitudinal shear loadings [21].

Maligno developed Zhao et. al's study with hexagonally packed RVEs in his PhD thesis [22]. In the first part of his thesis, moduli of an E-Glass fiber/epoxy matrix for different fiber volume fractions were obtained. The commercial name of the material was not mentioned in the thesis. Elastic modulus and the Poisson's ratio of the fibre are 76 GPa and 0.2 respectively and the resin has an elastic modulus of 4 GPa and Possion's ratio of 0.35. He compared the predicted results with some other micromechanical methods such as "Rule of Mixtures" and "Halpin-Tsai". In the second part, curing residual stresses induced in E-Glass/MY750/HY917/DY063-epoxy composite was investigated. Maximum principal stress distribution at the end of the cure-cycle is shown in Figure 1.32. Maximum principal stress occurred in resin was found around 26 MPa for a composite which has a fibre volume fraction of 60%. Afterwards, initiation and evolution of failure under subsequent loading was examined with respect to maximum principal stress and Raghava's modified

von Misses failure criteria. Damage assessment was investigated with and without the effect of residual stress. However, the subsequent loadings were limited to uniaxial normal loadings only. In further parts of the thesis, effect of interphase material and fibre packing geometry for hexagonally packed RUC on the damage mechanism was investigated.

It should be stated that, the analysis in References [20-22] are carried out by ABAQUS. Residual stress and failure predictions were modelled with user-defined subroutine UMAT [23]. Maligno found that not only residual stress affects the damage initiation and evolution but also loading direction, fibre volume fraction and failure criterion have considerable effects on damage and strength predictions of E-Glass/LY556/HT907/DY063 epoxy composite as seen in Figure 1.33 and 1.34.

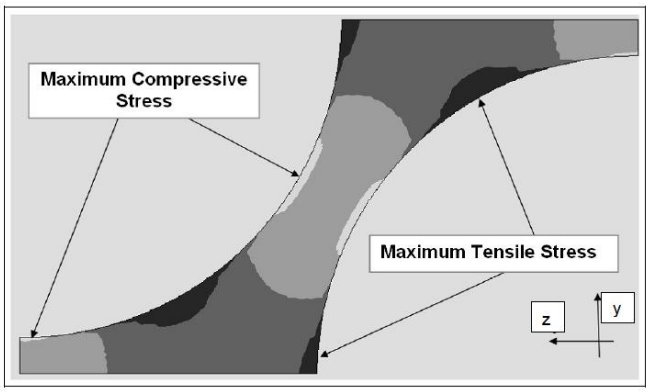

Figure 1.32. Distribution of residual stress in matrix after curing and cool-down [22].

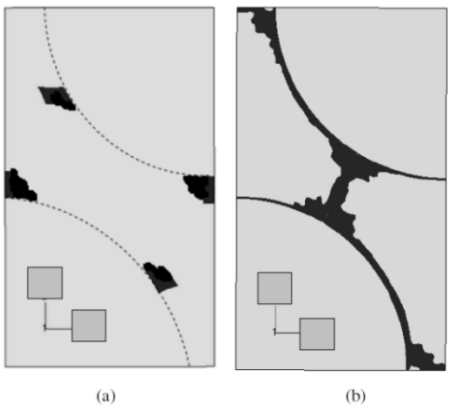

Figure 1.33. Comparison of damage onset prediction (V_f=60%) with residual stress (a) Maximum Principal Stress criterion (b) Raghava failure criterion [22].

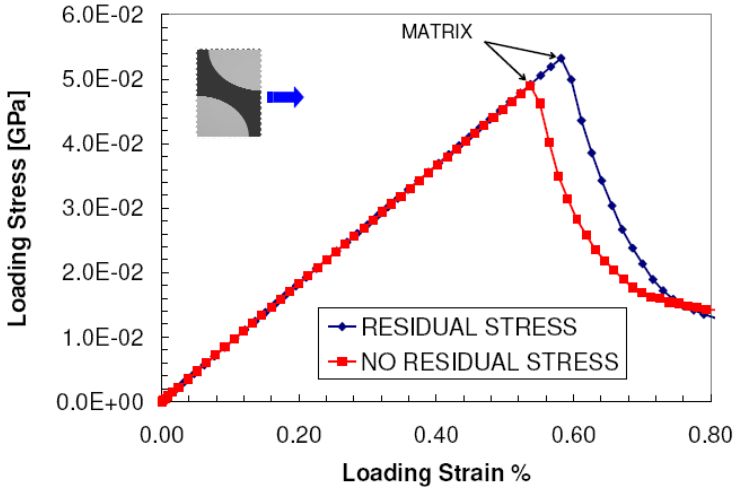

Figure 1.34. Global stress-strain curve under transverse tensile loading (V_f=60%) in direction-y direction [22].

In studies [17-22], when the material was defined as elastic, total induced incremental strain in resin due to chemical shrinkage and thermal cooling was expressed as given in Equation 1.32 and the incremental stress is defined in Equation 1.33.

$$d\varepsilon_{ij} = de_{ij} + \delta_{ij} ds + \delta_{ij} \alpha(T) \Delta T \tag{1.32}$$

$$d\sigma_{ij} = C_{ijkl} de_{kl} = C_{ijkl} \{ d\varepsilon_{ij} - \delta_{ij} ds - \delta_{ij} \alpha(T) \Delta T \} \tag{1.33}$$

in which $d\sigma_{ij}$ is the total stress increment, $d\varepsilon_{ij}$ is the total strain increment, de_{ij} is the elastic strain increment, ds is the free shrinkage strain increment due to chemical reaction, α(T) is the temperature dependent the coefficient of thermal expansion (CTE) and ΔT is the temperature change.

Ernst *et al.* [6] carried out a multi-scale failure analysis for a textile composite. Moduli of composite were predicted by finite element micromechanics method with square and hexagonally packed RVEs. Resin was modelled as an elasto-plastic material. Table 1.2 shows the comparison of moduli and strength values obtained in this study with experimentally measured values. The experimental and predicted moduli and strength values are very close to each other, showing the success of the finite element micromechanics approach. Afterwards, progressive damage model was applied. Effect of residual stress was not included in Ernst's study. Mesh dependency of the micromechanics

model is shown in Figure 1.35. Eventually, three-point bending test was applied in macro-scale. It was mentioned at the end of the study that, the algorithm developed within this study can replace experimental methods.

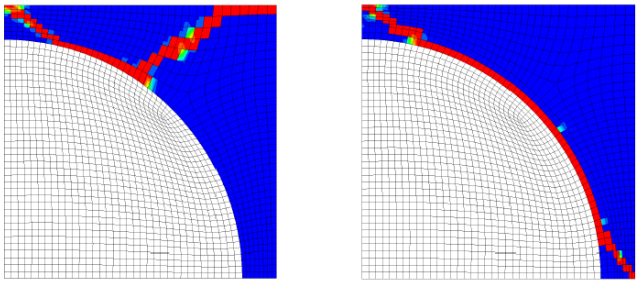

Figure 1.35. Mesh dependency on damage evolution under transverse compression [6].

Table 1.2. Mechanical properties of Silenka E-Glass/MY750/HY917/DY063-epoxy [6].

Properties	**Unit**	**WWFE (Experimental)**	**Unit cell [6]**	
			Hex.	**Square**
Longitudinal modulus (E_1)	GPa	45.6	45.7	45.7
Longitudinal tensile strength (${\sigma_1}^T$)	MPa	1280	1308	1308
Longitudinal tensile failure strain (${\varepsilon_1}^T$)	%	2.807	2.905	2.905
Longitudinal compressive strength (${\sigma_1}^C$)	MPa	800.	870.	870.
Longitudinal compressive failure strain (${\varepsilon_1}^C$)	%	1.75	1.96	1.96
Transverse modulus (E_2)	GPa	16.2	11.89	15.06
Transverse compressive strength (${\sigma_2}^C$)	MPa	145	118.5	149.5
Transverse compressive failure strain (${\varepsilon_2}^C$)	%	1.2	1.07	1.05
Transverse tensile strength (${\sigma_2}^T$)	MPa	45	41.7	38.3
Transverse tensile failure strain (${\varepsilon_2}^T$)	%	0.25	0.39	0.3
In-plane shear modulus (G_{12})	GPa	5.83	4.27	4.66
In-plane Poisson's ratio (ν_{12})		0.278	0.25	0.25
In-plane shear strength (${\tau_{12}}^S$)	MPa	73	56.0	51.7
In-plane shear failure strain (${\gamma_{12}}^S$)	%	4	2.98	3.42
Transverse shear modulus (G_{23})	GPa	–	4.11	3.3
Transverse Isotropy	GPa	5.79	4.25	5.97
Transverse Poisson's ratio (ν_{23})		0.4	0.4	0.262
Transverse shear strength (${\tau_{23}}^S$)	MPa	–	44.47	51.04
Transverse shear failure strain (${\gamma_{23}}^S$)	%	–	1.49	3.17

Ersoy et. al. [3] calculated the physical and mechanical properties of AS4/8552 through cure by using finite element micromechanics approach. Development of elastic modulus of resin was based on Group Interaction Modelling (GIM). In addition to this,

moduli of composite were calculated by an analytical approach which is named as self-consistent field micromechanics (SCFM) and finite element based micromechanics method (FEBM) for the glassy and rubbery properties of resin. A hexagonally packed RVE was considered for FEBM. Deformations under transverse tensile and in-plane shear loading are represented in Figure 1.36a and 1.36b respectively. Calculated moduli were compared to experimental values.

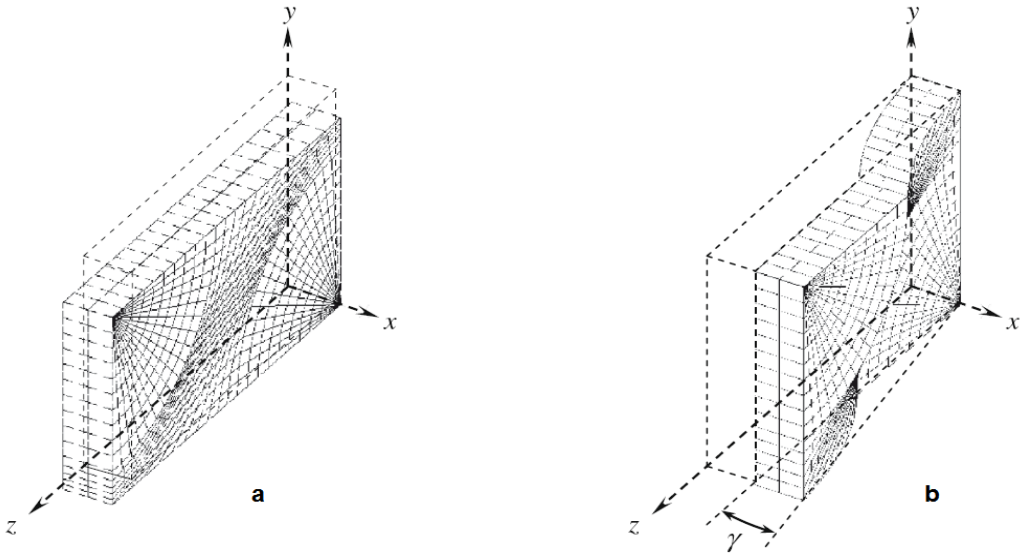

Figure 1.36. Resulting deformation of the hexagonally packed RVE under (a) transverse tensile (b) longitudinal shear loading [3].

Soden, Hinton and Kaddour, as WWFE (World wide failure exercise) [24] published the full details of experimental properties of four different composite material including the elastic constants and strengths of constituents, as well as the elastic constants, strengths and stress-strain curves of the composites. That paper has been very important for engineers and scientists who work with those materials. It is an asset to compare numeric or even experimental results. This paper is highly benefited in this study as a benchmark.

1.6. Problem Statement

Finite element micromechanical analysis is a solution for the situations where experiments are hard to do. Therefore, there is a great interest to implement this method. However, there are still some uncertainty in micromechanical analysis of composite structures.

First of all, the cure cycle process has not been fully represented by numerical analysis. Generally cooling stage has been considered only, and the residual stresses developed due to cure shrinkage are ignored. Secondly, much attention has been paid on glass/fibre composites and there is restricted amount of study on carbon fibre composites. Thirdly, few damage criteria have been investigated and there is no extensive comparison of damage criteria suitable for resin systems used in composites. Finally, all loading modes for a single material have not been fully analysed.

Moreover, the material used in this thesis is AS4/8552. In literature, one can find some properties of the composite or its constituents from a few sources [3, 24 and 25]. However, moduli or strength values in these studies do not match with each other. There are big differences in some properties between each study. Also, compression strength of neat resin has not been given in literature yet.

This study is a further improvement of Ersoy's study [3]. Its main goal is to develop a micromechanical model by using a commercial finite element package program (ABAQUS/Standard) to predict mechanical properties of a carbon-fibre-reinforced thermosetting composite and assess the damage initiation and evolution under resin dominated load types, such as, transverse tensile, transverse compression, in-plane shear and transverse shear loading, with and without the effect of thermal residual stress. Different failure criteria, such as, Maximum Principal, von Misses, Tresca and Raghava's and Bauwen's modified von Misses failure criteria are applied and compared to each other and as well as to experimental results.

In real life, the bond strength between the fibre and matrix are different than resin but it is very difficult to measure the interface strength even though some test methods are developed. The details of these methods can be found in [1]. However, in this thesis, the effect of different interfacial stiffness and strength are not taken into account. Its properties are assumed to be equal to resin.

The synopsis of this thesis as follows.

Firstly, elastic properties of a carbon-fibre reinforced composite are calculated and a comparison is presented for the verification of the model and approach. The material is

selected from Hyer's textbook [5] because all the material property data are available. It is a good case study for verification of the model and approach.

Secondly, elastic properties of AS4/8552 are obtained and compared with Ersoy's study [3] and experimental results [26]. Very good correlation is obtained with the results.

Thirdly, MRCC of AS4/8552 is modelled to investigate the process induced residual stress in resin and fibre. Non-linear behaviour and material properties of resin developed during its cure cycle are implemented into ABAQUS by using a user-defined subroutine UMAT. Residual stresses induced in fibre-resin interface are presented in details.

Finally, progressive damage analysis is performed. Several failure criteria are implemented into ABAQUS with user-defined subroutine USDFLD. Effect of residual stress, load mode and failure criterion on strength and damage progression are investigated. In order to validate the model and subroutines, progressive damage analysis of previously studied materials, are carried out. These materials are E-Glass Gevetex/LY556/HT907/DY063 epoxy and AS4/3501-6. After validating the progressive failure model, the same procedure is applied for AS4/8552 in more details.

2. FINITE ELEMENT MICROMECHANICAL METHOD

Micromechanical finite element analysis is carried out in ABAQUS/Standard version 6.10. The analysis consists of three main parts listed below:

- Prediction of elastic moduli of AS4/8552.
- Determination of residual stress at the end of Manufacturer's Cure cycle
- Failure assessment under various types of loading

First part does not consider the usage of user-defined subroutine but in the last 2 parts, user-defined subroutines, UMAT and USDLFD are required to simulate cure cycle and the damage assessment. Each part is discussed in more detail in further sections.

2.1. Finite Element Model

Only a 3D finite element model can give the response of a composite under different types of loading. Hexagonally packed representative volume elements are selected for this study. Proper boundary conditions should be satisfied to ensure periodicity and symmetry of the model. Validation of the boundary conditions is ensured by analysing a graphite/epoxy composite which is found in HYER's textbook [5].

2.1.1. Geometry of the Model

Regardless of the volume fraction of the composite to be analysed, geometry of the finite element model should follow the consideration shown in Figure 2.1 and through thickness of the element is chosen as 0.001 mm. Detailed dimensions of the model are given in further parts of the thesis. Representative volume elements with Cartesian coordinates system are presented in Figures 2.2 and 2.3. Definition of cylindrical coordinate systems with the fibre-resin interface and variation with angle is given in Figures 2.4 and 2.5 respectively. Highly grey parts indicate the fiber and darker parts indicate the resin.

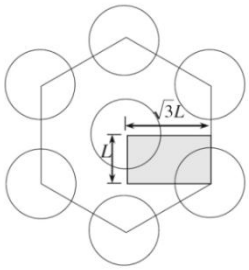

Figure 2.1. Geometry of a hexagonal packed RVE.

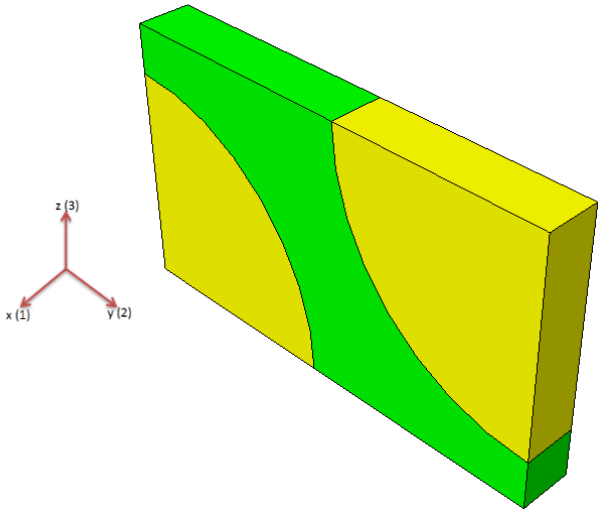

Figure 2.2. Quarter hexagonally packed RVE.

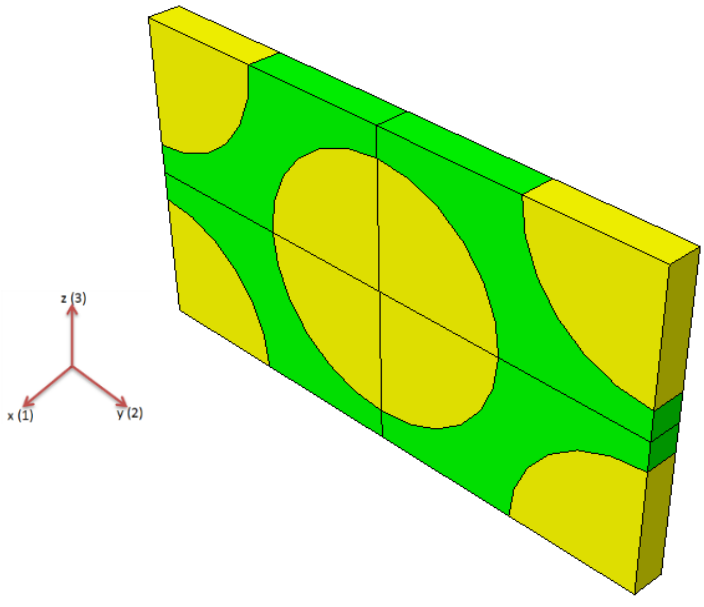

Figure 2.3. Full hexagonally packed RVE.

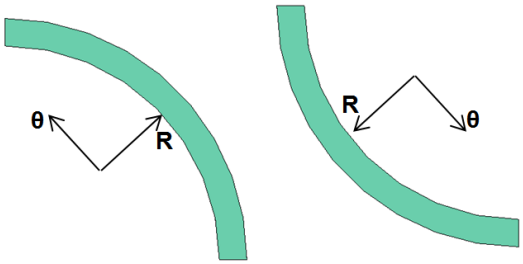

Figure 2.4. Two different cylindrical coordinate systems used in the analysis.

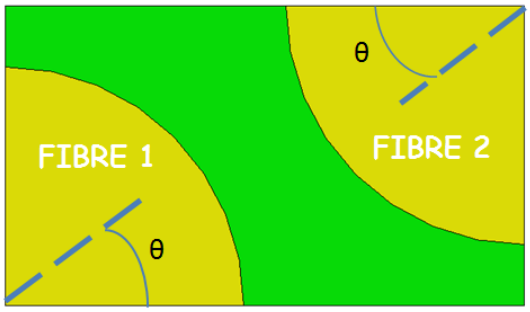

Figure 2.5. Definition of θ in cylindrical coordinate system.

2.1.2. Meshing

Selection of an appropriate type of mesh element for a finite element model is crucial to obtain the reliable results. In this study, linear and quadratic hexagonal elements are examined. The first mesh type is an 8-node linear brick element which is named as C3D8 in ABAQUS®.

Different mesh sizes are applied for these elements. Selected element sizes are; 0.0008, 0.0006, 0.0003, 0.0002, 0.0001 and 0.00005 mm. It is seen that the results converge when the mesh element is C3D20 and its size is less than or equal to 0.0002mm. Effect of different mesh element size on the stiffness and strength of the part can be seen in section 3.3.2. So, C3D30 elements with 0.0002mm are used for moduli prediction and residual stress analysis and in order to show the damage pattern in details, C3D20 type elements are used with 0.0001 mm element size. There is no difference between results of these two types of elements.

C3D20 type element is shown in Figure 2.6. Meshed part can be seen in Figure 2.7. It is seen that the model consists of a single layer through axial direction. If the number of layers is increased, numerical results do not change but required time to solve it increases.

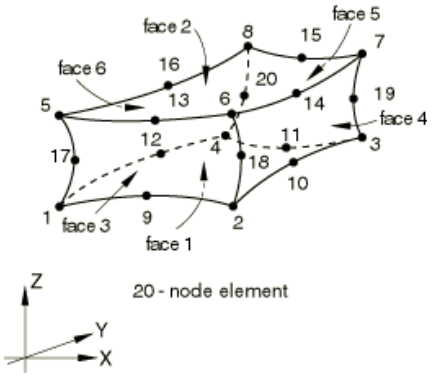

Figure 2.6. Quadratic mesh element (C3D20).

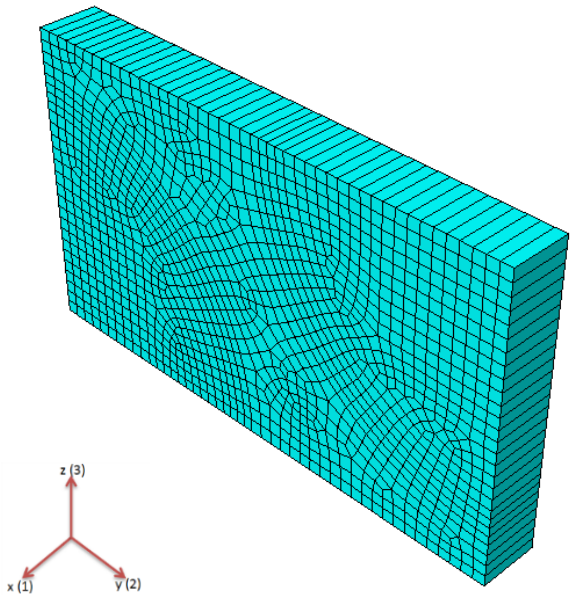

Figure 2.7. Meshing of the RVE.

2.1.3. Loading and Boundary Conditions

As mentioned in previous parts of this thesis, boundary conditions are one of the most important parameters that should be defined for a proper finite element micromechanical analysis. Characteristic boundary conditions are required to provide symmetry and periodicity to the model under each loading mode. These boundary

conditions are given in details in this part. All the coordinates in this chapter are considered with respect to Figure 2.7.

2.1.3.1. Normal Loading. In order to simulate the normal loading correctly, edges of the unit cell should remain planar after deformation as shown in Figures 1.6 and 1.7. To keep the edges planar, all the nodes on x=0, y=0 and z=0 planes are restricted to move in their normal directions. Also, all the nodes on x=1 plane are constrained to have the same x-displacement, the nodes on $y = L\sqrt{3}$ plane are constrained to have the same y-displacement and the nodes on z=L plane are constrained to have same z-displacement. Details of the boundary conditions are given in Table 2.1 where C stands for constrained, R stands for restrained and F means free to move.

These boundary conditions can be applied to both longitudinal and transverse tensile loading. However, loading modes are different for each of them.

In order to simulate longitudinal tensile loading, a displacement boundary condition can be given to a node on x=1 plane or a tensile stress can be applied to x=1 plane. For simplicity of calculations with Equation 1.4 and 1.5, unit tensile stress (σ_1=1 MPa) is applied on x=1 plane of the model. Similarly, to simulate transverse tensile loading, unit tensile stress is applied on $y = L\sqrt{3}$ in y-direction (σ_2=1 MPa) or z=L plane in z-direction (σ_3=1 MPa).

Table 2.1. Boundary Conditions for Normal Loading.

PLANE	**x**	**y**	**z**
x=0	R	F	F
x=1	C	F	F
y=0	F	R	F
$y = L\sqrt{3}$	F	C	F
z=0	F	F	R
z=L	F	F	C

To define these boundary conditions and constraints in ABAQUS®;

DISPLACEMENT/ROTATION type boundary conditions are defined for *x=0, y=0* and *z=0* planes with 0-displacement in the normal directions of each plane.

EQUATION type constraint is given to the nodes on *x=1*, $y = L\sqrt{3}$ and z=*L* planes with the following Equation

$$u_x(1,0,0) - u_x(1,y,z) = 0 \tag{2.1}$$

where $u_x(1,0,0)$ is the displacement of *"x=1, y=0, z=0"* node in x-direction, $u_x(1,y,z)$ is the displacement of rest of the nodes on x=1 plane in x direction.

Similarly:

$$u_y(0, L\sqrt{3},0) - u_y(x, L\sqrt{3},z) = 0 \tag{2.2}$$

$$u_z(0,0,L) - u_z(x,y,L) = 0 \tag{2.3}$$

2.1.3.2. Thermal Loading. As given in Figure 1.10, edges of the model should remain planar after thermal loading deformation. Therefore, same boundary conditions defined in 2.1.3.1 are used for thermal loading. Instead of applying a mechanical load in ABAQUS, a temperature increase is defined to the model. In addition to thermal loading with a temperature increase, same boundary conditions are used to simulate the generation of residual stress throughout the cure cycle.

2.1.3.3. Longitudinal Shear Loading. In order to model longitudinal (in-plane or axial) shear loading with a micromechanical finite element model, whether a displacement boundary condition can be applied to a node on $y = L\sqrt{3}$ plane in fibre direction or unit shear stress can be applied on $y = L\sqrt{3}$ plane in fiber direction. In order to do apply Equation 1.13 and 1.14 easily, unit shear stress is applied on $y = L\sqrt{3}$ plane in fibre direction.

All nodes of the RVE are allowed to move in fibre direction only. Only *y=0* plane is restricted to move in all directions. Additionally, the nodes with same y, z coordinates are constrained to move equally in fiber direction. The boundary conditions and constraints are presented in Table 2.2.

Table 2.2. Boundary Conditions for Axial Shear Loading.

PLANE	**x**	**y**	**z**
x=0	F	R	R
x=1	F	R	R
y=0	R	R	R
$y = L\sqrt{3}$	F	R	R
z=0	F	R	R
z=L	F	R	R

Definition of boundary conditions for axial shear loading in ABAQUS is described in details.

All nodes are allowed to move only in fiber direction with DISPLACEMENT type boundary conditions.

ENCASTRE type boundary condition is given to all nodes on y=0 plane.

EQUATION type constraint is defined for the nodes on $y = L\sqrt{3}$ plane. With this constraint, nodes with same y and z coordinates are obtained to move equally in fiber direction.

$$u_x(0, L\sqrt{3}, 0) - u_x(x, L\sqrt{3}, 0) = 0 \tag{2.4}$$

2.1.3.4. Longitudinal Shear Loading after Cure Cycle. Predefined constraints methods in ABAQUS do not allow the application of in-plane shear loading after cure cycle. Edges of the model should remain planar during cure cycle as in normal loading and while subsequent longitudinal shear loading is applied, deformation should be different than normal loading. Boundary conditions or constraints described in sections 2.1.3.1 or 2.1.3.3 do not provide this. Therefore a modification in boundary conditions and constraints are required.

During curing process, boundary conditions given in Table 2.1 and for the subsequent longitudinal shear loading boundary conditions given in Table 2.2 are used. However, constraints of each condition should be combined as given in 2.5-2.7.

$$u_x(1, y, z) - u_x(0, y, z) = u_x(1, 0, 0) - u_x(0, 0, 0) \tag{2.5}$$

$$u_y(x, L\sqrt{3}, z) - u_y(x, 0, z) = u_y(0, L\sqrt{3}, 0) - u_y(0, 0, 0) \tag{2.6}$$

$$u_z(x, y, L) - u_z(x, y, 0) = u_z(0, 0, L) - u_z(0, 0, 0) \tag{2.7}$$

By using Equation 2.5, the distance between the nodes with same y and z coordinates of x=0 and x=1 planes is kept equal to the distance of the corner nodes of these planes. Similar situation is provided with Equation 2.6 and 2.7 for transverse directions.

In order to obtain this combined constraint system in ABAQUS, a manipulation in nodes are required. In ABAQUS, node numbers are randomly attached to nodes when a part is meshed. These nodes are ranged in a node set in ascending order. It is generally independent of the part geometry. This situation limits the use of Equation constraint, because in an Equation constraint, ABAQUS automatically matches the nodes of node sets with respect to their order. Therefore node numbers should be ranged in a node set with respect to the geometry of the model.

First of all, nodes on edges of x=0 surface are re-numbered via graphical user interface. New numbers of nodes on each edge should follow the same order with respect to opposite edge on this surface. Then, all nodes on x=0 surface are copied to x=1 surface by using input file of the model. These copied nodes can cause a conflict, to prevent this, new nodes on x=1 surface are merged with existing ones. So, node sets of each surface and edge have the same number order with respect to the geometry.

Definition of these boundary conditions in ABAQUS is given below.

In first step of the simulation, i.e, during cure cycle, x=0, y=0 and z=0 planes are restricted to move in their normal directions as in Section 2.1.3.1.

In next step, during subsequent in-plane shear loading, all nodes are allowed to move in fiber direction only but the y=0 plane is suppressed in all directions.

DISPLACEMENT/ROTATION type boundary condition with "Fixed at Current Position" method is defined for all nodes to keep them in their current positions in directions 2-3. Same boundary condition with same method is applied for y=0 plane which keeps all nodes in their current positions in all directions. In graphical user interface of ABAQUS, constraining node sets which contain multiple nodes is not available. Thus, combined constraint system is defined in input file with Equation constraints.

2.1.3.5 Transverse Shear Loading. Quarter RVE does not enable to predict the transverse shear loading correctly. Therefore, a whole hexagonally packed RVE is used to simulate shear loading in transverse direction. Until now, appropriate boundary conditions are defined to keep the edges planar after deformation. The distortions of the boundaries under pure shear loading in transverse direction are seen with a whole hexagonally packed RVE. The origin of the model is the mid-node of the model.

It is not totally a correct assumption to model transverse shear loading with a quarter RVE. In addition to this, applying shear traction to the surfaces of the model does not provide correct method. Pure transverse shear loading of a whole RVE is sketched with Figure 2.8. Displacements are given to each surface. In this sketch, $a = L\sqrt{3}, b = L$

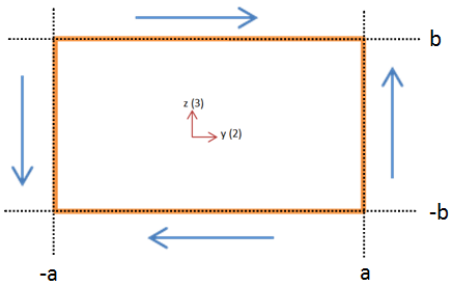

Figure 2.8. Transverse shear loading of a whole RVE

Similar boundary conditions are applied as in [15]. All nodes are suppressed to move in fiber direction. So the problem is reduced to a 2D problem.

Movement of y=0, z=0 nodes of the model is restrained in each directions. (Mid-Edge of the model)

Further constraints are applied to model to enable the screw-symmetry such as:

$$u_y(x,y,b) = - u_y(x,y,-b) \tag{2.8}$$

$$u_z(x,a,z) = - u_z(x,-a,z) \tag{2.9}$$

In addition to the different boundary conditions, different loading mode is required. Applying unit shear stress in transverse directions does not sufficiently enable to simulate transverse shear loading. Therefore, another option is required. Displacement boundary conditions are applied to the corner nodes of the model. Equation 1.11 and 1.12 are applied after calculating the average transverse shear stress by dividing the reaction forces induced in corner nodes to the area of the transverse surfaces of the model.

These boundary conditions and constraints are defined in ABAQUS in details.

ENCASTRE type boundary condition is defined for the (x=0, y=0, z=0) nodes.

All nodes are suppressed in fiber direction. $u_x(x,y,z) =0$

DISPLACEMENT type boundary conditions are defined to each corner nodes to give constant displacement as shown in Figure 2.8.

$$u_y(0,a,b) = -u_y(0, -a, -b) = \delta_y \tag{2.10}$$

$$u_z(0,-a,-b) = -u_z(0, -a, b) = \delta_z \tag{2.11}$$

EQUATION type constraints are defined to obtain equal amount of displacement with screw-symmetry on each surface nodes.

$$u_y(0,a,b) - u_y(0,y,b)=0 \tag{2.12}$$

$$u_y(0,-a,-b) - u_y(0,y,-b)=0 \quad (2.13)$$

$$u_z(0,-a,-b) - u_z(0,-a,z)=0 \quad (2.14)$$

$$u_z(0,a,-b) - u_z(0,a,z)=0 \quad (2.15)$$

It is shown that, each load type requires different boundary and loading conditions in finite element micromechanical modelling of composites.

2.2. Prediction of Elastic Moduli

Firstly, a graphite/epoxy composite is analysed by using the constituent material properties in [5]. Boundary and loading conditions given in section 2.1.3 are applied. After validating the model, same procedure is applied to predict the elastic moduli of AS4/8552.

2.2.1. A Graphite/Epoxy Composite

A graphite epoxy with a fibre volume fraction of 60% is considered. The constituents material properties are given in [5]. This study will provide a validation test case for the models developed throughout this thesis.

Dimensions of the model are not mentioned in the reference. RVE shown in Figure 2.7 is used for analysis. The diameter of fiber is chosen as 8 μm = 0.008 mm. The dimensions of the RVE are calculated with respect to fibre volume fraction and diameter of fibre as shown in Equation 2.16. Also, the properties of the constituents are given in Tables 2.3 and 2.4.

$$V_f = 0.6 = \frac{(\pi \cdot (0.004)^2/2)}{L^2\sqrt{3}} \quad (2.16)$$

where $L = 0.0049177\ mm$ and $L\sqrt{3} = 0.0085177\ mm$.

Table 2.3. Material Properties of Graphite Fibre [5].

$\mathbf{E_{11}}$	233	GPa
$\mathbf{E_{22}=E_{33}}$	23.1	GPa
$\mathbf{\nu_{12}=\nu_{13}}$	0.2	
$\mathbf{\nu_{23}}$	0.4	
$\mathbf{G_{12}=G_{13}}$	8.96	GPa
$\mathbf{G_{23}}$	8.27	GPa
$\mathbf{\alpha_1}$	-0.54	$10^{-6}/^{o}$C
$\mathbf{\alpha_2=\alpha_3}$	10.1	$10^{-6}/^{o}$C

Table 2.4. Material Properties of Epoxy Resin [5].

E [Gpa]	**ν**	**α [$10^{-6}/^{o}$K]**
4.62	0.36	41.4

2.2.2. AS4/8552

The material studied in this thesis is aunidirectional AS4/8552 laminae. Its manufacturer is HEXCEL. This prepreg is generally named as HexPly® 8552. HexPly® 8552 is a high performance epoxy matrix developed for use in especially aerospace structures. It exhibits good impact resistance and damage tolerance.

Fibre volume fraction of the composite is 57.42% and the diameter of the fibre is 8 μm. Edges of the representative volume element are $L = 0.0050278\,mm$, $L\sqrt{3} = 0.008708\,mm$. Mechanical properties of its constituents are given in Tables 2.5 and 2.6.

Table 2.5. Material Properties of AS4 [3].

$\mathbf{E_{11}}$	228	GPa
$\mathbf{E_{22}=E_{33}}$	17.2	GPa
$\mathbf{\nu_{12}=\nu_{13}}$	0.2	
$\mathbf{\nu_{23}}$	0.5	
$\mathbf{G_{12}=G_{13}}$	27.58	GPa
$\mathbf{G_{23}}$	5.733	GPa
$\mathbf{\alpha_1}$	-0.9	$10^{-6}/^{o}$C
$\mathbf{\alpha_2=\alpha_3}$	7.2	$10^{-6}/^{o}$C

Table 2.6. Material Properties of 8552 [25].

E [Gpa]	**ν**	**α [$10^{-6}/^{o}$K]**
4.67	0.37	65

2.3. Residual Stress Analysis of AS4/8552

Generation of residual stress in a unidirectional AS4/8552 ply throughout its cure cycle is investigated. Manufacturer's recommended cure cycle (MRCC) is described in product data shet [25] which is a 6 hours long process and consists of 5 steps. In the first step, part is heated up to 120 °C with 2 °C/min. In the second step, the part is held at this temperature for 60 minutes. In the third step, it is heated to 180 °C with 2 °C/min. Then in fourth step, it is held at 180 °C for 120 minutes. Finally, the part is cooled down to room temperature with 2 °C/min. A pressure of 0.7 bars is applied from the beginning until the end of the process.

2.3.1. Cure Kinetics

In this study, only resin is assumed to generate residual stress during cure cycle. In order to investigate the residual stresses in it, GIM of 8552 resin developed by Ersoy et. al [3] is taken into account. GIM of 8552 is carried out by the "Composites Research Group" in the department of Aerospace Engineering of University of Bristol. It presents the "Cure Kinetics" of this resin.

Cure kinetics study enables us to reach the instantaneous linear strain data and see the development of stiffness of 8552 resin through cure. Instantaneous linear strain and stiffness data of resin were saved for every 2.5 minutes. Figure 2.9 represents the MRCC of AS4/8552 together with the variation of strain throughout the cure cycle. Figures 2.10 and 2.11 represent the variation of elastic modulus and instantaneous strain of Hexcel 8552 resin during the cure cycle with respect to time and temperature respectively.

In Figures 2.9, 2.10 and 2.11 one can easily realize that HEXCEL 8552 resin has a non-linear behaviour with respect to time. In Figure 2.9, in the first step of MRCC, strain increases linearly. From the second step, it shows non-linear behaviour. At gelation point, the resin modulus increases rapidly and the prepreg can sustain in-plane loading after this point. Gelation point of the composite is more noticeable in Figure 2.11. It is the 130^{th} min. of the cure cycle. Rapid development of the elastic modulus after this point can be seen in Figure 2.11. In the second dwell (fourth step), strain decreases rapidly. Due to the

polymerization of resin, shrinkage occurs. Vitrification point is found to be 45 minutes after 180 °C begins. They are pointed in Figures 2.9 and 2.11.

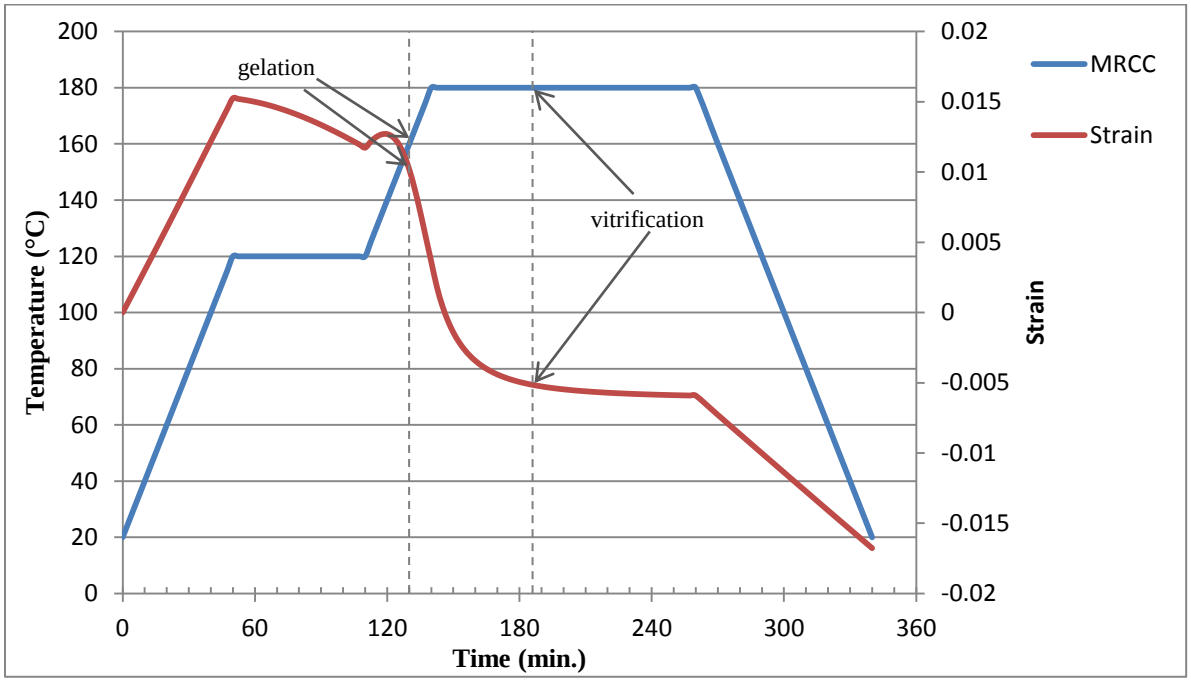

Figure 2.9. Incremental strain of HEXCEL 8552 during MRCC of AS4/8552.

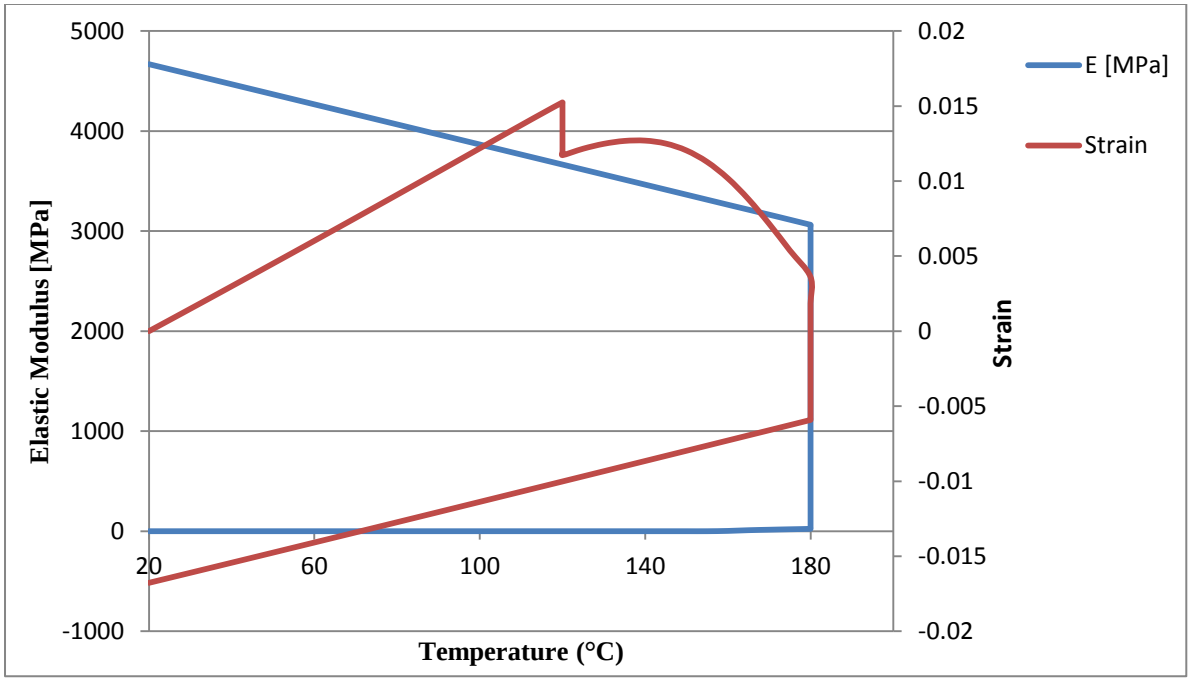

Figure 2.10. Development of elastic modulus and incremental linear strain of Hexcel 8552 resin with respect to temperature.

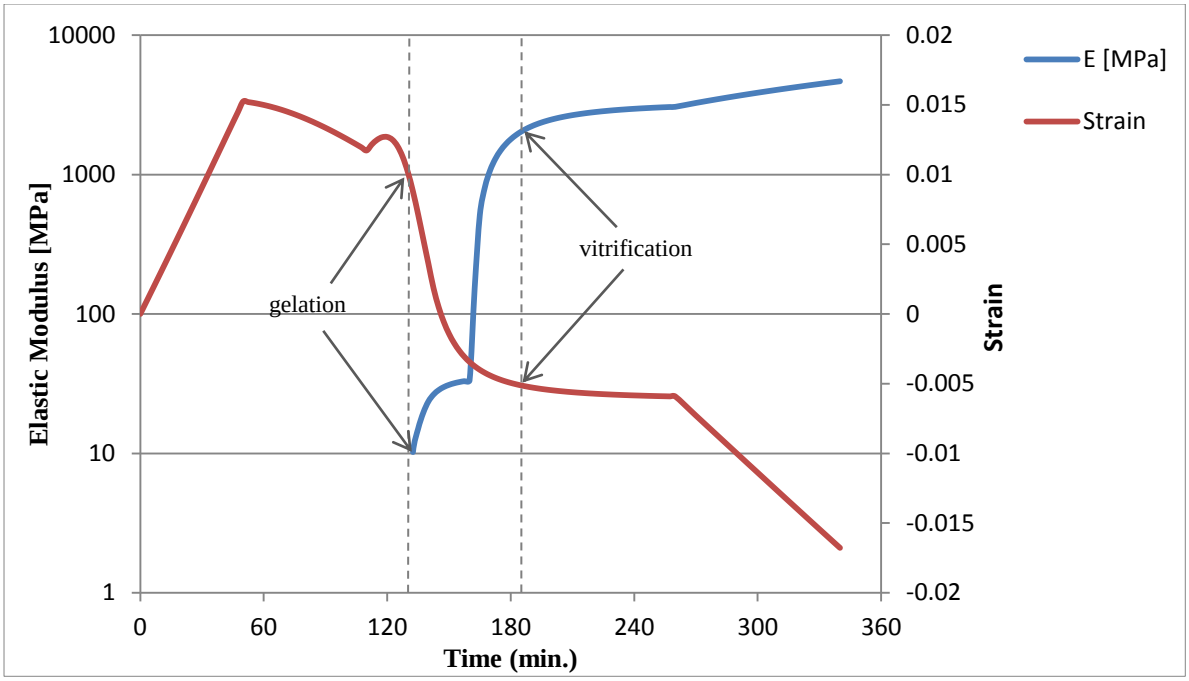

Figure 2.11. Development of elastic modulus and incremental linear strain of Hexcel 8552 resin with respect to time.

2.3.2. Modelling MRCC with Finite Elements Method

As mentioned in previous section, only the residual stress induced in resin is considered. For this purpose, resin is modelled as a temperature-dependent, non-linear material and fibre is modelled as a linear, elastic, temperature-independent material in ABAQUS.

Incremental strain and elastic modulus of the resin throughout the cure cycle is implemented into a user-defined subroutine UMAT. With UMAT, stiffness matrix and stress of the material are calculated incrementally. Total induced strain in resin due to chemical shrinkage and thermal cooling can be expressed as Equation 1.36 and the stress-strain relationship of the resin is defined as in Equation 1.37.

In this study, temperature-dependent coefficient of thermal expansion and cure shrinkage are not taken into account separately. Instead of this, strain change and elastic modulus development due to the polymerization reaction are considered. Incremental stress-strain relationship is expressed as shown in Equation 2.17. In this Equation, δ_{ij} ·

$d\varepsilon_{th}$ represents the given amount of incremental strain change due to chemical and/or thermal effects.

$$\{DSTRESS(i,j)\} = [C] \cdot \{DSTRAN(i,j) - \delta_{ij} \cdot d\varepsilon_{th}\} \quad (2.17)$$

in which [C] is the stiffness matrix, DSTRESS(i,j) is the Array of stress increments, DSTRAN(i,j) is the array of mechanical strain increments (the total strain – thermal strain) and $\delta_{ij} \cdot \varepsilon_{ij}$ is the thermal strain increment.

2.4. Progressive Damage Modelling

In order to simulate mechanical loading same boundary conditions given in section 2.1 are used under each loading modes but different load types are defined in ABAQUS. For a simple calculation of moduli, unit tensile pressure or shear traction are applied to the surfaces of RVE. However applying pressure does not enable to simulate progressive damage modelling, because it does not show the decrease of global stress when an element is failed. Global stress continues to increase after failure. Instead of this, global strain is given in regarding directions like in a real mechanical testing. Equation type constraint defined in section 2.1 provides to gather the reaction forces to a single node. That is the resulting average force in that direction. Then, force is divided to the area of the surface to calculate average global stress. Thus, incremental global stress-strain values are calculated during subsequent loading.

Progressive failure is modelled with stiffness reduction method. There are two stiffness reduction schemes used in literature. They are selective and non-selective reduction schemes. In this study, non-selective reduction scheme is used because in isotropic materials, damage is independent of material orientation. When stress in an element reaches to the critical value according to the failure criterion, degradation is applied only on the stiffness of the resin by reducing it to a near zero value [22]. Stiffness reduction method is applied with user-defined subroutines USDFLD and UMAT into ABAQUS.

User-defined subroutine USDFLD allows defining field variables at a material point as functions of any material point quantities. The values of the field variables defined

in this routine are used to calculate values of material properties that are defined to depend on field variables and are passed into other user subroutines that are called at the material point. Conjunction is achieved by state variables. State variables are passed into UMAT and the stiffness of the material is updated [23]. Failure criteria are defined in USDLFD. Field and state variables in USDFLD are set to 1 when a parameter at an integration point reaches the critical value during loading with respect to the failure criteria.

Two materials are investigated by using the progressive damage model developed in this thesis. Because the elastic properties and strength values of constituents and the composites are available in literature. So, they are proper test cases for testing the models developed in this study. Firstly, E-Glass Gevetex/LY556/HT907/DY063 Epoxy material is simulated. Its transverse tensile strength and damage progression under this type of loading are investigated with respect to Maximum Principal, Raghava's and Bauwen's MVM failure criteria in each directions. Then, progressive failure analysis of carbon-fibre reinforced AS4/3501-6 is performed. Predictions are compared with previous studies [22,24].

After validating the user-defined subroutines and the model, strength and damage assessment of AS4/8552 are investigated with respect to several failure criteria such as Maximum Principal, Von-misses, Tresca, Raghava's and Bauwen's modified von Misses criteria under various types of loading with and without the presence of residual stress to investigate its effect on composite strength and damage path after damage initiation.

Only resin dominated strength values are investigated. Therefore tensile and compression strength of 8552 neat resin should be known. In product data sheet of 8552 resin [25], the tensile strength is given as 120 MPa. However, compression strength of 8552 resin is not available. Therefore, an assumption is done for the compression strength of resin. 8552 resin is more toughened polymer than 3501-6 as mentioned in [25] and the strength values of 3501-6 resin are known from [24] in which the compression strength of 3501-6 is found as 250 MPa. With respect to this information, the compression strength of 8552 resin is assumed as 300 MPa. Interfacial strength of fibre-resin interface is different than the properties of resin in real life [1]. However, in this thesis, strength and stiffness of

the fibre-resin interface is assumed to be equal to resin. Its different mechanical properties are not taken into account.

Strength values obtained in this study are compared to each other, product data sheet [25], statistical test report of AS4/8552 [26] and some experimental results carried out in Mechanical Testing Laboratory of Mechanical Engineering Department of Bogazici University. Least square difference between the predicted and measured strength values of the composite are averaged for various types of loading. Equation 2.18 shows the formulation applied.

$$\frac{1}{n}\sum_{i=1}^{n}\sqrt{\left(\frac{PS-EXP}{EXP}\right)^{2}}\cdot 100 \tag{2.18}$$

where n is the number of predicted strength, PS is the predicted strength and EXP is the experimental result

3. RESULTS AND DISCUSSION

Results of the numerical analysis and some experiments are presented in this chapter. Numerical analysis is carried out in ABAQUS/Standard version 6.10. Experiments are done in Mechanical Testing Laboratory of Mechanical Engineering Department of Bogazici University. In numerical analysis, applied loading and boundary conditions are given in previous chapter, so there is no need to write them again.

3.1. Elastic Moduli Prediction

As mentioned in section 2.1, elastic moduli of two different composites are predicted. First material is a graphite/epoxy given in Ref. [5]. By comparing the results with reference values, the finite element micromechanical model with applied loading and boundary conditions are verified. Then elastic moduli of AS4/8552 are predicted.

3.1.1. Elastic Moduli of Graphite/epoxy composite

Elastic properties of the constituents of this material and the geometry of the micromechanical model are given in Section 2.2.1 as $x = 0.001, y = L\sqrt{3} = 0.0085177$ and $z = L = 0.0049177$. Tables 2.3 and 2.4.present the elastic properties of the constituents.

3.1.1.1. E_{11} and ν_{12}. Figure 3.1 illustrates the resulting deflections in the material under a tensile loading in fibre direction. Deformations occur on the free planes. It is seen from Figure 3.1 that the edges of the model remain planar after deformation. Values of the resulting displacements in each directions after loading are given below.

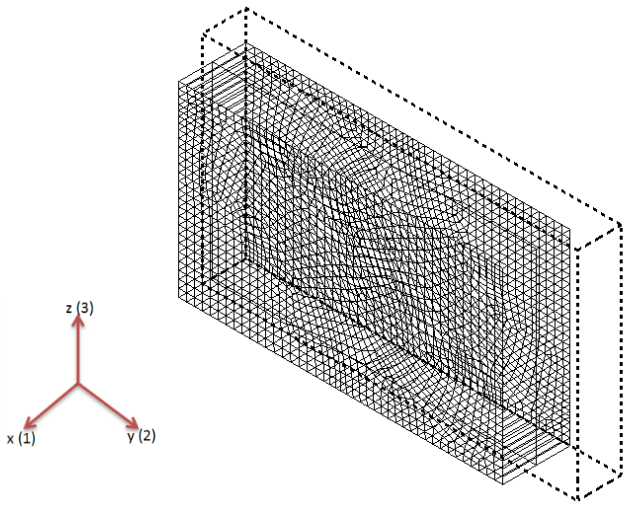

Figure 3.1. Deflections under axial tensile loading.

The resulting deflections are:

$$du_x = 7.05788 \cdot 10^{-9} mm$$

$$du_y = -1.548 \cdot 10^{-8} mm$$

$$du_z = -8.95283 \cdot 10^{-9} mm$$

By applying Equation 2.4 and 2.7:

$$\varepsilon_1 = \frac{du_x}{dx} = 7.05788 \cdot 10^{-6}$$

$$\varepsilon_2 = \frac{du_y}{y} = -1.81739 \cdot 10^{-6}$$

The required material properties; E_{11} and ν_{12} are calculated with Equation 1.5 and 1.6 as follows:

$$E_{11} = \frac{1}{\varepsilon_1} = 141685\ MPa \rightarrow E_{11} = 141.7\ GPa$$

$$\nu_{12} = \nu_{13} = \frac{\varepsilon_2}{\varepsilon_1} = 0.257$$

3.1.1.2. E_{22}, ν_{21} and ν_{32}. The resulting displacements in each directions due to tensile loading in z direction are shown below and the resulting deformations are sketched in Figure 3.2.

The resulting displacements are:

$$du_x = -1.81938 \cdot 10^{-9} mm$$

$$du_y = -3.53605 \cdot 10^{-7} mm$$

$$du_z = 4.35667 \cdot 10^{-7} mm$$

By applying Equation 1.4 and 1.7, linear strains in each directions:

$$\varepsilon_1 = \frac{du_x}{dx} = -1.81938 \cdot 10^{-6}$$

$$\varepsilon_2 = \frac{du_y}{dy} = -4.1514 \cdot 10^{-5}$$

$$\varepsilon_3 = \frac{du_z}{dz} = 8.85914 \cdot 10^{-5}$$

By using Equation 1.8, 1.9 and 1.10, E_{22}, ν_{21} and ν_{23} are calculated as follows:

$$E_3 = \frac{1}{\varepsilon_3} = 11288\ MPa \ \rightarrow \ E_3 = E_2 = 11.29\ GPa$$

$$\nu_{31} = -\frac{\varepsilon_1}{\varepsilon_3} = 0.0205$$

$$\nu_{32} = -\frac{\varepsilon_2}{\varepsilon_3} = 0.468$$

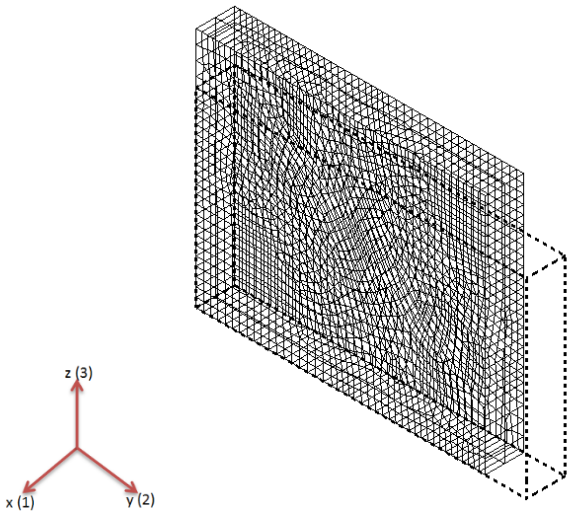

Figure 3.2. Resulting deflections under transverse tensile loading.

3.1.1.3. G_{12}. Simple shear procedure is followed to determine G_{12}. Resulting deformations under axial shear loading is shown in Figure 3.3.

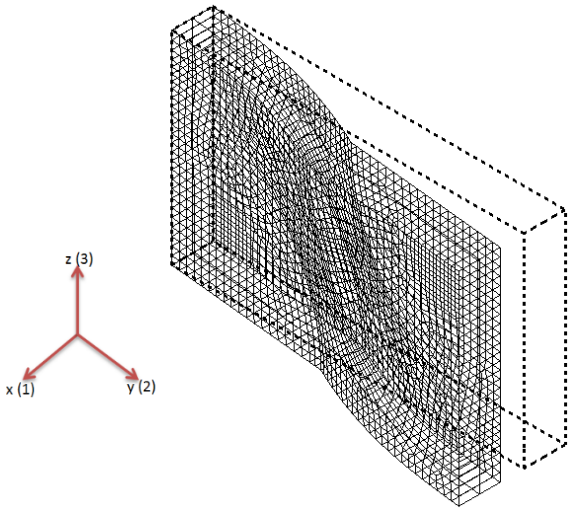

Figure 3.3. Resulting deformations under axial shear loading.

The maximum deflection in fiber direction under axial shear loading:

$$du_x = 2.10119 \cdot 10^{-6} mm$$

Axial shear strain is calculated with Equation 1.14 as:

$$\gamma_{12} = \frac{du_x}{dy} = 2.4668 \cdot 10^{-4}$$

The Shear Modulus in the Axial Direction is:

$$G_{12} = G_{13} = \frac{1}{\gamma_{12}} = 4054\ MPa$$

3.1.1.4. G_{23}. As mentioned in previous sections composite materials are transversely isotropic materials. Therefore Equation 1.21 should be satisfied.

According to Transverse Isotropy Rule:

$$G_{23} = \frac{11290}{2 \cdot (1 + 0.468)} \rightarrow G_{23} = 3850\ MPa$$

G_{23} is calculated with respect to boundary conditions described in Section 2.1.3.6. 0.0001mm displacements are given in each direction to each corner nodes.

Resulting deformations of the model in yz plane is shown in Figure 3.4. Periodic boundary conditions can be seen clearly in Figure 3.4. Every node on each surface have the same deformations with the ones on the opposite surface.

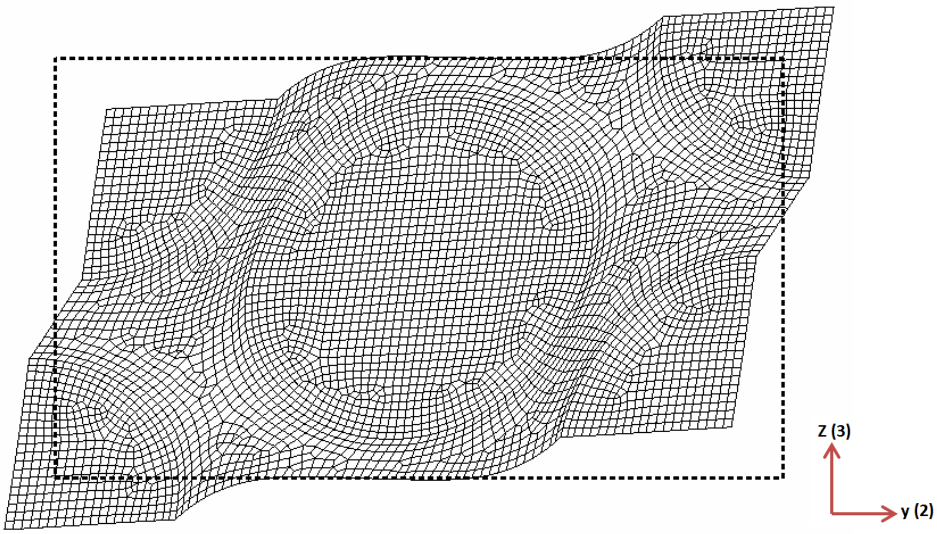

Figure 3.4. Resulting deformations under pure shear loading in transverse direction.

Transverse shear modulus (G_{23}) of the composite is calculated by using the method given in section 2.1.3.5.

Reaction force induced in direction-y is: 0.00210183 N

Reaction force induced in direction-z is: 0.00121349 N

Average shear stress in transverse direction:

$$\sigma_{23} = \frac{0.00210183}{(2 \cdot 0.008707 \cdot 0.001)} = \frac{0.00121349}{(2 \cdot 0.0050278 \cdot 0.001)} = 123.38\ MPa$$

Transverse shear strain:

$$\gamma_{23} = \frac{du_z}{dy} + \frac{du_y}{dz} = \frac{0.0001}{0.0085177} + \frac{0.0001}{0.0049177} = 0.032075$$

Transverse shear modulus:

$$\frac{\sigma_{23}}{\gamma_{23}} = 3.847 \approx 3.85\ GPa$$

According to the transverse isotropy rule: G_{23}=3.85 GPa

As it is seen from results whole RVE gives close solution with the transverse isotropy rule. Therefore, transverse isotropic structure of this composite is proven and this model is appropriate for further transverse shear modelling.

3.1.1.5. Coefficient of Thermal Expansion (CTE). A predefined field of 100 ^{o}C temperature increase is defined for the model. Resulting deformation of the model due to thermal loading is sketched in Figure 3.5. Due to the low negative CTE of fibre and its high stiffness, contraction of composite in fibre direction is very smaller than the expansion in transverse directions. Coefficients of thermal expansion of this composite in each direction are calculated with respect to Equation 1.16 and 1.17.

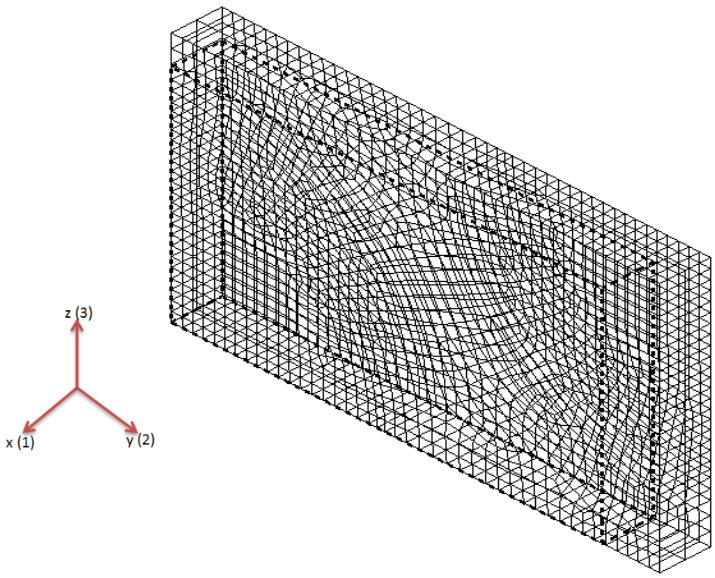

Figure 3.5. Resulting deflection in material after thermal loading.

Deflections in each direction are found to be:

$$dx = 7.87618 \cdot 10^{-9} mm \quad dy = 2.27367 \cdot 10^{-5} mm \quad dz = 1.31319 \cdot 10^{-5} mm$$

Coefficients of thermal expansion (CTE):

$$\frac{\mathrm{du}_x}{dx} = \alpha_1 \cdot 100 \rightarrow \alpha_1 = 0.0786 \cdot 10^{-6} \, /℃$$

$$\frac{\mathrm{du}_y}{dy} = \frac{\mathrm{du}_z}{dz} = \alpha_2 \cdot 100 = \alpha_3 \cdot 100 \rightarrow \alpha_2 = \alpha_3 = 26.7 \cdot 10^{-6} \, /℃$$

All of the engineering properties of graphite-reinforced composite are predicted with finite elements micro-mechanical method. Table 3.1 compares the results of this study with reference values.

Table 3.1. Engineering properties of graphite-reinforced composite.

V_f=60%	[5]	This Study		% Err.
E_1	141.9	141.7	GPa	0.14
$E_2=E_3$	11.3	11.3	GPa	0.0885
$G_{12}=G_{13}$	4.05**	4.05	GPa	0.099
G_{23}	3.85*	3.85	GPa	0
$\nu_{12}=\nu_{13}$	0.257	0.257	-	-
ν_{21}	0.0205	0.0205	-	-
ν_{23}	0.468	0.468	-	-
α_1	0.0766	0.0786	x $10^{-6}/^oC$	2
$\alpha_2=\alpha_3$	26.6	26.7	x $10^{-6}/^oC$	0.38
*: Transverse Isotropy Rule **: Elasticity Model, Not any RVE Approach				

All of the material property data are available in HYER's textbook [5]. Therefore, it is a good case for comparison. Results obtained within this study show excellent correlation with [5]. It demonstrates the validation of the model. So, this model can be used for further micromechanical analysis

3.1.2. Elastic Moduli of AS4/8552

Since same procedure is applied to predict the mechanical properties of AS4/8552, same deformation modes are obtained but with different values for sure. Therefore, visual representation of resulting deformation is not presented for AS4/8552. Only predicted mechanical properties of AS4/8552 are given here and they compared with reference values.

Table 3.2 presents the predicted and analytically calculated elastic properties of AS4/8552. These values show good agreement with numerical [3] and experimental [26] values. G_{23} is accurately predicted with whole RVE method in this study. Numerical values of G_{23} were calculated with transverse isotropy rule in [3] but its experimental value was not mentioned in [26]. One interesting situation in [26] is, there are two different values were found for some elastic moduli. Appearently, AS4/8552 has different behaviour during

compression and tension as shown in Table 3.2 in which superscript C stands for compression and T for tension.

Table 3.2. Comparison of predicted glassy properties of AS4/8552 with reference values.

V_f=%57.4	**SCFM [3]**	**FEBM [3]**	**Measurement [26]**		**This Study**		
E_1	133000	134000	129000^T	113200^C	133000		MPa
$E_2=E_3$	9130	9480	9050^T	9850^C	9755		MPa
$G_{12}=G_{13}$	5210	5490	4830		5228		MPa
G_{23}	3210	3272	-		3194^f	3194^{TI}	MPa
$\nu_{12}=\nu_{13}$	0.272	0.271	0.302^T	0.335^C	0.267		-
ν_{21}	-	-	0.029		0.0196		-
ν_{23}	0.465	0.448	0.45		0.527		-
α_1	-	-	-		0.232		x 10^{-6}/ºC
$\alpha_2=\alpha_3$	39.9	40	32.6**		40.03		x 10^{-6}/ºC

^{T}: Tension – ^{C}: Compression

**: [14]

^{f}: Full RVE Model – ^{TI}: Transverse Isotropy

3.2. Residual Stress Analysis

Incremental strain and stiffness values of resin are entered in user defined subroutine (UMAT) to model the Manufacturer's recommended cure cycle (MRCC) of AS4/8552. Strain variation of resin with respect to time is modelled in ABAQUS as shown in Figure 3.6. This is similar to Figures 2.9 and 2.11. Gelation point, vitrification point and beginning of cooling stage are marked with their abbreviations in Figure 3.6.

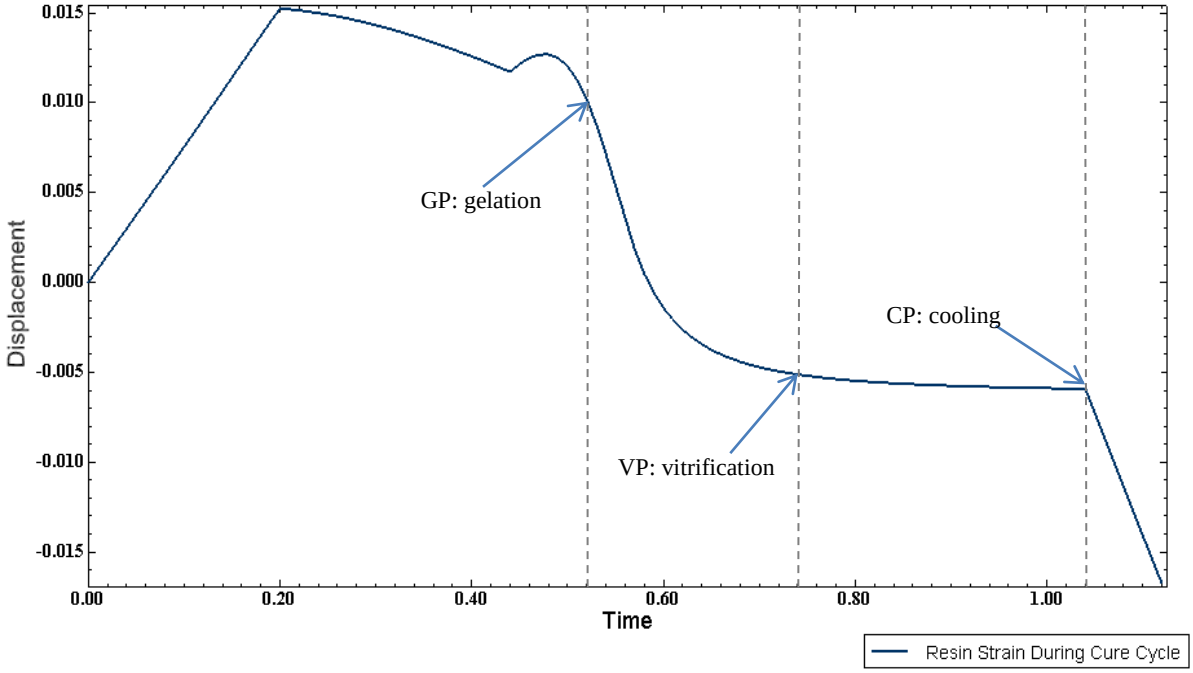

Figure 3.6. Strain variation of resin throughout MRCC.

Resulting deformation of AS4/8552 at the end of cure cycle is sketched in Figure 3.7. At the end of the cure cycle, AS4/8552 shrinks. Strain of composite in some specific points are presented in Table 3.3.

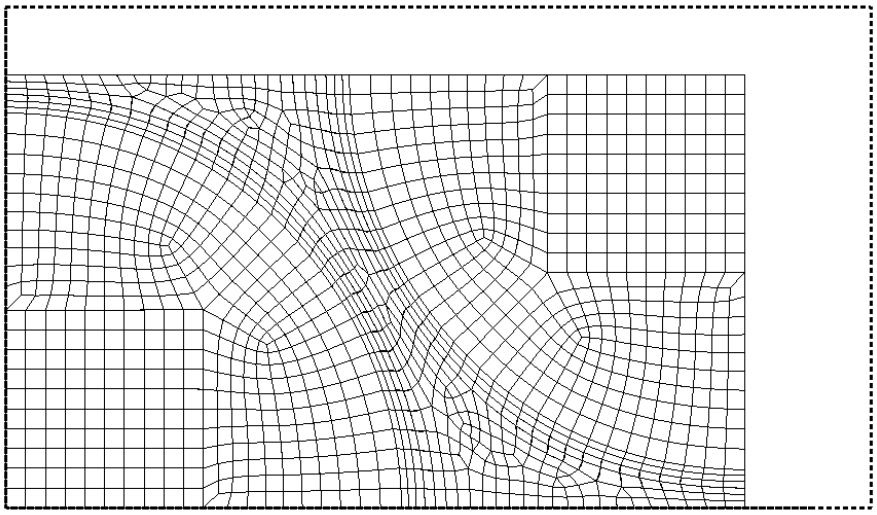

Figure 3.7. Resulting deformations at the end of the MRCC.

Table 3.3. Total strains and strain changes at some specific points during cure cycle.

	ε_1	ε_2	ε_3
GP	$-1.39141 \cdot 10^{-8}$	0.00645	0.00655
VP	$-8.507 \cdot 10^{-9}$	-0.00315	-0.00306
CP	$-1.63931 \cdot 10^{-5}$	-0.00367	-0.00358
END	-0.0001776	-0.00941	-0.00933
VP-GP	$5.4071 \cdot 10^{-9}$	-0.00960	-0.00961
CP-VP	$-1.63846 \cdot 10^{-5}$	-0.000517	-0.00052
END-CP	-0.000161207	-0.00574	-0.00575

Results indicate that, RVE expands until gelation point and shrinks until the end of cure cycle in transverse directions. Most of the shrinkage occurs at the cooling stage. Amount of expansion and shrinkage is almost equal to each other in transverse directions. Variation of residual stress throughout the MRCC is given in details in next chapter.

3.2.1. Stress in Fibre Direction

As mentioned in previous studies [6, 18-22], damage initiates at fibre-matrix interface, so it is a critical part of the RVE. Therefore, detailed analysis of residual stress is presented for the interface in this section.

As in previous studies [19-22], tensile residual stresses are generated in resin and compressive residual stresses are induced in fibres at the end of cure cycle. Residual stresses induced in fibre direction (σ_{11}) at the end of the cure cycle are represented with Figure 3.8. Tensile stresses in resin and compressive stresses in fibre can be seen clearly. Stress distribution in resin can be seen in Figure 3.9 in details. The average value of the stress in fibre direction at the end of the cure cycle is 63.77 MPa. It is 6.48 MPa before cooling down to room temperature. So, most of the process induced residual stress in produced due to cooling processs.

Variation of residual stress at fibre matrix interface in resin and fibre with respect to the fibre angle are plotted in Figure 3.10. Maximum tensile stress in resin is induced in

resin-rich region, however minimum tensile stress in resin and maximum compressive stress in fibre are induced in resin-low regions as presented in Figure 3.10.

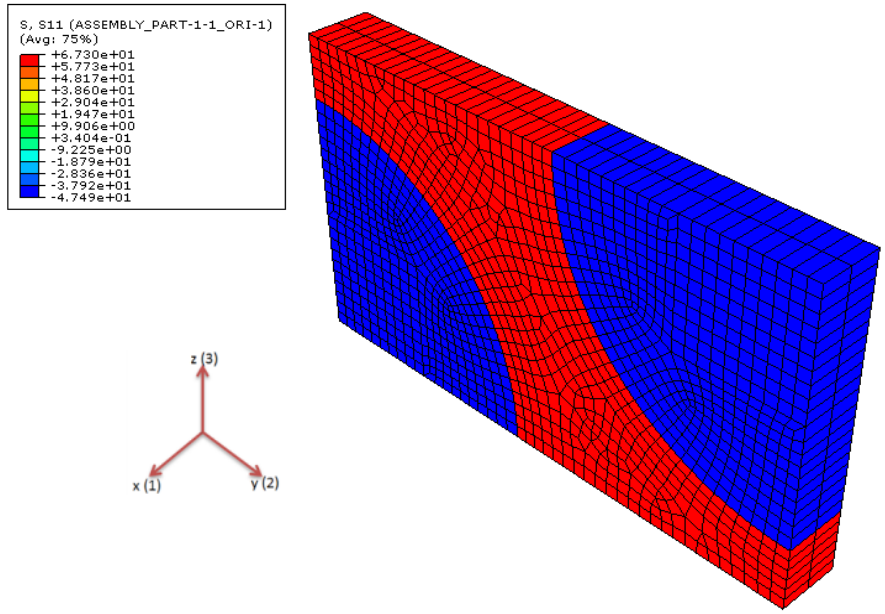

Figure 3.8. Stresses induced in fibre direction.

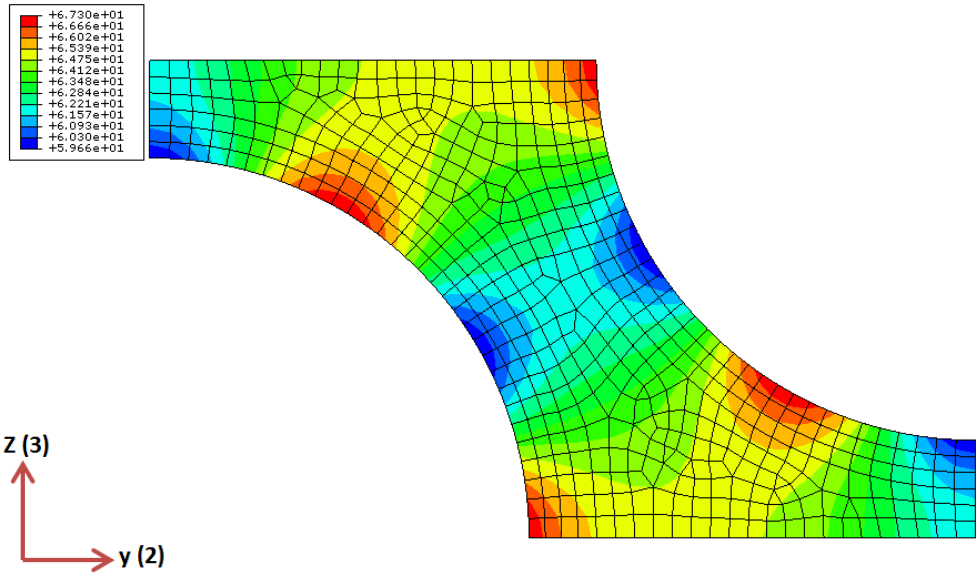

Figure 3.9. Stresses induced in resin in fibre direction.

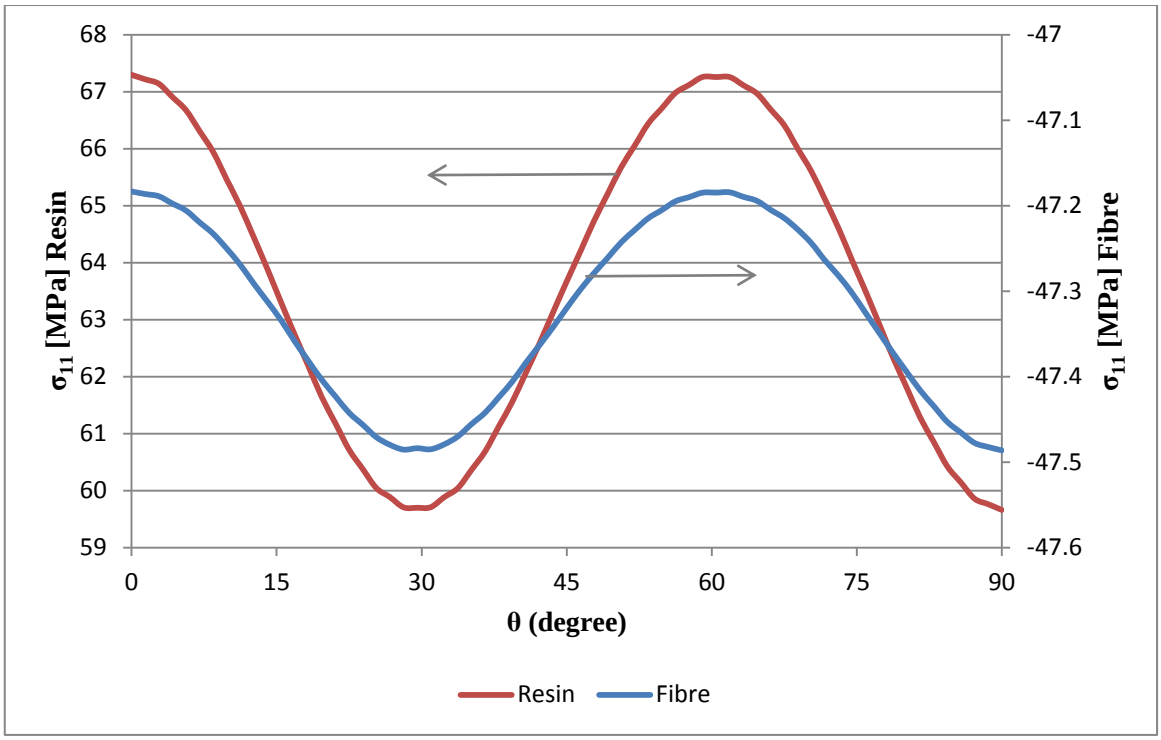

Figure 3.10. Variation of stress in fibre direction along the fibre matrix interface.

3.2.2. Von Misses Stress Distribution

Residual stresses generated in a composite at the end of the cure cycle are consequences of polymerisation of matrix during curing and the mismatch of thermal contraction of fiber and matrix while cooling down to room temperature. As mentioned in section 3.2.1, most of the residual stress is induced during cooling stage. Visual representation of this situation for von Misses stress is presented in this section. Von Misses stress distribution at the end of curing at 180 °C (just before cooling stage) and at the end of cure cycle (after cooling to 20^{o}C) are presented in Figures 3.11 and 3.12 respectively. Before cooling, maximum von Misses stress is 7.85 MPa and at the end of cooling it increases to 85.64 MPa in resin. Distribution of von Misses stress at the end of cooling in fibre-resin interface can be seen in Figure 3.13. In resin-low areas, maximum stress is induced in resin however, minimum stress is induced in fibres.

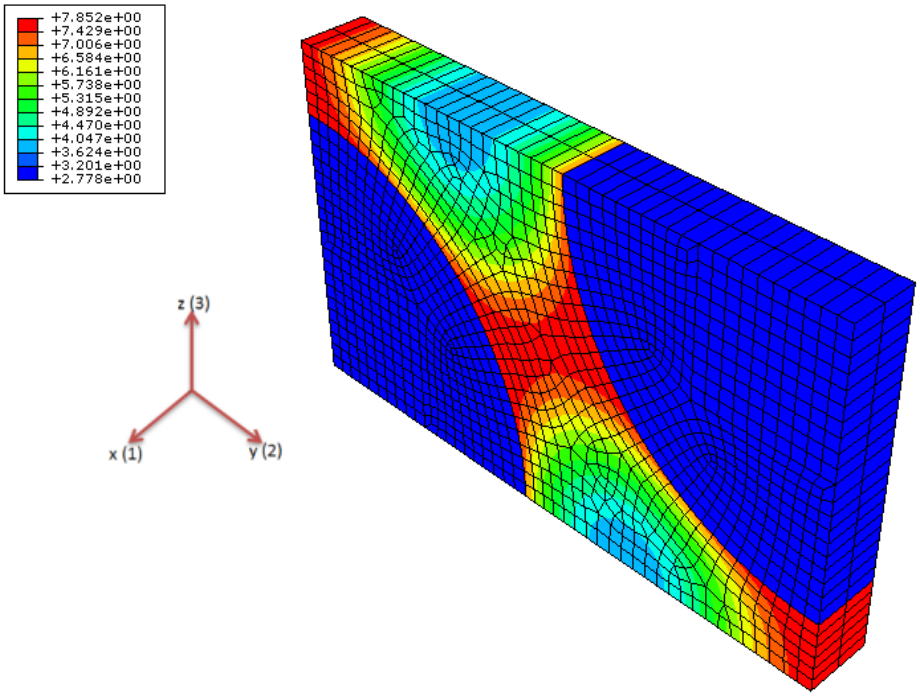

Figure 3.11. Misses stress distribution just before cooling stage (at 180^{o}C).

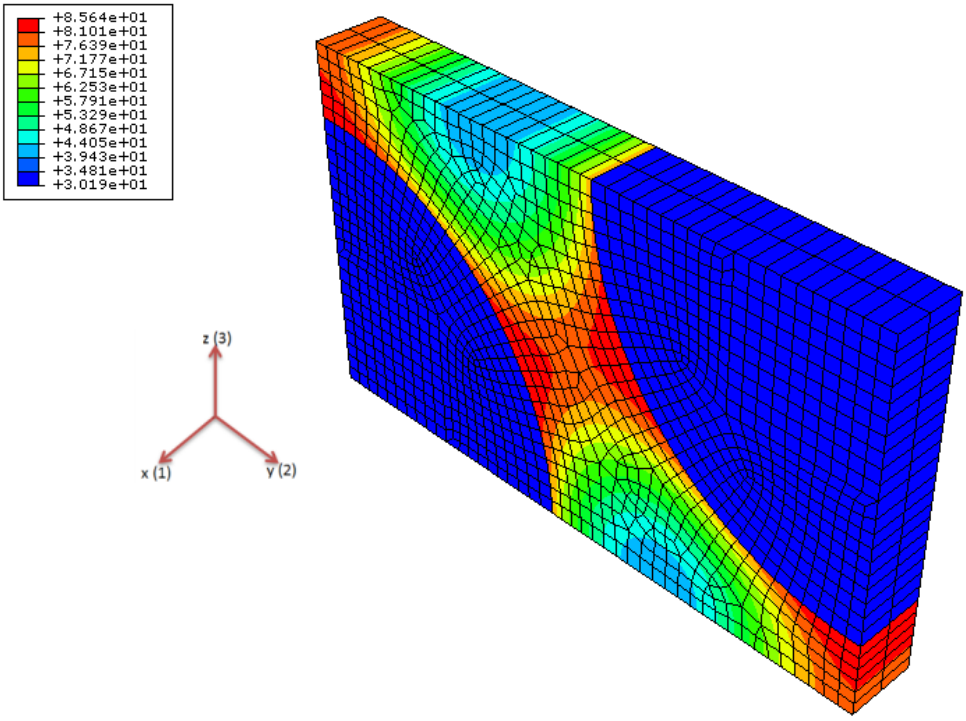

Figure 3.12. Misses stress distribution at the end of cooling (at 20^{o}C).

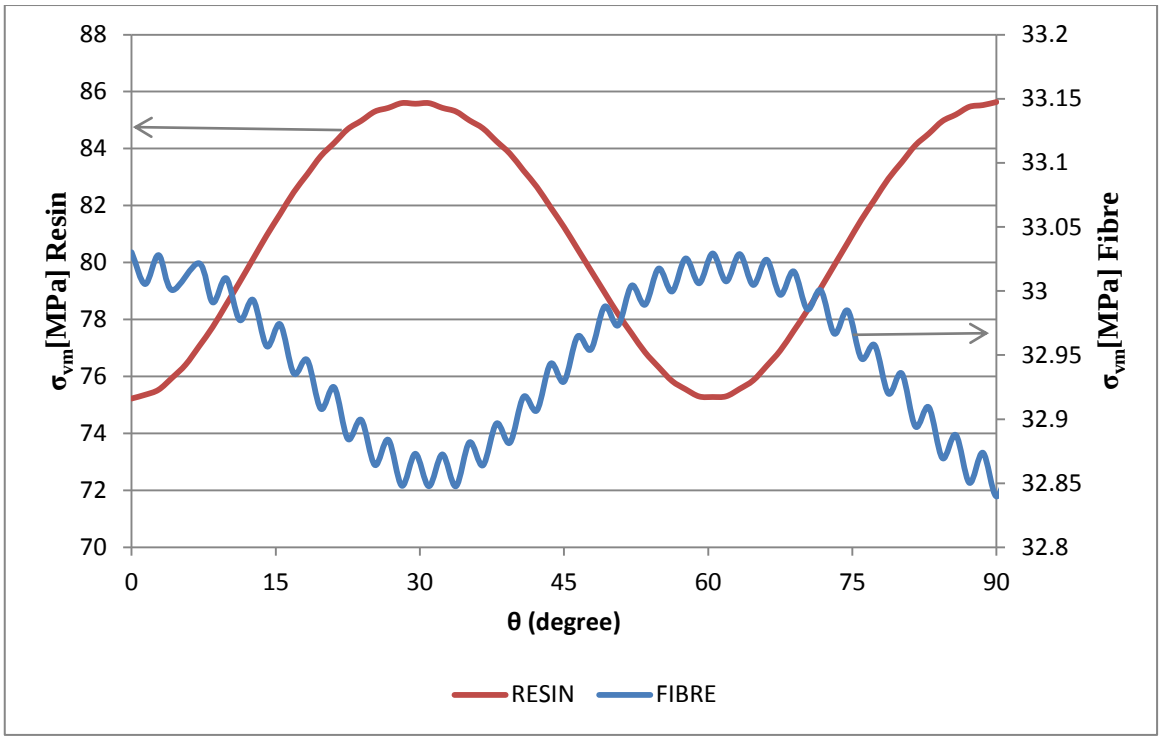

Figure 3.13. von Misses stress variation along fibre matrix interface.

3.2.3. Maximum principal stress distribution

Max. Principal Stress distributions in bulk resin and the fibre-matrix interface are shown in Figures 3.14 and 3.15 respectively. As it is seen in Figure 3.14, maximum principal stress is induced in fibre direction in bulk resin but Figure 3.15 shows that in some parts of the interface, maximum principal residual stress is induced in hoop directions with respect to cylindrical coordinate system. So, it can be said that, maximum principal stress is in fibre direction at the resin rich parts of the model and it is in radial direction where the resin content is low. Figure 3.16 plots the stress variation in resin at the fibre-matrix interface.

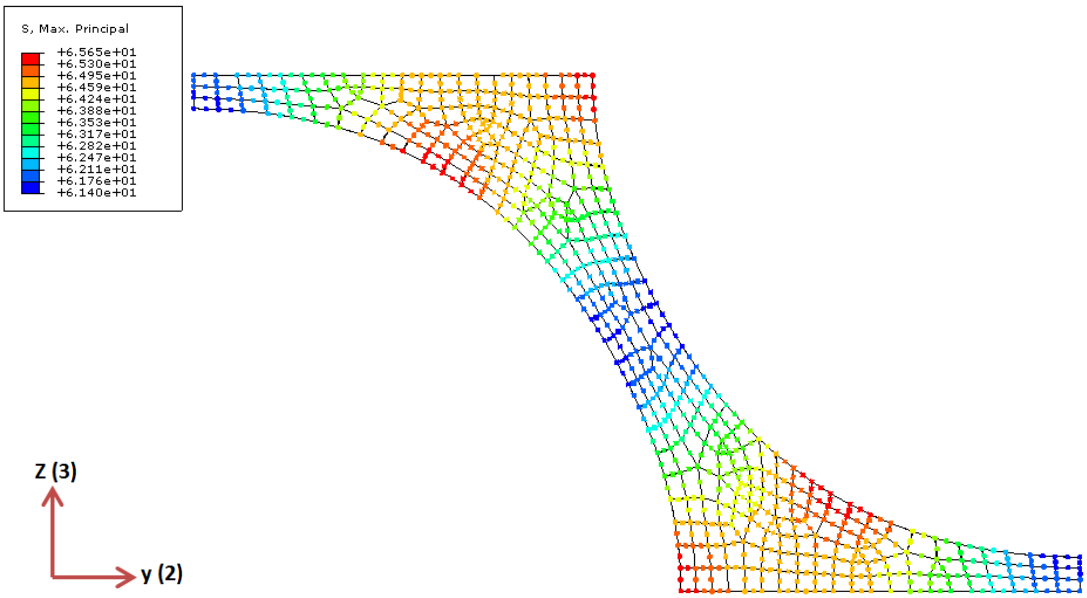

Figure 3.14. Maximum principal residual stress distribution in bulk resin.

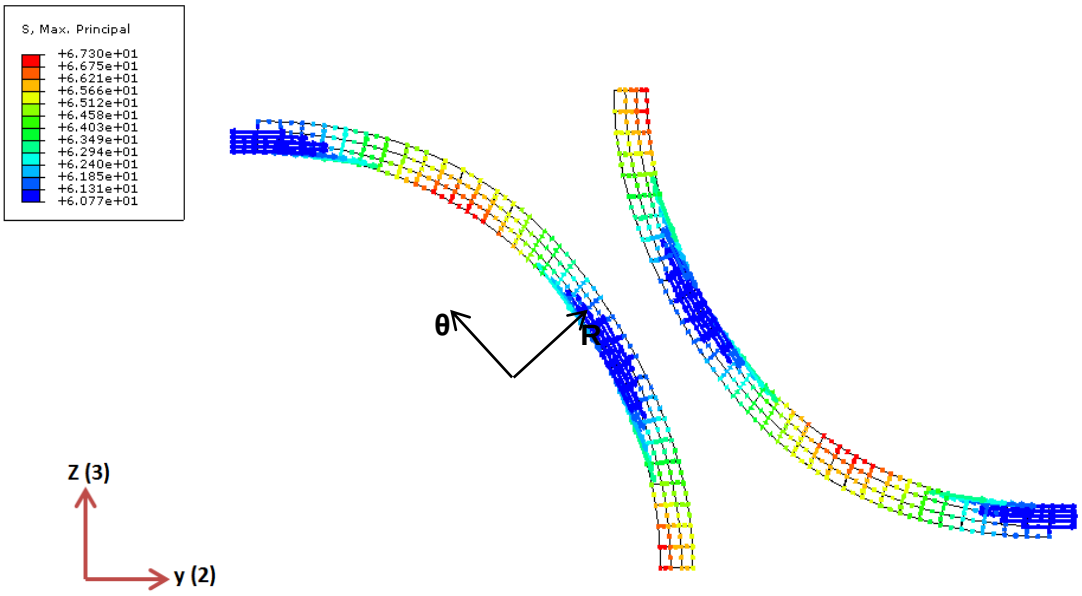

Figure 3.15. Maximum principal residual stress distribution in interfaces.

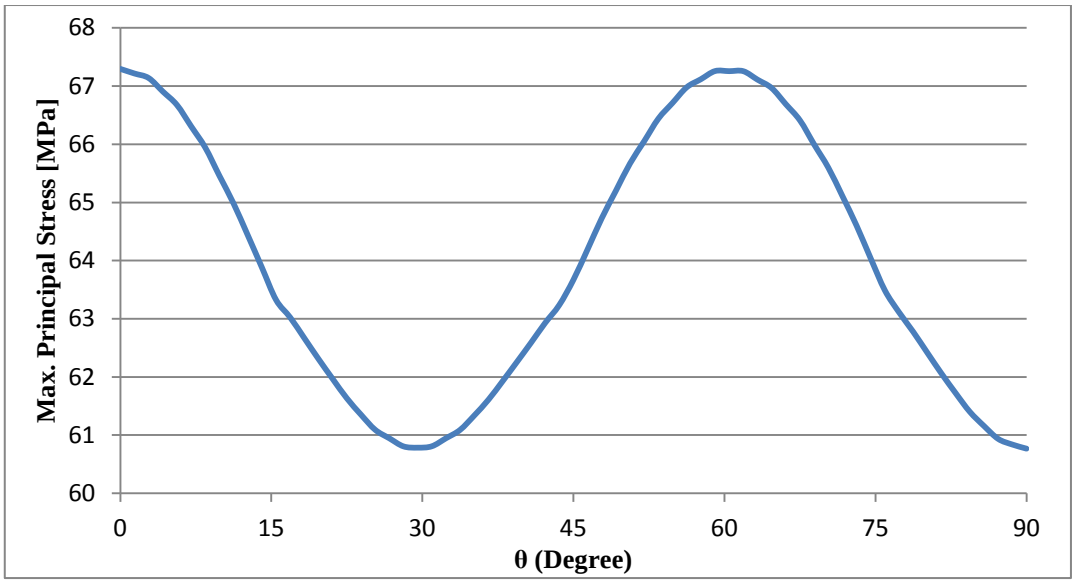

Figure 3.16. Variation of maximum principal stress in resin at the fibre-matrix interface.

3.2.4. Stresses in Radial Direction (σ_r)

Cylindrical coordinate systems are defined as shown in Figure 2.4. Magnitudes of the stresses with respect to each of these two coordinate systems are same but the distribution is symmetric. Due to the symmetry, it is sufficient to present radial stress distribution only in one cylindrical coordinate system. Stresses induced in radial directions at the interfaces after cure cycle with respect to 1st cylindrical coordinate system is shown in Figures 3.17. Magnitude of radial stress at fibre-matrix interface around fibre 1 is same for fibre and resin. Radial stress distribution around fibre 1 is presented with Figure 3.18.

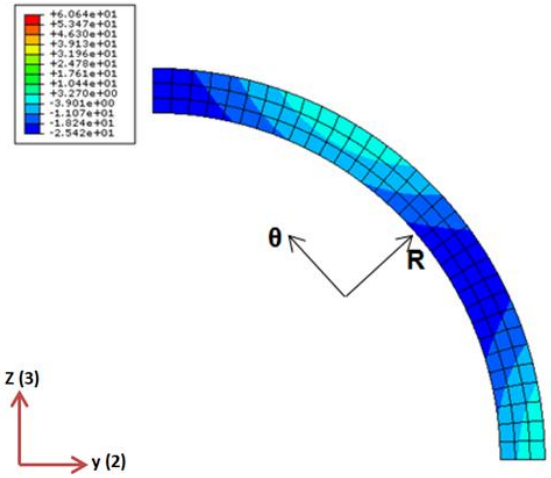

Figure 3.17. Radial stress distribution at the interface in 1st cylindrical coordinate system.

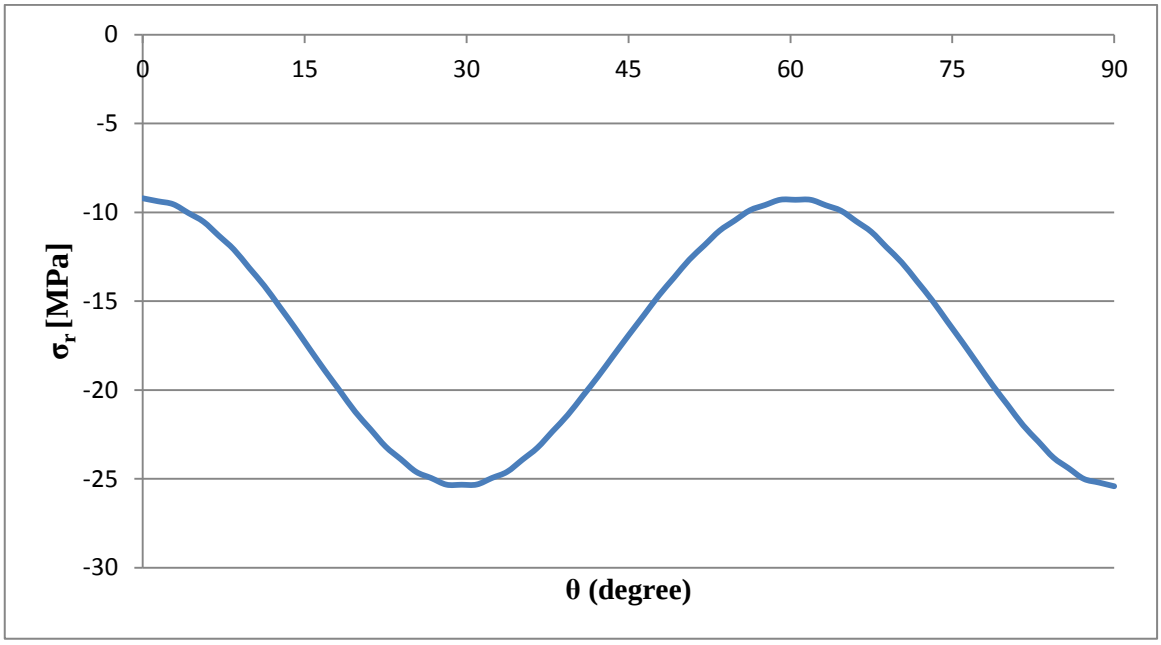

Figure 3.18. Radial stress variations around fibre 1.

3.2.5. Stresses in hoop direction (σ_θ)

As in radial stresses, only the 1st cylindrical coordinate system is considered here. Residual stresses induced in θ direction in the interface with respect to 1st cylindrical coordinate system are shown in Figure 3.19. Stress variations along fibre-matrix interfaces of fibre 1 are plotted in Figures 3.20.

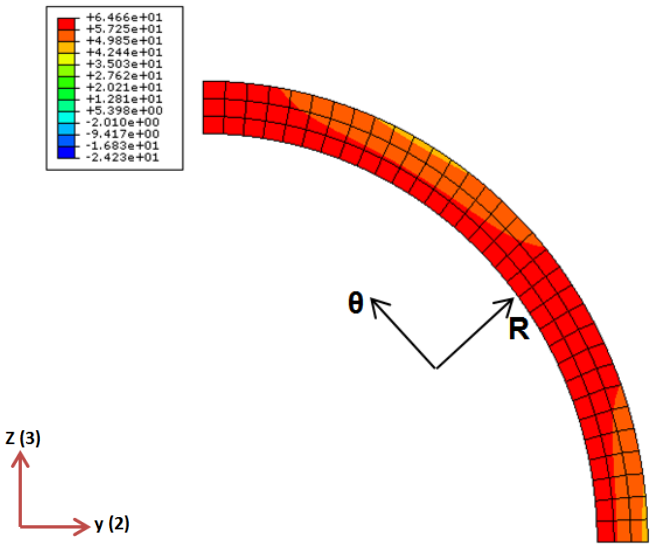

Figure 3.19. Hoop stress distribution.

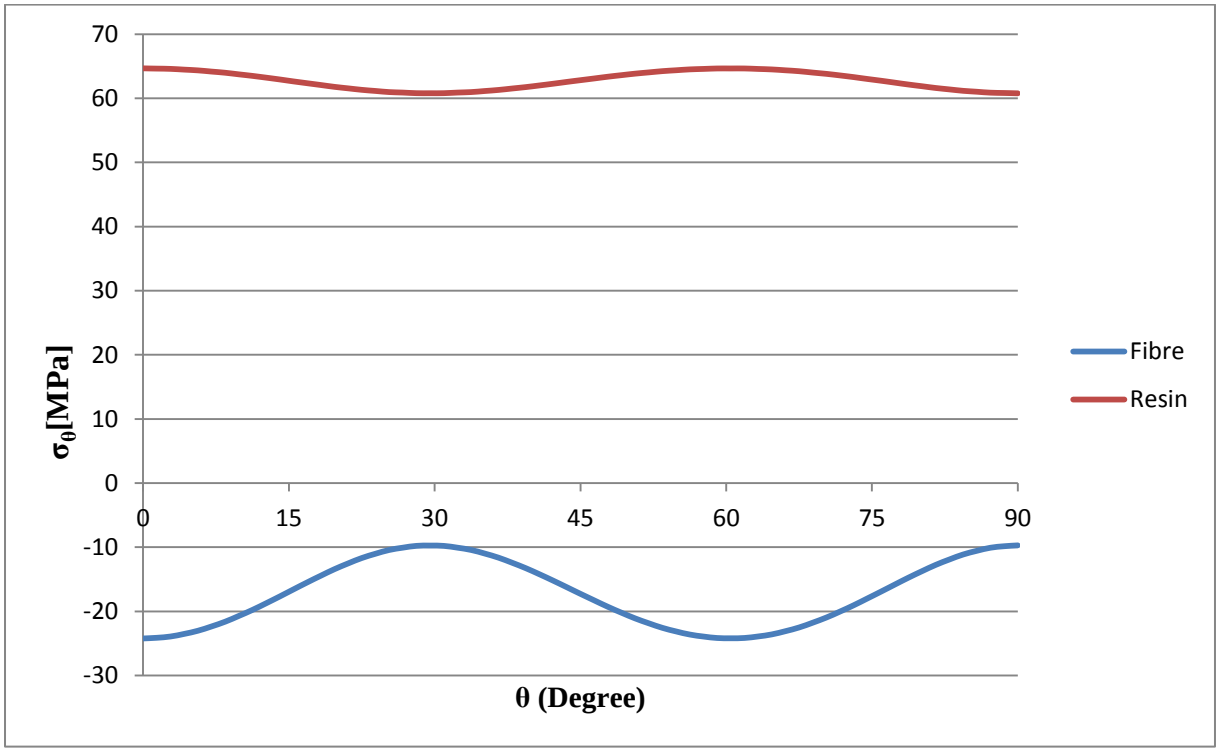

Figure 3.20. Hoop stress variation around fibre1.

3.2.6. Coefficient of Thermal Expansion (CTE)

Taking into account the deformation of the RVE during the cooling stage, Coefficients of Thermal Expansions (CTE) in fibre and transverse directions during cooling from 180 ^{o}C to 20^{o}C are calculated and compared with literature in Table 3.4.

Table 3.4. Comparison of CTE with experimental value.

AS4/8552	**With residual stress**	**[3]**
α_1 (10^{-6} /°C)	1.01	-
$\alpha_2=\alpha_3$ (10^{-6} /°C)	35.6	32.6

In this section, process-induced residual stress in AS4/8552 is investigated. Since the interface is the critical part of the RVE, different types of residual stresses are investigated at the interface level. Also, detailed behaviour of resin at some critical increments, such as, gelation point, vitrification point and just before cooling stage are presented in details. It is found that, most of the residual stresses are induced during cooling from cure temperature to room temperature and at the end of the cure cycle, tensile residual stresses are induced in resin and compressive residual stresses are induced in fibres as expected. Magnitude of residual stresses is greater at resin rich areas. These areas give an idea of where damage is expected to begin. The detailed analysis of damage assessment is presented in next chapter.

3.3. Progressive Damage Assessment

In this section, firstly, the strength values of a glass-fibre and carbon-fibre reinforced composites are predicted with maximum principal, Rahgava's and Bauwen's MVM failure criterion. Then, progressive damage assessment of AS4/8552 is presented. In addition to the criteria given, von Misses and Maximum Shear Stress failure criterion are applied for failure assessment of AS4/8552. Different interfacial properties are not taken into account. Strength and stiffness of the fibre-matrix interface are assumed to be equal to resin.

3.3.1. Strength Prediction of Various Composite Materials

The main aim of this thesis is the damage assessment of AS4/8552. In order to validate the user-defined subroutines USDFLD and UMAT developed in this thesis, a previously completed study [22] is used as a benchmarking study first. Micromechanical analysis of E-Glass Gevetex/LY556/HT907/DY063 Epoxy and AS4/3501-6 is examined and compared with experimental results [24]. In this section, damage paths or final failure of composite are not presented, only the strength values of each composite material are given.

3.3.1.1. E-Glass Gevetex/LY556/HT907/DY063 Epoxy. In Maligno's thesis [22], the composite has a volume fraction of 60 % and the cure temperature is 149 °C. The thermal residual stress is produced when the composite cooled down from 149 to 20 °C. At the end of the cure cycle, maximum of 26 MPa maximum principal residual stress is induced in resin. Also, Soden [24] performed experimental tests for the same material. Constituents properties given in [22,24] are shown in Table 3.5. $\sigma_r{}^T$ and $\sigma_r{}^C$ are tensile and compressive strengths of resin respectively.

Table 3.5. Constituents' properties of E-Glass/Epoxy

	E-Glass Gevetex	LY556/HT907/DY063 Epoxy	
E	80	3.35	GPa
ν	0.2	0.35	
α	4.9	58	10^{-6}/°C
$\boldsymbol{\sigma_r{}^T}$	-	80	MPa
$\boldsymbol{\sigma_r{}^C}$	-	120	MPa

Table 3.6 presents the comparison of transverse tensile and longitudinal shear strength of E-Glass Gevetex/LY556/HT907/DY063 Epoxy obtained by micromechanical approach [22] and experimental measurements [24]. It is seen from Table 3.6 that results obtained by the model in this thesis show good agreement with micromechanical results [22], however they are far away from experimental results. In-plane shear test was not carried out in [22].

Table 3.6. Comparison of predicted strength of E-Glass/Epoxy with reference values.

		Maximum Principal	**Raghava's MVM**	**Bauwen's MVM**	**EXP [24]**
PRESENT STUDY	σ_y^T **[MPa]**	61	66.3	70.5	35
	σ_z^T **[MPa]**	51.5	58.2	66.6	
	τ_{yz}^S **[MPa]**	43.1	41	40	72
REFERENCE [22]	σ_y^T **[MPa]**	**61**	**66**	-	-
	σ_z^T **[MPa]**	**52**	**58**	-	

3.3.1.2. AS4/3501-6. This material is a composite which is similar to AS4/8552. Properties of AS4 are given in Table 2.5 and material properties of 3501-6 given in [24] are shown in Table 3.7. Cure temperature of this composite is 180 °C and when cooled down to 20 °C, maximum von Misses and principal residual stresses induced in resin are 49 MPa and 41 MPa respectively.

Table 3.7. Elastic properties of 3501-6 epoxy [24].

	LY556/HT907/DY063 Epoxy	
E	4.2	GPa
ν	0.34	
α	45	10^{-6}/°C
σ_r^T	69	MPa
σ_r^C	250	MPa

Table 3.8 shows the comparison of predicted strength values with experimental results found by Soden et al. [24]. According to Table 3.8, the micromechanical model with maximum principal stress failure criterion gives close result with experimental results for normal loading conditions and under in-plane shear loading, predicted values diverge from experimental results. When Table 3.6 is compared with Table 3.8, it can easily be seen that, for each loading mode, difference between each criteria is higher for AS4/3501-6. This is the consequence of different material types and difference between the compression and tensile strength of resin. Both fibre and resin are isotropic in E-Glass/Epoxy, however AS4 is a transversely-isotropic fibre and 3501-6 is an isotropic resin material. Different fibre structures affect the strength prediction of composite materials.

Difference between the compression and tensile strength of LY556/HT907/DY063 is less than 3501-6 resin. This situation highly affects the predicted strength results for each failure criteria.

Table 3.8. Comparison of predicted strength values of AS4/3501-6 with experimental results.

	Max. Principal	**Raghava's MVM**	**Bauwen's MVM**	**Experimental [24]**
σ_y^T **[MPa]**	51.6	27.1	30.4	48
σ_z^T **[MPa]**	48.7	26.3	28	
σ_y^C **[MPa]**	-209.1	-180.2	-123.4	-200
σ_z^C **[MPa]**	-211	-169.2	-178.4	
τ_{yz}^S **[MPa]**	43.7	37.6	33.6	79

Difference between each loading direction for each material is due to the geometry of the hexagonally packed RVE regardless of its type. Because a hexagonally packed RVE does not have a fully symmetric conditions in each planes. Same predictions are made with quarter and whole hexagonally packed RVEs in each loading direction for these materials. Therefore, for a shorter computation time, quarter hexagonally packed is preferred for AS4/8552.

3.3.2. Failure Assessment of AS4/8552

As in previous section, resin dominated strength properties of AS4/8552 are predicted and damage patterns under each load mode are presented in this section. According to the product data sheet of 8552 resin [25], tensile strength of 8552 is 120 MPa but the compression strength is not given. Also, it is not available in literature. Therefore an assumption is done. 8552 resin has higher strength than 3501-6 and the strength values of 3501-6 resin are known from [24]. The compression strength of 8552 resin is assumed as 300 MPa.

Transverse tensile & compression, in-plane shear tests are simulated. Also progressive damage behaviour with damage pattern is presented.

3.3.2.1. Transverse Tensile Strength. First, the failure assessment of AS4/8552 is investigated under transverse tensile loading in both transverse directions (y & z) to see the

effect of loading direction on the transverse tensile strength and damage pattern of the composite.

Mesh convergence analysis is carried out for subsequent transverse tensile loading of AS4/8552 after its cure cycle with respect to Maximum Principal Failure criterion. It is presented in Figure 3.21. It is seen in Figure 3.21 that, mesh size mostly effects the elastic modulus of the material. Since, stress based failure criteria are used in this thesis, mesh size does not considerably affect the strength of the material. In figure 3.21, the coarse element size 0.0008 mm and the slope of that element is 9720 MPa. With decreasing the element size to 0.0001 mm, light blue and pink lines coincide with each other, the slope of both curves is 9755 MPa. It means that, results converge when mesh element type is C3D20 and its size is less than or equal to 0.0002 mm.

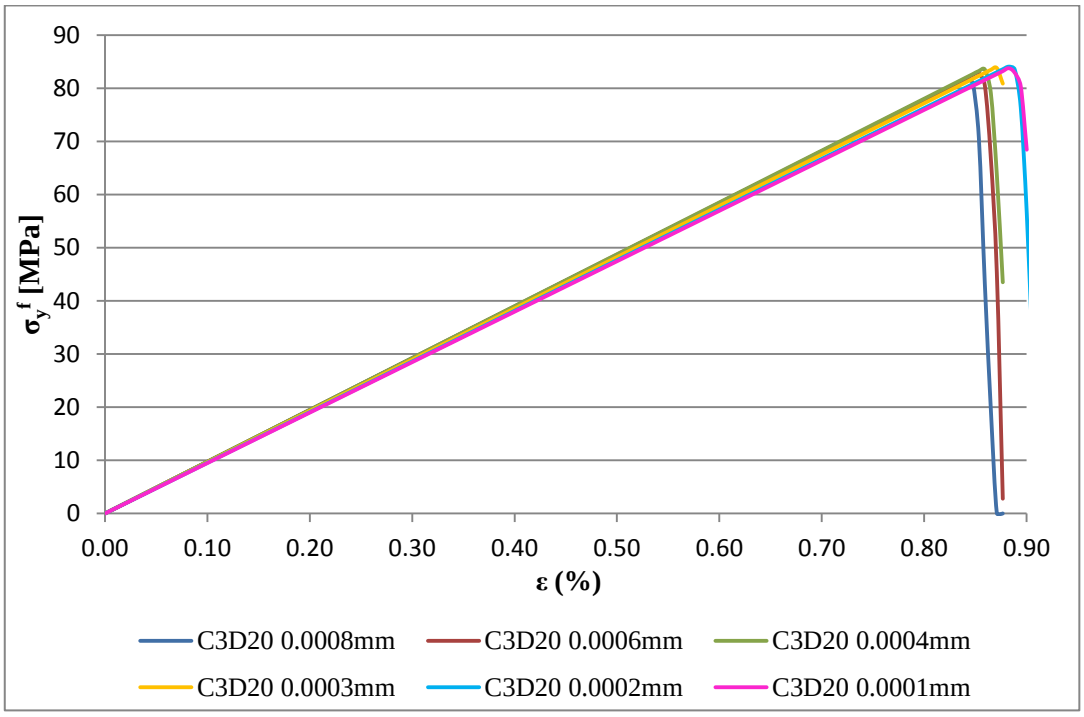

Figure 3.21. Transverse tensile strength prediction with different mesh sizes.

In order to show the damage pattern in details, mesh size is chosen as 0.0001 mm. Figure 3.22 presents the damage initiation and its progression according to the maximum principal failure criterion. Damage initiates at where maximum principal stress is greater than or equal to the tensile strength of resin. In order to show an example of this moment, maximum principal stress distribution of Figure 3.22a is presented in Figure 3.23. Damage

initiation is similar when loaded in different directions with residual stress. It initiates in fibre-resin interface as can be seen in Figure 3.22a. However, without residual stress, damage initiates very differently when loaded in different directions. It initiates in bulk resin at the corners of RVE when loaded in z direction as shown in 3.22b.

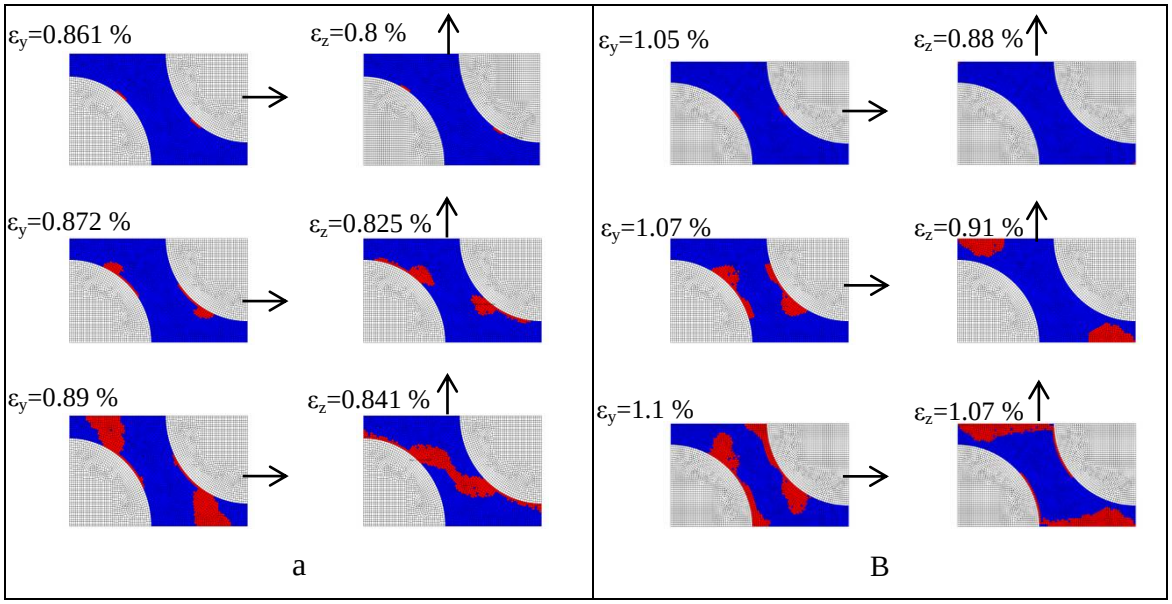

Figure 3.22. Damage progression under transverse tensile loading with respect to Maximum Principal Failure Criterion (a) with residual stress; (b) without residual stress.

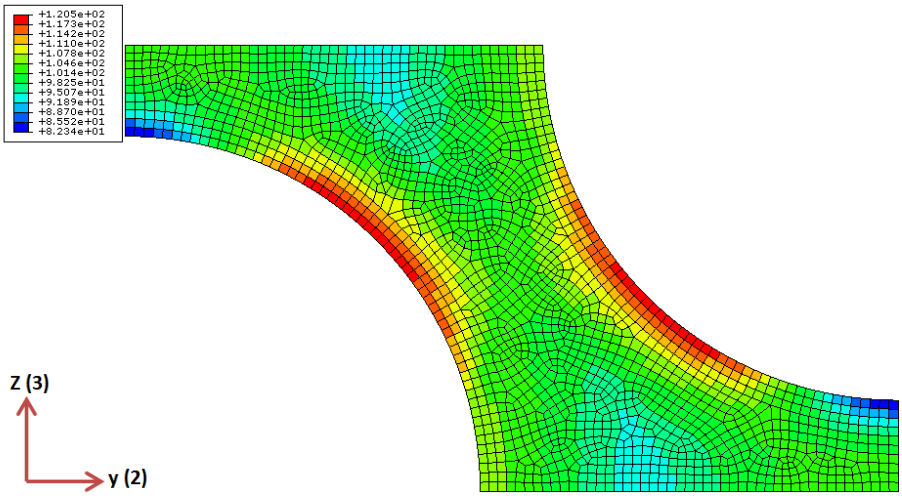

Figure 3.23. Max. Principal stress distribution in resin after loaded in y-direction with presence of residual stress.

Effect of residual stress to the strength of composite can be seen clearly in Figure 3.24. Transverse tensile strength of composite reduces from 102 MPa to 84 MPa in y-direction and it reduces from 85 MPa to 77 MPa in z-direction with presence of residual stress. It can elongate to 1.05 % in y direction and 0.88 % in z-direction without residual stress, however its elongation without any failure is limited to 0.861 % in y-direction and 0.80 % in z-direction with the presenc of residual stress in resin.

Residual stress does not affect the strength of AS4/8552 when loaded in z-direction as it affects its strength under loading in y-direction. However, damage progression is highly affected with presence of residual stress in each directions.

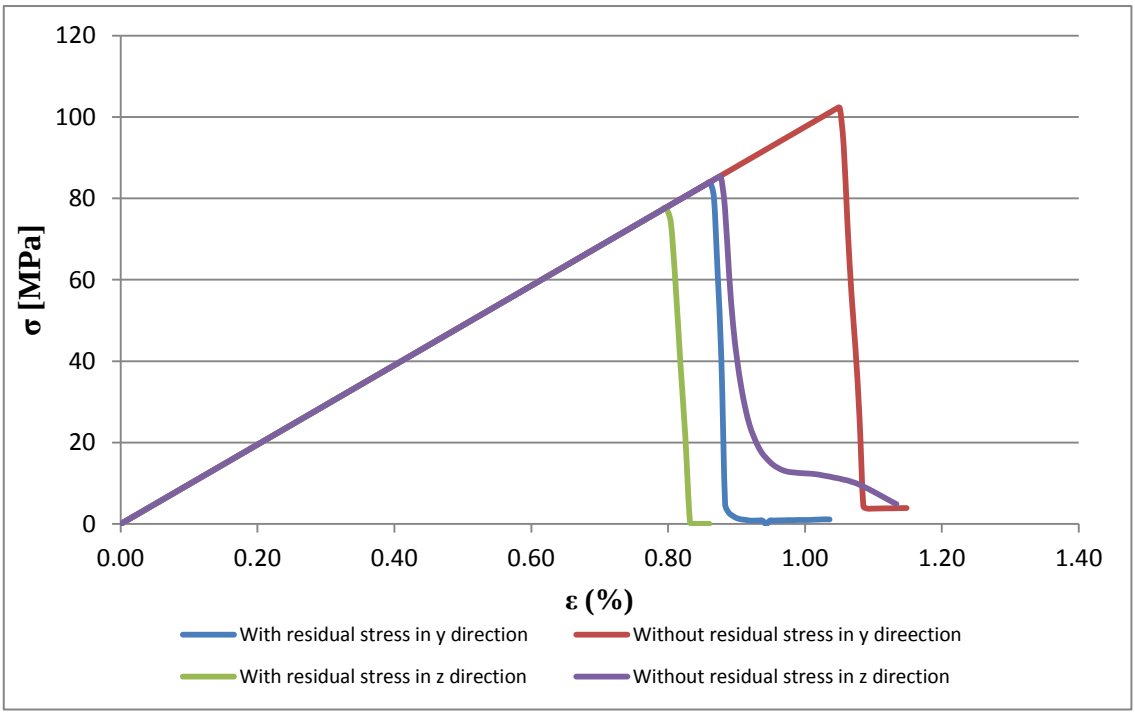

Figure 3.24. Tensile stress-strain curve for AS4/8552 in transverse directions with respect to maximum principal stress criterion.

Strength and damage pattern significantly change when this material is analysed with respect to Raghava's MVM failure criterion. Figure 3.25 shows damage initiation and evolution under transverse tensile loading in each directions according to Raghava's MVM failure criterion with and without the effect of residual stress. Damage patterns are perpendicular to loading directions. Residual stress with respect to Raghava's MVM

failure criterion has more influence on transverse tensile strength than Maximum Principal failure criterion, this situation can be seen clearly when Figure 3.26 is compared with Figure 3.24.

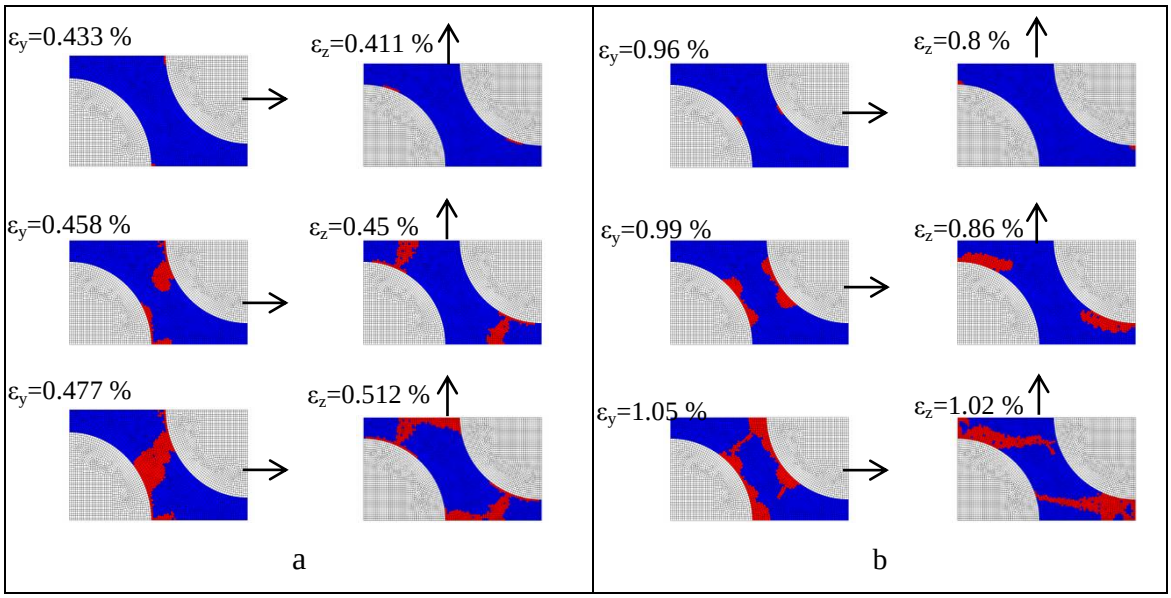

Figure 3.25. Damage progression under transverse tensile loading with respect to Raghava's MVM Failure Criterion (a) with residual stress; (b) without residual stress.

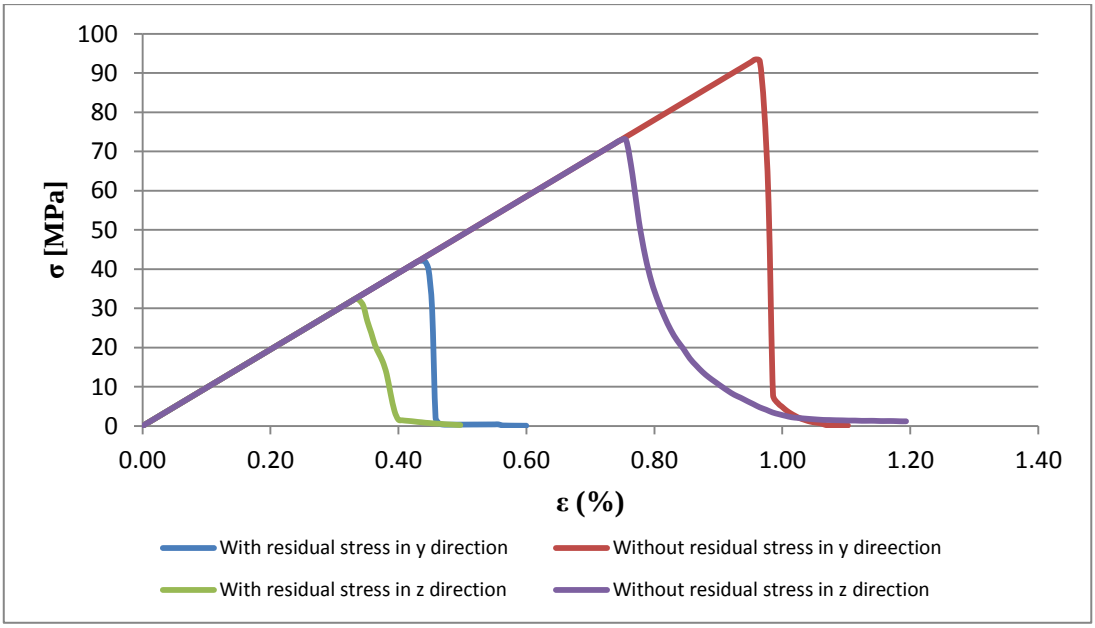

Figure 3.26. Tensile stress-strain curve for AS4/8552 in transverse directions with respect to Raghava's MVM criterion.

According to Bauwen's MVM failure criterion, with presence of residual stress, damage initiates in fibre/matrix interface and propagates towards the corners of RVE and causes debonding when loaded in y-direction. When it is loaded in z-direction with residual stress, it causes a shear band. If resin does not carry residual stress during loading, the damage pattern is different. Damage patterns under transverse loading conditions with respect to Bauwen's MVM failure criterion can be seen in Figure 3.27.

Effect of residual stress and loading direction to the transverse tensile strength and of AS4/8552 is similiar with respect to Bauwen's and Raghava's MVM failure criteria. Figure 3.28 shows the effect of residual stress and loading direction on the transverse tensile strength of the composite with respect to Bauwen's MVM.

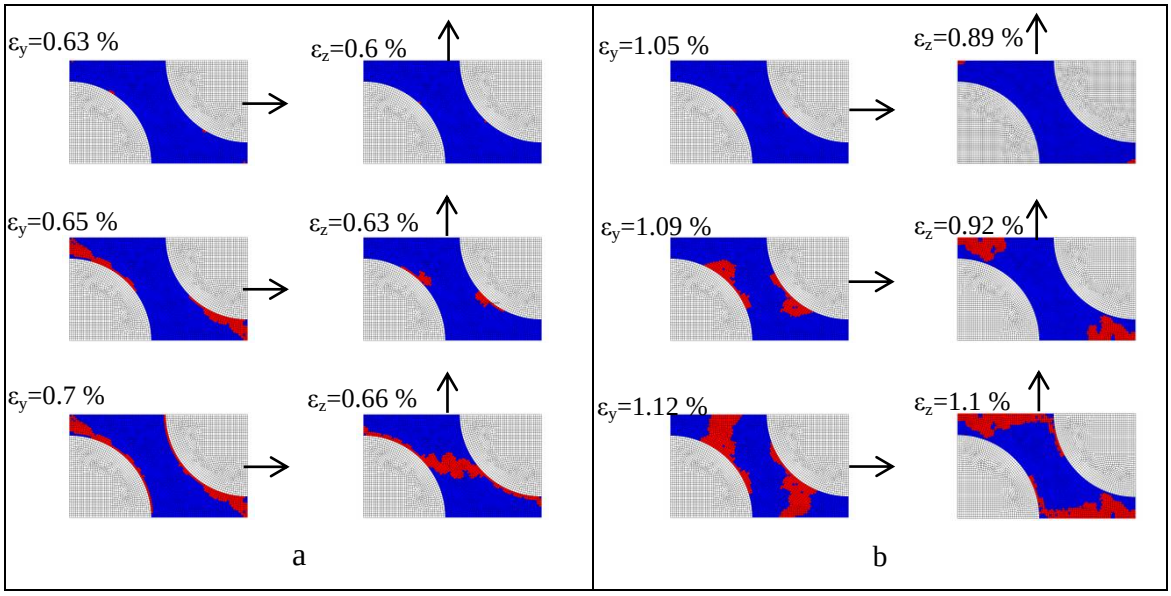

Figure 3.27. Damage progression under transverse tensile loading with respect to Bauwen's MVM Failure Criterion (a) with residual stress; (b) without residual stress.

From progressive damage assessment of AS4/8552, Figures 3.24, 3.26 and 3.28 show that, presence of residual stress causes a significant strength reduction in fibre-reinforced polymeric composites. Especially this reduction is greater according to Raghava's and Bauwen's MVM failure criterion. These two criteria consider the interactions between volumetric and deviatoric stress invariants.

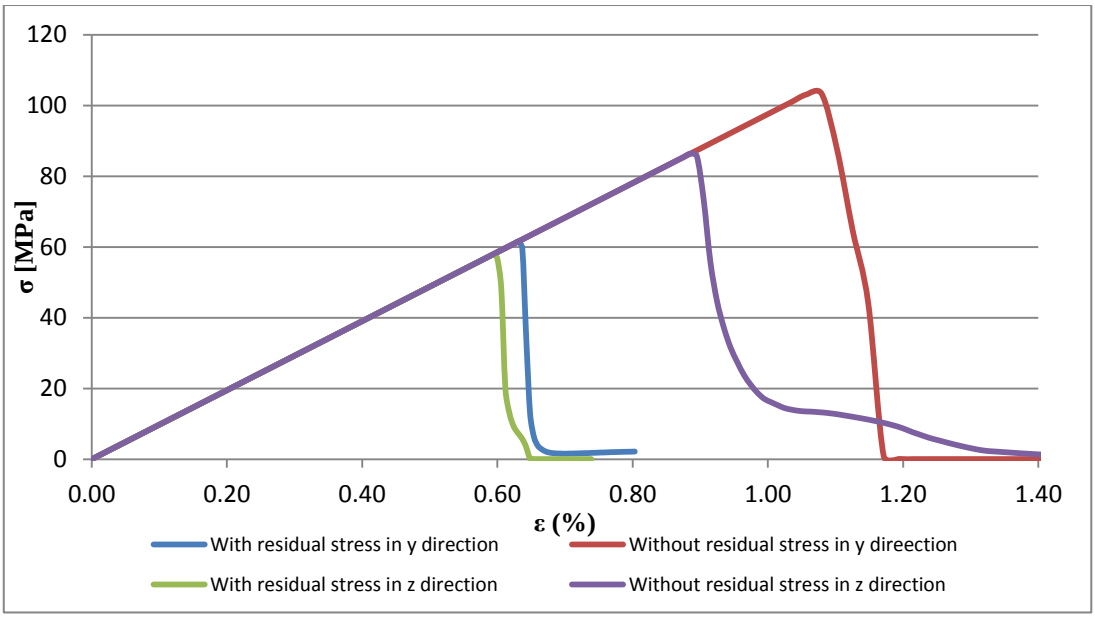

Figure 3.28. Tensile stress-strain curve for AS4/8552 in transverse directions according to Bauwen's MVM failure criterion.

Although von Misses and maximum shear stress criterion are not necessary for composite materials, strength of AS4/8552 is investigated with respect to these criteria. A comparison between predictions, experimental results and product data sheet is shown in Table 3.9. According to Table 3.9, Tresca and von Misses failure criterion do not seem appropriate for AS4/8552, because it gives pretty far predictions when loaded in each directions. Raghava's and Bauwen's MVM failure criteria seem more appropriate for AS4/8552.

Table 3.9. Comparison of transverse tensile strength and failure strain prediction of AS4/8552.

	With Residual Stress		**Without Residual Stress**	
	σ_y^T [MPa]	**σ_z^T [MPa]**	**σ_y^T [MPa]**	**σ_z^T [MPa]**
MAX. PRINC.	83.9	77.6	102.2	85.2
RAGHAVA	42.1	39.7	93	77
BAUWEN	61.5	57.8	103.3	86.3
TRESCA	47.3	71.5	103.1	103.5
VON-MISSES	59.6	88.2	117.2	118
EXP	50 (STD = 8.86)			
[25]	81			
[26]	63 (STD = 5.982)			

3.3.2.2. Transverse Compression Strength. Compressive strength of AS4/8552 is predicted with respect to maximum principal stress, Raghava's MVM and Bauwen's MVM failure criteria. Tresca and von Misses are not taken into account.

Damage initiation and evolution under compression loading in y-direction is similiar with and without residual stress according to maximum principal failure criterion. Similarly, damage pattern occured as a consequence of subsequent loading in z-direction after cure-cycle resembles the path after loading without the presence of residual stress in resin. Figure 3.29 presents the damage path for each load modes. As seen in Figure 3.29, loading direction changes the location of damage initiation.

Maximum principal stress distribution in resin when damage initiates under subsequent loading in y-direction can be seen in Figure 3.30. Effect of loading direction to transverse compression strength of AS4/8552 has more influence than the effect of presence of residual stress. Figure 3.31 compares the prediction of compressive strength with respect to Maximum Principal Failure criterion for each load direction.

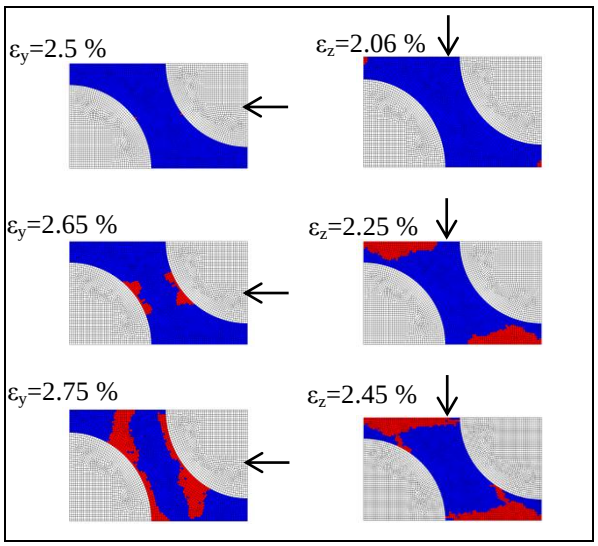

Figure 3.29. Damage progression under transverse compressive loading according to Maximum Principal Failure Criterion.

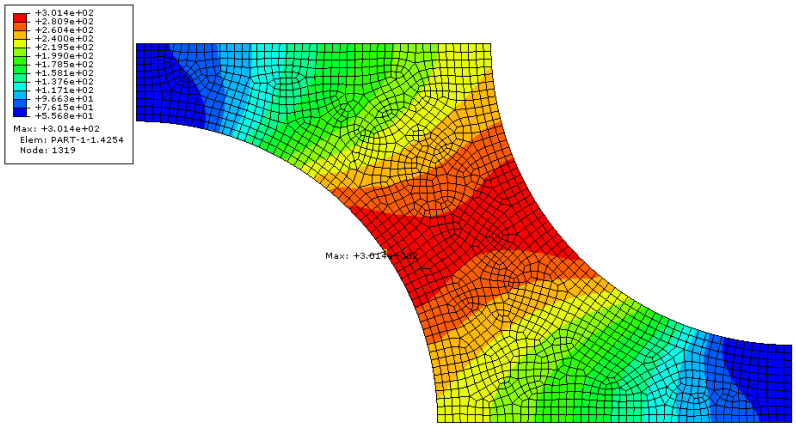

Figure 3.30. Maximum principal stress distribution in resin when damage initiates under compression in y-direction.

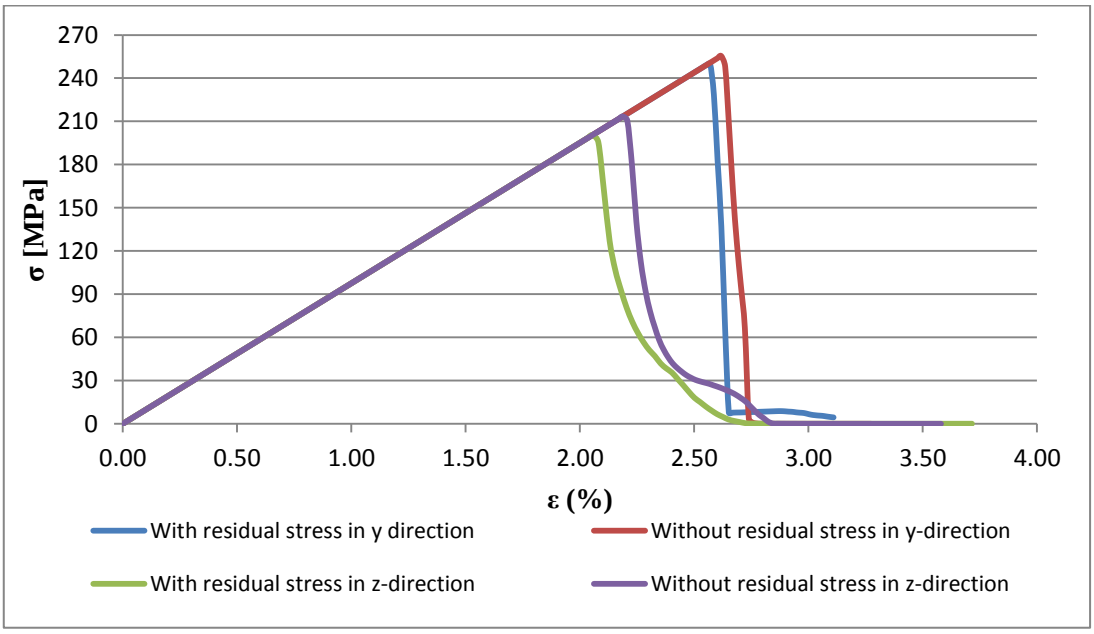

Figure 3.31. Compressive stress-strain curve of AS4/8552 according to maximum principal stress criterion.

Damage pattern is completely different with respect to Raghava's MVM failure criterion than maximum principal stress criterion but similarly, presence of residual stress does not have an important effect on damage pattern but loading direction has. Although final failure is similar, loading direction and residual stress both effect damage initiation. Figure 3.32 presents damage progression for every situation.

According to Raghava's MVM failure criterion, residual stress has more influence than loading direction on the transverse compression strength of AS4/8552 as can be seen in Figure 3.33.

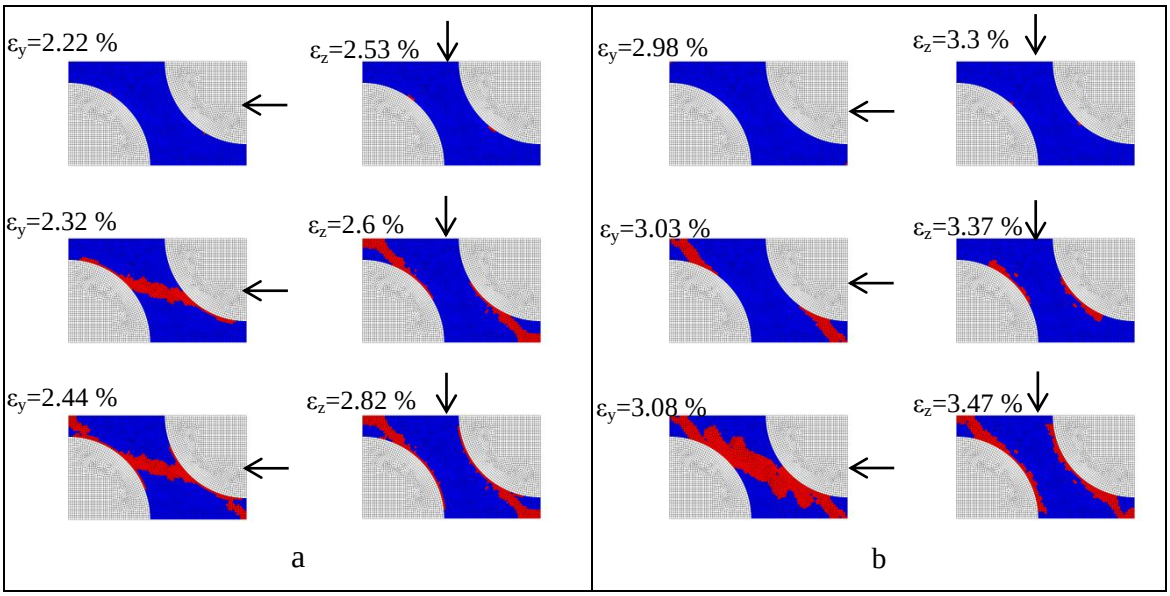

Figure 3.32. Damage progression under transverse compressive loading with respect to Raghava's MVM Failure Criterion (a) with residual stress; (b) without residual stress.

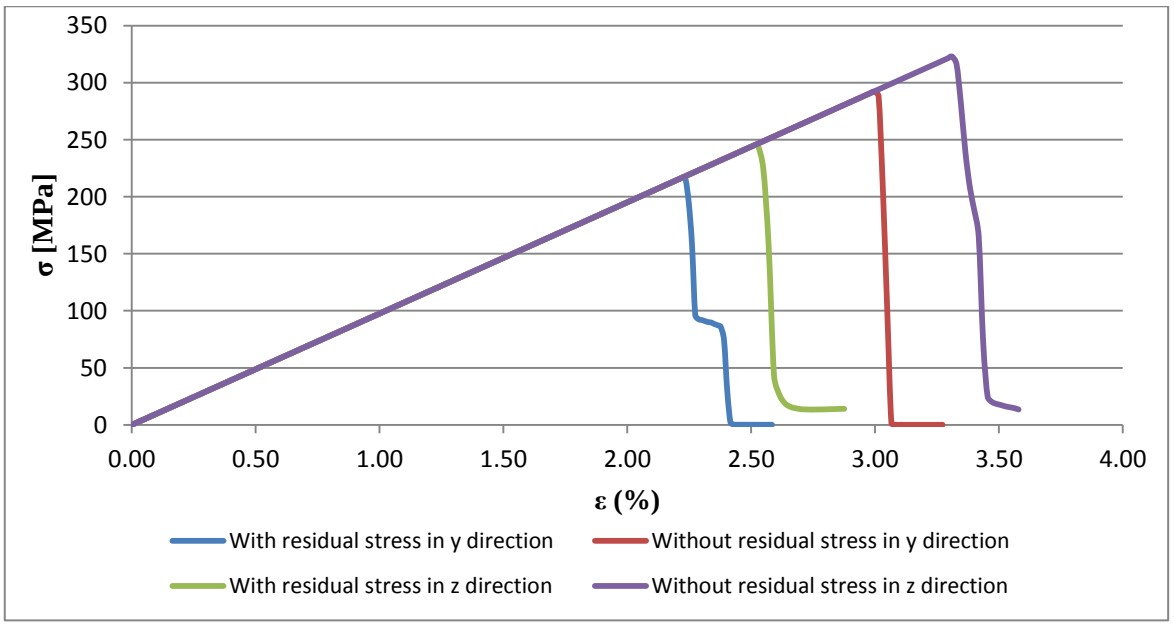

Figure 3.33. Compression stress-strain curve of AS4/8552 according to Raghava's MVM failure criterion.

Progressive damage behaviour of AS4/8552 with respect to Bauwen's MVM failure criterion can be seen in Figure 3.34. When it is compared with 3.32, similar behaviour can be noticed. Damage initiation is influenced by residual stress but the final failure is similar for each loading mode. While a shear band is induced under loading in y-direction, a debonding in fibre-resin interface is a consequence of loading in z-direction. So, one can say that progressive damage behaviour of AS4/8552 under transverse compressive loading with respect to Bauwen's MVM failure criteria is similar to Raghava's MVM failure criterion. Figure 3.35 presents the compressive stress-strain curve for AS4/8552 with respect to Bauwen's MVM failure criterion.

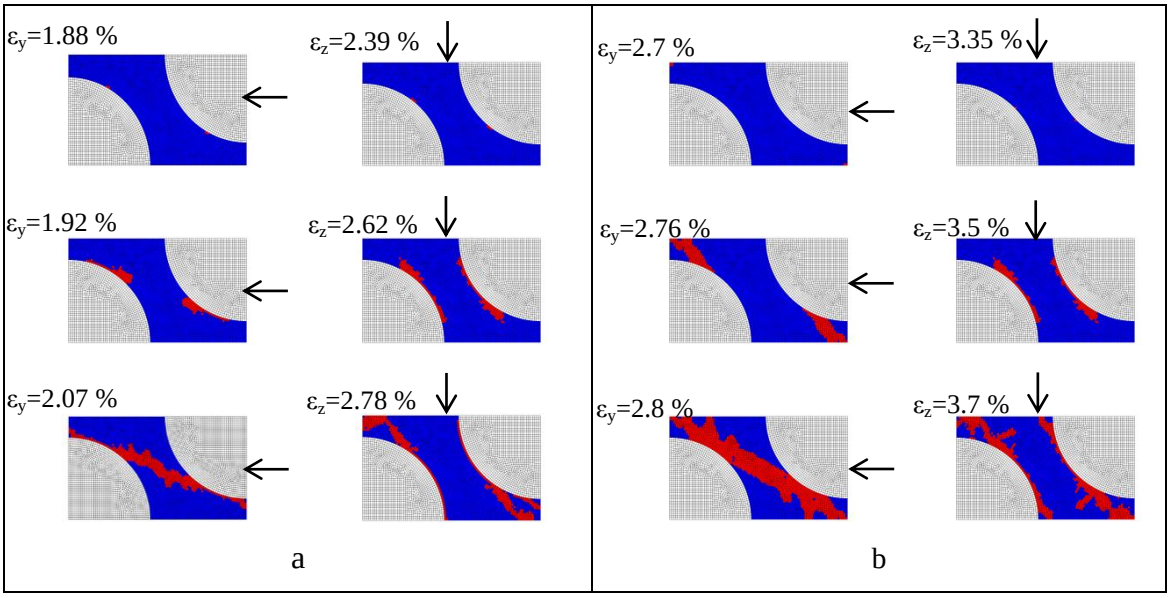

Figure 3.34. Damage progression under transverse tensile loading with respect to Bauwen's MVM Failure Criterion (a) with residual stress; (b) without residual stress.

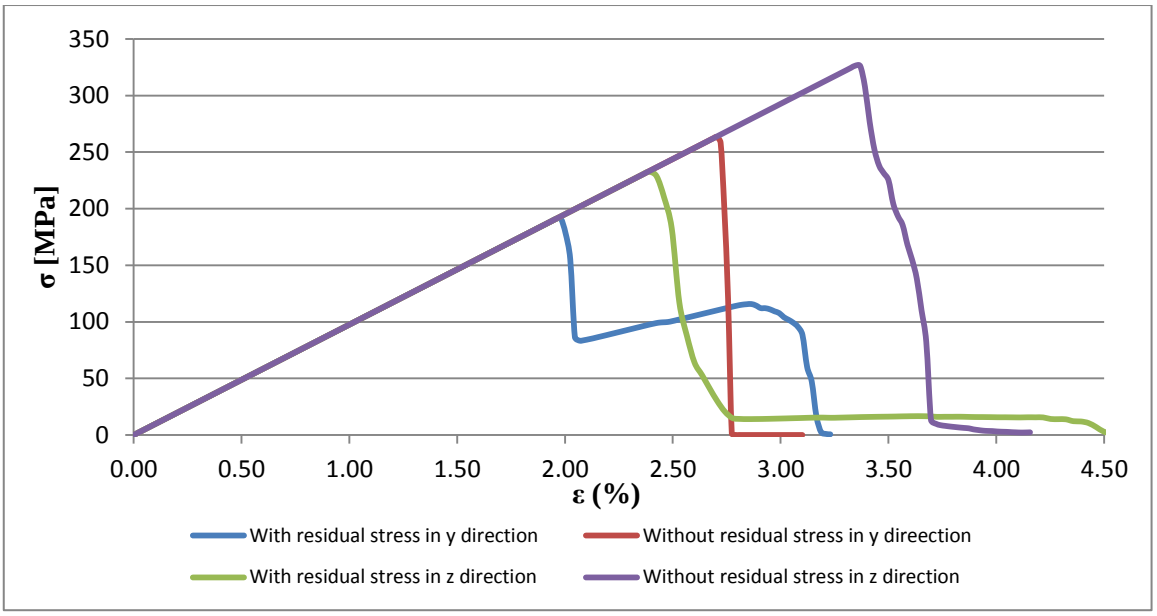

Figure 3.35. Compression stress-strain curve of AS4/8552 according to Bauwen's MVM failure criterion.

Compressive strength values of AS4/8552 in transverse directions with respect to each failure criteria are presented in Table 3.10. Difference between strength values of AS4/8552 with and without residual stress is about 35 % for Raghava's and Bauwen's MVM failure criteria but it is around 5 % for maximum principal failure criterion.

A compression test is not done in mechanics laboratory of mechanical engineering department of Bogazici University and transverse compression strength of AS4/8552 is not available in product data sheet but statistical report [26] presents the results of a bunch of compression test.

Table 3.10. Comparison of transverse compressive strength prediction of AS4/8552.

	With Residual Stress		**Without Residual Stress**	
	σ_y^C [MPa]	**σ_z^C [MPa]**	**σ_y^C [MPa]**	**σ_z^C [MPa]**
MAX. PRINC.	250	200.6	255.4	213.4
RAGHAVA	216.8	244.8	292.1	323
BAUWEN	190.2	232.6	263.3	326.5
[26]	267 (STD = 6.276)			

3.3.2.3. Longitudinal Shear Strength. Longitudinal shear strength can be considered as the short beam shear strength of AS4/8552. Details of the boundary conditions and constraints are given in chapter 2.

Figure 3.36 presents the final failure at the end of longitudinal shear loading. Detailed sketch of incremental failure as a consequence of longitudinal shear loading with presence of residual stress can be seen in Figure 3.37. With the effect of residual stress, damage progression is very similiar with respect to every failure criteria and damage pattern is same regardless of the failure criteria without the effect of residual stress as represented in Figure 3.38. When in-plane shear loading is applied without the presence of residual stress, damage begins in the middle of fibre-matrix interface and spreads through the interface toward the upper and transverse edges of the model regardless of failure criteria. In order to show an example of stress distribution in resin and the deformation at damage initiation moment, Figure 3.39 represent Equation 1.31 which is Raghava's failure stress. Only free edges of the model are sketched in Figure 3.39 for a clear view.

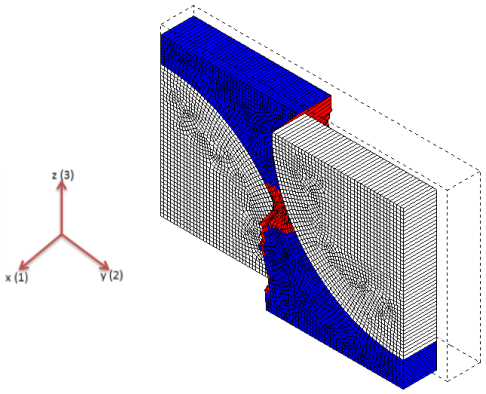

Figure 3.36. Final failure under subsequent in-plane shear loading.

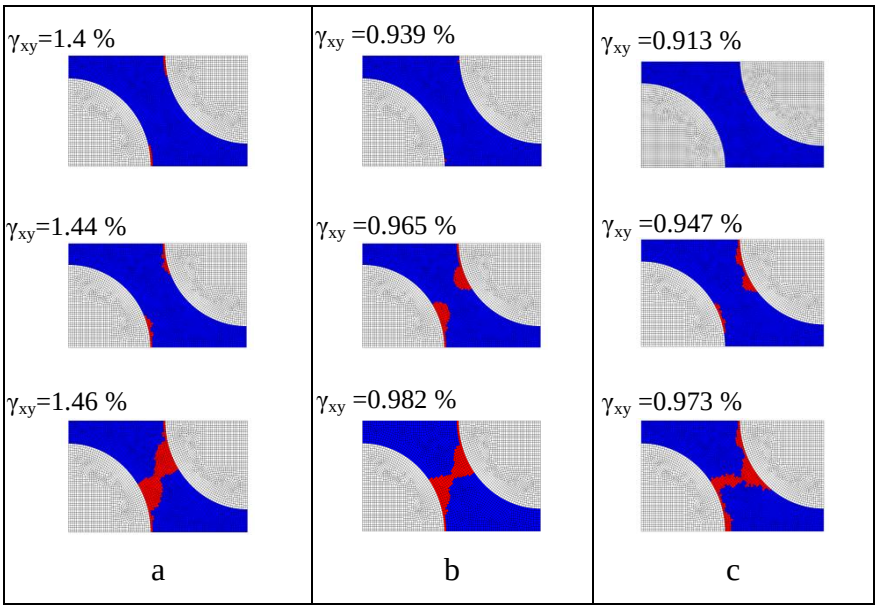

Figure 3.37. Damage progression under longitudinal shear loading (a) Maximum Principal (b) Raghava's MVM (c) Bauwen's MVM failure criteria.

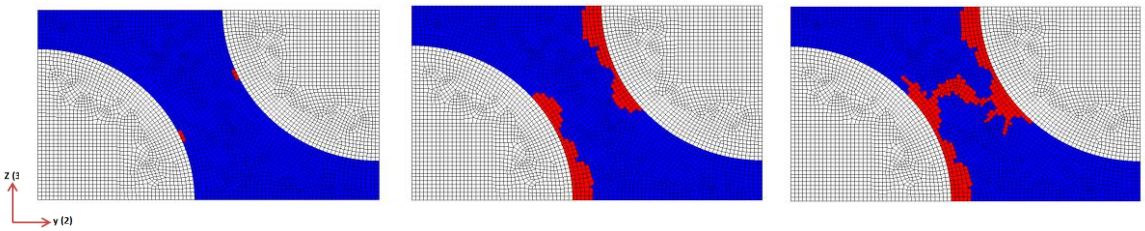

Figure 3.38. Damage progression under longitudinal shear loading without the effect of residual stress.

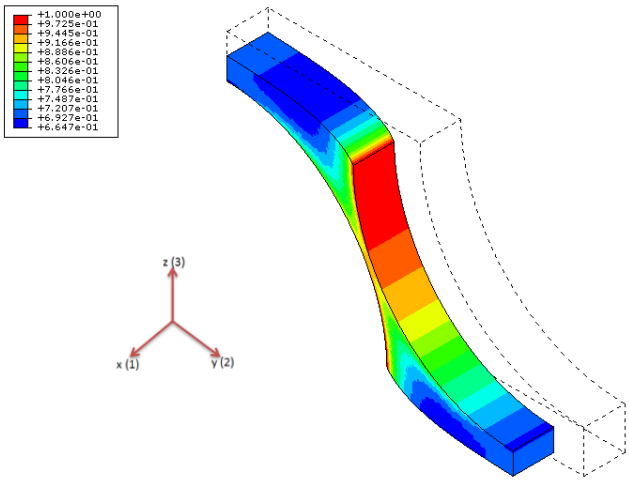

Figure 3.39. Representation of deformation and Equation 1.31 when damage initiates with respect to Raghava's MVM failure criterion.

Figure 3.40 is the plot of shear stress-strain curve of AS4/8552 under in-plane shear loading. Detrimental effect of residual stress on shear strength can be seen clearly. In-plane shear strength prediction of AS4/8552 is presented in Table 3.11. In order to make a comparison, statistical report [26] is taken into account. In this report, non-linear behaviour is observed during short-beam shear tests, therefore the in-plane shear strength of the material is determined by 0.2 % offset and its value is 55 MPa.

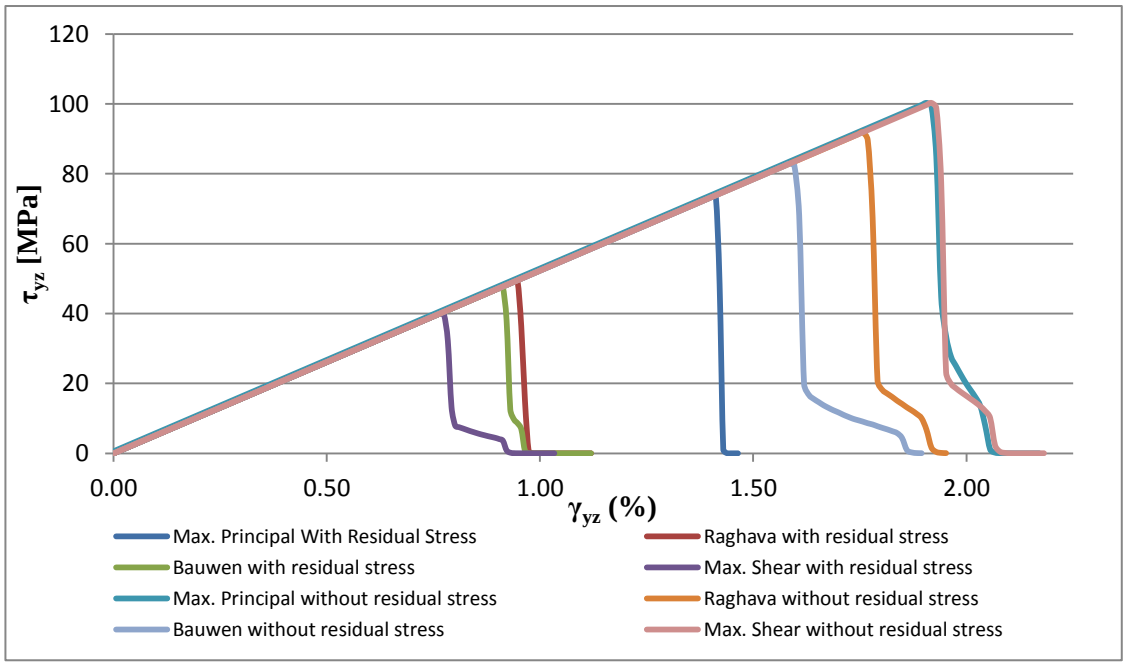

Figure 3.40. Shear stress-strain curve of AS4/8552 under in-plane shear loading.

According to the Least Square Difference method given with Equation 2.18 the error between each failure criteria and experimental results are given in Table 3.12. With respect to these results, the most adequate criteria seems Maximum Principal Stress Criteria.

Table 3.11. Comparison of in-plane strength prediction of AS4/8552.

	With Residual Stress	**Without Residual Stress**
	τ_{yz}^{S} [MPa]	**τ_{yz}^{S} [MPa]**
MAX. PRINC.	73.4	100.3
RAGHAVA	49.5	93
BAUWEN	47.4	83
MAX. SHEAR	35.6	100.3
[26]	55 [0.2 % offset] (STD = 1.654)	

Table 3.12. Error between each criteria and experimental result.

	Maximum Principal	Raghava	Bauwen
Error %	9.4	12	13.2

4. CONCLUSION AND FUTURE WORK

In this thesis, a finite element micromechanical model is developed to calculate the elastic moduli of a composite, to investigate process-induced residual stress in constituents and the effect of the presence of residual stresses on progressive damage behaviour of the composite. For this purpose, a hexagonally packed 3D representative volume element is constructed in ABAQUS. For this model, a user defined subroutine UMAT is developed to model incremental elastic modulus of resin, thermal expansion, contraction and chemical shrinkage of resin during its cure cycle. In addition to this, another user defined subroutine USDFLD is developed to model failure criteria for resin.

A quarter hexagonally packed RVE with C3D20 mesh elements sized of 0.0002 mm is sufficient to calculate the elastic moduli, predict the strength of a fibre-reinforced composite but it is not adequate to predict transverse shear properties, therefore a whole, symmetric RVE should be used with proper periodic and symmetric boundary conditions and constraints for modelling transverse shear. Elastic moduli of a carbon/reinforced composite are predicted with excellent correlation with reference value [5]. Then, elastic moduli of AS4/8552 is predicted. It also shows great agreement with numerical [3] and experimental [26] results. Thus, the model and the approach are verified for further micromechanical analysis.

Manufacturer's Recommended Cure Cycle (MRCC) of AS4/8552 is modelled. Incremental strain and development of elastic modulus of resin during its cure cycle are implemented in user defined subroutine, UMAT. Non-linear behaviour of resin and the composite through cure cycle are presented. Especially, total strain of composite in gelation, vitrification and beginning of cooling points are emphasised. It is observed that most of the residual stress is induced during cooling from cure temperature to room temperature. Maximum residual stresses are induced in resin rich regions of the RVE. For different stress criterion, fibre-matrix interface is found to be the critical region at the end of cure cycle as in previous studies [19-22].

In the final part of the thesis, effect of residual stress on the strength and progressive damage behaviour of AS4/8552 is investigated. A new user defined subroutine, USDFLD, is developed to model failure criteria. Before performing

progressive damage analysis of AS4/8552, the verification of the model is required by comparing it to previously done studies [22,24] as the model is verified for predicting elastic moduli. Therefore, transverse tensile, compression and longitudinal shear strengths and failure behaviour of E-Glass Gevetex/LY556/HT907/DY063 Epoxy composite is predicted. The difference between the compressive and tensile strength of the resin is not big. Predictions show great correlation with previously complete finite element results [22], but they are far from experimental results [24]. Also, there is slight difference between the predictions of loadings in different directions. Secondly, failure assessment of AS4/3501-6 is carried out. The difference between the compressive and tensile strength of 3501-6 is very high. Loadings in different directions resulted with more difference than E-glass fibre/epoxy. In addition to this, each failure criteria gave different results.

Similarly with AS4/3501-6, strength and damage pattern of AS4/8552 varied with loading direction and failure criteria. Also, the difference between compressive and tensile strength of 8552 is very high. While some criteria approach to experimental results, some do not. So, it can be concluded that, for E-glass fibres, loading directions and failure criteria for resin do not have an important influence on strength prediction but for carbon-reinforced epoxy composites, these parameters highly affect the strength and progressive damage behaviour. This situation has never been mentioned in literature before.

According to the least square difference criteria, maximum principal failure criterion seems to be the most adequate failure criter for prograssive failure analysis of fibre-reinforced composites.

As a future work to continue this study, generally in literature, square packed RVEs are considered and transverse strengths of the RVE does not vary with loading direction for any type of composite. However this situation is not valid for hexagonally packed RVE as proved in this thesis. In order to determine which loading direction is more important, a sensitive tensile test is required for AS4/8552. First failure stress should be determined with acoustic emission monitoring. Also, damage pattern should be viewed to compare and determine which loading direction is the most important one.

This thesis is carried out for unidirectional lamine. Mechanical behaviour of a cross-ply or even an anlge ply composite can be investigated. Also, effect of fibre packing geometry and randomly packed RVEs can be compared.

Transverse shear strength of composite is not performed in this thesis. As a future work, the same procedure carried out for each load mode can be applied to determine transverse shear strength of AS4/8552 with the effect of residual stress.

5. REFERENCES

1. Hull, D., *An Introduction to Composite Materials*, Cambridge University Press, New York, 1981.

2. Unluhisarcikli, O., *Control and Optimization of Cure Cycle for Thick-Sectioned Thermoset Composites Manufacturing*, M.S. Thesis, Bogazici University, 2008.

3. Ersoy, N., T., Garstka, K., Potter, M. R., Wisnom, D., Porter, M., Clegg and G., Stringer, "Development of the Properties of A Carbon Fibre Reinforced Thermosetting Composite Through Cure", *Composites: Part A*, Vol. 41, pp. 401–409, 2010.

4. Authar, K. K., *Mechanics of Composite Materials*, 2nd Edition, Taylor & Francis Inc., Florida, 2006.

5. Hyer, M. W., *Stress Analysis of Fibre-Reinforced Composite Materials*, McGraw-Hill, Michigan, 1998.

6. Ernst, G., M., Vogler, C., Hühne and R., Rolfes, "Multiscale Progressive Failure Analysis of Textile Composites", *Composites Science and Technology*, Vol. 70, No. 1, pp. 61–72, 2010.

7. Li, S., "General Unit Cells for Micromechanical Analyses of Unidirectional Composites", *Composites: Part A*, Vol. 32, pp. 815–826, 2001.

8. Garnich, M. R. and V. M. K., Akula, "Review of Degradation Models for Progressive Failure Analysis of Fiber Reinforced Polymer Composites", *Applied Mechanics Reviews*, Vol. 62, No. 1, 2009.

9. Gentz, M., D., Armentrout, P., Rupnowski, L., Kumosa, E., Shin, J. K., Sutter and M., Kumosa, "In-Plane Shear Testing of Medium and High Modulus Woven Graphite Fiber Reinforced/Polyimide Composites", *Composites Science and Technology*, Vol. 64, pp. 203–220, 2004.

10. Raghava, R. S., R. M., Caddell, and G. S. Y., Yeh, “The Macroscopic Yield Behaviour of Polymers”, *Journal of Material Science,* Vol. 8, pp. 225-232, 1973.

11. Bauwens, J. C., “Yield Condition and Propagation of Lüders' Lines in Tension-Torsion Experiments on Poly(Vinyl Chloride)”, *Journal of Polymer Science Part A-2: Polymer Physics*, Vol. 8, No. 6, pp. 893-901, 1973.

12. Adams, D. F. and D. A., Crane, “Combined Loading Micromechanical Analysis of A Unidirectional Composite”, *Composites*, Vol. 15, No. 3, pp. 181–192, 1984.

13. King, T. R., D. M., Blackketter, D. E., Walrath and D. F., Adams, “Micromechanics Prediction of the Shear Strength of Carbon Fibre/Epoxy Matrix Composites: The Influence of the Matrix and Interface Strengths”, *Journal of Composite Materials*, Vol. 26, No. 4, pp. 558–573, 1992.

14. Nedele, M. R. and M. R., Wisnom, “Finite Element Micromechanical Modelling of a Unidirectional Composite Subjected to Shear Loading”, *Composites,* Vol. 25, pp. 263–272, 1994.

15. Sun, C. T. and R. S., Vaidya, “Prediction of Composite Properties from a Representative Volume Element”, *Composites Science and Technology,* Vol. 56, pp. 171–179, 1996.

16. Chamis, C. C., “Simplified Composite Micromechanics for Predicting Micro Stresses”, *Journal of Reinforced Plastic Composites*, Vol. 6, pp. 268–288, 1987.

17. Lee, J. W. and I. M., Daniel, “Progressive Transverse Cracking of Cross-Ply Composite Laminates”, *Journal of Composite Materials*, Vol. 24, pp. 1225–1243, 1990.

18. Chen, Y., Z., Xia and F., Ellyin, “Evolution of Residual Stresses Induced During Curing Processing Using a Viscoelastic Micromechanical Model”, *Journal of Composite Materials*, Vol. 35, pp. 522–542, 2001.

19. Zhang, Y., Z., Xia and F., Ellyin, "Evolution and Influence of Residual Stress/Strains of Fibre Reinforced Laminates", *Composites Science and Technology*, Vol. 64, pp. 1613–1621, 2004.

20. Zhao, L. G., N. A., Warrior and A. C., Long, "A Micromechanical Study of Residual Stress and Its Effect on Transverse Failure in Polymer-Matrix Composites", *International Journal of Solids and Structures*, Vol. 43, pp. 5449–5467, 2006.

21. Zhao, L. G., N. A., Warrior and A. C., Long, "A Thermo-Viscoelastic Analysis of Process-Induced Residual Stress in Fibre-Reinforced Polymer–Matrix Composites", *Materials Science Engineering*, Vol. 453, pp. 483–498, 2007.

22. Maligno, A. R., *Finite Element Investigations on the Microstructure of Composite Materials*, Ph.D. Thesis, University of Nottingham, 2008.

23. *ABAQUS/Standard User's Manual*, Version 6.10, Vol. 1, included in the related software package.

24. Soden, P. D., M. J., Hinton and A. S., Kaddour, "Lamina Properties, Lay-Up Configuration and Loading Conditions for a Range of Fibre-Reinforced Composite Laminates", *Composites Science and Technology*, Vol. 58, No. 7, p. 1011, 1998.

25. Hexcel Composites, *HexPly 8552 Epoxy Matrix*, 2008, http://www.hexcel.com, accessed at July 2010.

26. K., Marlett, "Hexcel 8552 AS4 Unidirectional Prepreg at 190 gsm & 35 % RC Qualification Material Property Data Report", *NCAMP Test Report, Revision A*, 2011.